

**MOLECULAR REGULATORS OF INNERVATION AND PATTERNING
IN THE DEVELOPING CHICKEN INNER EAR**

by

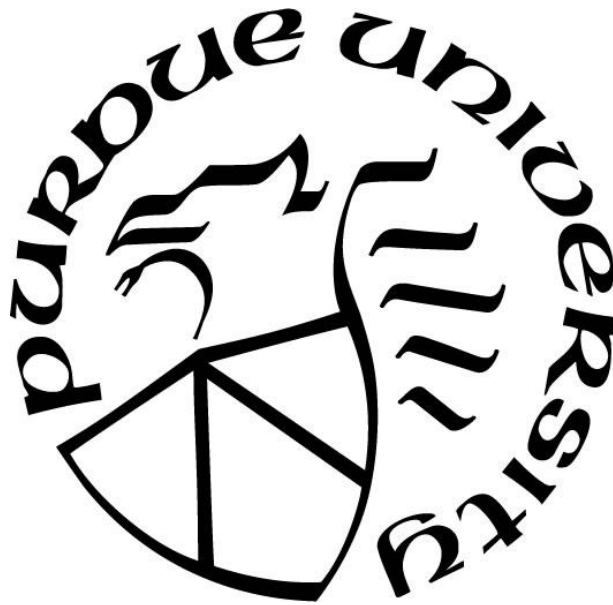
Mary Katherine Scott

A Dissertation

Submitted to the Faculty of Purdue University

In Partial Fulfillment of the Requirements for the degree of

Doctor of Philosophy



Department of Biology

West Lafayette, Indiana

December 2018

**THE PURDUE UNIVERSITY GRADUATE SCHOOL
STATEMENT OF COMMITTEE APPROVAL**

Dr. Donna M. Fekete, Chair

Department of Biology

Dr. Daniel M. Suter

Department of Biology

Dr. Jer-Yen Yang

Department of Basic Medical Sciences

Dr. Michael G. Heinz

Department of Speech, Language, and Hearing Sciences

Department of Biomedical Engineering

Approved by:

Dr. Jason Cannon

Head of the Graduate Program

To my daughter.

ACKNOWLEDGMENTS

First, I would like to thank my advisor, Donna Fekete. Under her mentorship, I have become a better critical thinker, teacher, and scientist. I am grateful for everything I have learned from her. I thank my committee: Daniel Suter, Jer-Yen Yang, Michael Heinz, and Eri Hashino for their support and feedback on this project. I would also like to thank my previous research mentors: Ryan Lau, Aimee Mayeda, and John Hofstetter for inspiring my passion for research and encouraging me to pursue my PhD. I am grateful for your continued support throughout my undergraduate, professional, and graduate career.

I would like to thank my lab mates, previous and current, for their support. Thank you to Michelle Stoller, Kaidi Zhang, and Vidhya Munnamalai for patiently training me in many of the techniques that were instrumental to this project and for your professional advice as I navigated graduate school. I thank Ankita Thawani, Deb Bieseemeier, and Vidhya Munnamalai for your direct and meaningful contributions to this project, your scientific feedback, and your friendship throughout graduate school. You have been integral to my success. I would like to thank the undergraduate trainees that I have had the pleasure to mentor during my time here at Purdue. Julie Lee, Bella Yue, Lucas Mondo, Alix Bikker, and Katie Pagel: your technical assistance on this project has been invaluable. I sincerely appreciate your contributions to this work and I wish you the best in your future endeavors.

I thank the National Institute of Deafness and Communication Disorders for funding my work. Thank you to Gaby Sincich for providing artwork to enhance the figures used in my first author publication and in this dissertation. I thank Nadia Atallah for providing her expertise and assistance on the RNA sequencing project. I thank Nicolas Daudet, Yoshiko Takahashi, Christophe Marcelle, and Sheri Holmen for sharing their plasmids with us. Thank you to Tom Coate for providing the opportunity to strengthen my publication record by inviting me to coauthor a review. I also thank Rupa De and Donna Fekete for providing the opportunity to assist in teaching your courses.

I wish to thank my friends and family who supported me throughout graduate school. Finally, I thank my husband, Ryan Scott, for always being by my side, encouraging me through the challenges and celebrating my successes throughout graduate school. I could not have done this without your love and support.

TABLE OF CONTENTS

LIST OF TABLES	9
LIST OF FIGURES	10
LIST OF ABBREVIATIONS	12
ABSTRACT	15
CHAPTER 1. INTRODUCTION	18
1.1 The anatomy of the avian inner ear.....	18
1.1.1 The vestibular system	18
1.1.2 The auditory system.....	18
1.1.3 Nonsensory domains of the cochlear duct	19
1.2 Chicken inner ear development and innervation	22
1.3 Molecular regulators of innervation in the inner ear	22
1.3.1 Molecular regulators of vestibular innervation	23
1.3.2 Molecular regulators of cochlear innervation	24
1.3.2.1 Axon guidance factors regulate afferent innervation to inner hair cells	24
1.3.2.2 Molecular regulators of afferent innervation to the outer hair cells	26
1.4 Significance and study objectives.....	27
CHAPTER 2. MATERIALS AND METHODS	31
2.1 Plasmid design and construction.....	31
2.1.1 Design and construction of tools for <i>Wnt9a</i> knock down.....	31
2.1.1.1 Artificial intron	32
2.1.1.2 RCAS(Y)-siWnt9a.....	34
2.1.1.3 RCAN(X)-siWnt9a	34
2.1.1.4 Tol2-siWnt9a	34
2.1.2 Design and construction of tools for Sema3D overexpression	35
2.1.3 Design and construction of <i>in situ</i> probe DNA templates	37
2.2 Virus preparation and injection.....	41
2.2.1 Virus preparation	41
2.2.2 Virus injection.....	43
2.3 Electroporation.....	44

2.4 Blood vessel infusion.....	46
2.5 Tissue preparation.....	46
2.5.1 Whole mount preparation.....	47
2.5.2 Cryosectioning	47
2.5.3 Perfusion fixation.....	48
2.6 Real-time quantitative polymerase chain reaction.....	48
2.7 RNA deep sequencing	52
2.8 <i>In situ</i> hybridization	52
2.8.1 Making probes for alkaline phosphatase <i>in situ</i> hybridization	53
2.8.2 Alkaline phosphatase <i>in situ</i> hybridization on whole mount tissue.....	54
2.8.3 Alkaline phosphatase <i>in situ</i> hybridization on sectioned tissue.....	54
2.8.4 RNAScope <i>in situ</i> hybridization on sectioned tissue.....	56
2.9 Immunohistochemistry	57
2.9.1 Immunofluorescence.....	57
2.9.2 Chromogenic immunohistochemistry	57
2.10 Efferent labeling	58
2.11 Microscopy	60
CHAPTER 3. WNT9A OVEREXPRESSION AND KNOCKDOWN IN THE CHICKEN BASILAR PAPILLA	61
3.1 Wnt signaling and inner ear development	61
3.2 Knock down of <i>Wnt9a</i> using small-interfering RNA.....	62
3.2.1 Delivery of si <i>Wnt9a</i> using viral-mediated gene transduction.....	63
3.2.2 Delivery of si <i>Wnt9a</i> using tol2 transposase-mediated gene transduction	64
3.3 RNA deep sequencing in <i>Wnt9a</i> -overexpressing BPs.....	65
3.4 Discussion.....	67
3.4.1 si <i>Wnt9a</i> is ineffective to knock down <i>Wnt9a</i> in the chicken inner ear.....	67
3.4.2 RNA deep sequencing identified axon guidance genes downstream of <i>Wnt9a</i>	68
CHAPTER 4. EXPRESSION AND MISEXPRESSION OF SLIT2 LIGAND AND ROUNDOABOUT RECEPTOR	70
4.1 Slit-Robo Signaling and Inner Ear Development	70
4.2 Expansion of Slit2 expression domain in the presence of ectopic <i>Wnt9a</i>	71

4.3 Radial expression of Slit2 and Robos	73
4.4 Misexpression of Slit2 in the CD.....	74
4.5 Misexpression of dominant-negative Robo1 in the CD.....	75
4.6 Discussion.....	76
CHAPTER 5. EXPRESSION OF CONTACTIN-6 IN THE BASILAR PAPILLA	78
5.1 Contactins	78
5.2 Low levels of Cntn6 expression in the chicken inner ear.....	78
5.3 Discussion.....	79
CHAPTER 6. CLASS 3 SEMAPHORINS AND THEIR RECEPTORS IN THE INNER EAR	80
6.1 Semaphorin signaling	80
6.2 Changes in Semaphorin signaling genes in response to <i>Wnt9a</i> overexpression.....	81
6.3 Time course of Semaphorin signaling gene expression in the inner ear	83
6.3.1 Expression results in the cristae, semicircular canals and endolymphatic sac.....	83
6.3.2 Expression results in the saccule, utricle, and vestibular ganglion.....	87
6.3.3 Expression results in the lagena.....	91
6.3.4 Expression results in the cochlear duct and cochlear ganglion.....	94
6.4 Misexpression of Semaphorin3D in the inner ear results.....	98
6.5 Discussion.....	101
6.5.1 Semaphorin3D and Neuropilin2 are downstream of <i>Wnt9a</i>	101
6.5.2 Semaphorin signaling genes in the ganglia suggest role in innervation	101
6.5.3 Semaphorin signaling genes in the hair cells suggest role in synaptogenesis	102
6.5.4 The presence of Semaphorin signaling genes in the mesenchyme suggest a role in endothelial migration	103
6.5.5 Semaphorin signaling genes in the nonsensory epithelium of the cochlear duct may influence boundary formation.....	104
6.5.6 Semaphorin signaling genes in the vestibular dark cells suggest role in producing endolymph and Meniere's disease	105
CHAPTER 7. ANATOMY AND TIMECOURSE OF EFFERENT INNERVATION IN THE BASILAR PAPILLA	107
7.1 Efferent projections from the auditory brainstem to the basilar papilla	107
7.2 Filter implant analysis.....	108

7.2.1 Filter implant approaches.....	108
7.2.2 Filter placement analysis.....	112
7.3 Time course of ipsilateral and contralateral auditory efferents in the BP	115
7.3.1 Ipsilateral auditory efferents at HH stage 37	115
7.3.2 Contralateral auditory efferents at HH stage 37.....	117
7.3.3 Ipsilateral auditory efferents at HH stage 38	119
7.3.4 Contralateral auditory efferents at HH stage 38.....	121
7.3.5 Ipsilateral auditory efferents at HH stage 41	123
7.3.6 Ipsilateral auditory efferents at HH stage 42	125
7.3.7 Ipsilateral auditory efferents at HH stage 43	127
7.4 Tracing auditory projections from the cochlear ganglion to the brainstem.....	129
7.5 Discussion.....	132
7.5.1 Optimal filter implant conditions.....	132
7.5.2 Efferent labeling in the BP and cochlear ganglion	132
7.5.3 Examining populations of efferent cell bodies in the brainstem.....	133
CHAPTER 8. SUMMARY, CONCLUSIONS, AND FUTURE DIRECTIONS.....	135
REFERENCES	138
VITA.....	150
PUBLICATIONS.....	151

LIST OF TABLES

Table 2.1 Target sequences for shRNAs.....	31
Table 2.2 Primers used to amplify the MOEC.....	34
Table 2.3 Primers for site directed mutagenesis of pT2K-CAG-GFP	35
Table 2.4 Primers used for In-Fusion Cloning of RCAS(A)-Sema3D	37
Table 2.5 Primers for amplifying probe template out of cDNA	38
Table 2.6 Retroviral plasmids	42
Table 2.7 Expression plasmids used in electroporation.....	44
Table 2.8 Primer sequences for RT-qPCR.....	50
Table 2.9 DNA Templates for RNA Probe.....	53
Table 6.1 Summary of <i>in situ</i> and immunohistochemistry replicates for uninfected embryos	83
Table 7.1 Summary of filter implants	110
Table 7.2 Summary of filter angle and depth analysis.....	113
Table 8.1 Candidates downstream of <i>Wnt9a</i>	136

LIST OF FIGURES

Figure 1.1 Anatomy of the avian inner ear	20
Figure 1.2 Hypothesis	29
Figure 2.1 Inserting shRNA into expression vectors using Gateway	32
Figure 2.2 RCAS-Sema3D.....	36
Figure 2.3 Sema3D DNA template for <i>in situ</i> probe	39
Figure 2.4 Sema3F DNA template for <i>in situ</i> probe.....	40
Figure 2.5 Cntn6 DNA template for <i>in situ</i> probe	41
Figure 2.6 Electrode placement	45
Figure 2.7 Tissue preparation	47
Figure 2.8 NeuroVue filter implants.....	59
Figure 3.1 <i>Wnt9a</i> knock down using retrovirus to deliver siRNA	64
Figure 3.2 <i>Wnt9a</i> knock down using Tol2-mediated gene transduction	65
Figure 3.3 Differentially expressed axon guidance factors	66
Figure 4.1 Slit activated β -catenin in the BP	71
Figure 4.2 Slit2 expression in the presence of ectopic <i>Wnt9a</i>	72
Figure 4.3 Expression of <i>Slit2</i> , <i>Robo1</i> , and <i>Robo2</i>	73
Figure 4.4 Misexpression of <i>Slit2</i>	75
Figure 4.5 Misexpression of dominant-negative <i>Robo1</i>	76
Figure 5.1 Low levels of <i>Cntn6</i> in <i>Wnt9a</i> -overexpressing and control BPs.....	79
Figure 6.1 Semaphorin3D and <i>Nrp2</i> decrease in the presence of exogenous <i>Wnt9a</i>	82
Figure 6.2 Semaphorin signaling gene expression in the posterior crista.....	85
Figure 6.3 Semaphorin signaling gene expression in the saccule, utricle, and vestibular ganglion	89
Figure 6.4 Semaphorin signaling gene expression in the lagena	92
Figure 6.5 Semaphorin signaling gene expression in the cochlear duct, basilar papilla, and cochlear ganglion.....	96
Figure 6.6 <i>Sema3D</i> misexpression in the sensory epithelium of the utricle.....	99
Figure 6.7 Misexpression of <i>Sema3D</i> in the mesenchyme and cochlear duct.....	100
Figure 7.1 Ipsilateral stage 37 (E11) cochlear ganglion and BP.....	116

Figure 7.2 Contralateral stage 37 (E11) cochlear ganglion and BP.....	118
Figure 7.3 Ipsilateral stage 38 (E12) cochlear ganglion and BP.....	120
Figure 7.4 Contralateral stage 38 (E12) cochlear ganglion and BP.....	122
Figure 7.5 Ipsilateral stage 41 (E15) cochlear ganglion and BP.....	124
Figure 7.6 Ipsilateral stage 42 (E16) cochlear ganglion and BP.....	126
Figure 7.7 Ipsilateral S43 cochlear ganglion and BP.....	128
Figure 7.8 Projections from the cochlear ganglion to the brainstem	130

LIST OF ABBREVIATIONS

ABC	avidin-biotin complex
ABR	auditory brainstem response
ACr	anterior crista
BDNF	brain derived neurotrophic factor
BP	basilar papilla
CD	cochlear duct
cDNA	complementary deoxyribonucleic acid
Celsr	cadherin epidermal growth factor laminin G seven-pass G-type receptor
Cntn6	Contactin-6
CtBP2	C-terminal-binding protein 2
DAB	3, 3'-diaminobenzidine
DAPI	4',6-diamidino-2-phenylindole
DEPC	diethyl pyrocarbonate
DIG	digoxigenin
DNA	deoxyribonucleic acid
dsDNA	double stranded deoxyribonucleic acid
E	embryonic day
EDTA	Ethylenediaminetetraacetic acid
Efna	EphrinA
env	envelope
FBS	fetal bovine serum
Fzd	Frizzled class receptor
gag	group-specific antigen
GFP	Green fluorescent protein
GPI	glycosylphosphatidylinositol
HBS	HEPES buffered saline
HC	hair cell
HH	Hamburger Hamilton stage

HINGS	Heat inactivated goat serum
LCr	lateral crista
LM	lagenar macula
LTR	long terminal repeat
miRNA	microRNA
MOEC	microRNA operon expression cassette
mRNA	messenger RNA
Nrp	Neuropilin
NF	neurofilament
NrCAM	neuronal cell adhesion molecule
NT	neurotrophin
oC	organ of Corti
P	post-natal day
PCR	polymerase chain reaction
PCr	posterior crista
PBS	phosphate buffer saline
PCP	planar-cell polarity
PFA	paraformaldehyde
Plxn	Plexin
pol	polymerase
RCAN	replication-competent avian sarcoma-leukosis virus long terminal repeat no splice acceptor
RCAS	replication-competent avian sarcoma-leukosis virus long terminal repeat with a splice acceptor
RIN	RNA integrity number
RNA	ribonucleic acid
RO	reverse osmosis
Robo	roundabout receptor
RPM	revolutions per minute
Rspo2	roof plate-specific spondin 2
RSV	Rous sarcoma virus

RT-qPCR	real-time quantitative polymerase chain reaction
SC	supporting cell
SA	splice acceptor
Sema	Semaphorin
Ser	Serrate
SD	splice donor
shRNA	short-hairpin RNAs
siRNA	small interfering RNA
SM	saccular macula
SSC	saline-sodium citrate
TBS	Tris-buffered saline
Trk	tyrosine kinase receptor
UM	utricle macula
Vangl	Van Gogh like
Wnt	Wingless/integrated

ABSTRACT

Author: Scott, Mary, K. PhD

Institution: Purdue University

Degree Received: December 2018

Title: Molecular Regulators of Innervation and Patterning in the Developing Chicken Inner Ear

Committee Chair: Donna Fekete

Normal hearing and balance relies on the detection of sound, orientation and acceleration by sensory hair cells (HCs) located in the inner ear. Once sound is detected, that information must be transmitted to the brain by sensory neurons. Damage to the HCs and/or neurons in the auditory or vestibular organs of the inner ear can result in hearing loss or balance disorders. In mammals, these disorders can be permanent, as HCs do not regenerate after damage. While hearing aids and cochlear implants can restore some ability to hear, there are currently no molecular therapies for hearing loss. By examining genes involved in HC development and innervation, basic science can identify candidate genes for potential molecular therapies. This dissertation focuses on molecular regulators involved in establishing and/or maintaining innervation in the chicken inner ear during embryonic development.

The basilar papilla (BP) is the auditory sensory organ in the chicken and is homologous to the mammalian organ of Corti (oC). The BP houses two types of sensory HCs – tall HCs and short HCs. On the neural side of the BP, tall HC receive primarily afferent innervation (neural-side identity). On the abneural side, short HC receive primarily efferent innervation (abneural-side identity). The patterning of these two identities along the radial axis is dependent upon the precise spatiotemporal expression of certain genes during embryonic development. One such gene is *Wingless/integrated (Wnt)9a*.

Previous work has shown that *Wnt9a* is expressed on the neural edge of the BP and is likely secreted in a gradient across the prosensory domain during crucial time points when proliferation, differentiation, and innervation are occurring. When *Wnt9a* was overexpressed, we observed an increase in the width of the BP as well as an expansion of the neural-side identity, likely at the expense of the abneural-side identity. RNA sequencing of *Wnt9a*-overexpressing and control BPs identified genes involved in the Wnt signaling pathway, cytoskeletal remodeling, and axon guidance signaling that were differentially expressed. This dissertation focuses on axon guidance

genes, specifically those involved in Slit/Robo (Roundabout), Contactin (Cntn), and Semaphorin (Sema) signaling, that were differentially expressed in this RNA sequencing data set.

Slits typically act as repulsive cues for neurites expressing Robo receptors. RNA sequencing data indicates that *Slit2* transcripts increased by 1.2 fold when *Wnt9a* was overexpressed. When examining Slit2 spatial expression pattern in *Wnt9a*-overexpressing BPs, we did not observe an upregulation of *Slit2* but rather an expansion of the *Slit2*-expression domain that is likely due to increased proliferation in response to *Wnt9a*. To better understand the role of Slit/Robo signaling in the developing BP, we examined the radial expression patterns of *Slit2*, *Robo1*, and *Robo2*. *Slit2* is expressed on the anterior and posterior walls of the cochlear duct (CD). *Robo1* and *Robo2* had graded expression in the prosensory domain of the BP, highest on the abneural side. *Robo1* is also present in the auditory ganglion. While only a small population of cochleovestibular ganglion neurites have been previously shown to respond to Slits, Slit-Robo has also been shown to activate TCF transcription factor by non-canonically activating β -catenin through Abl kinase. We examined Abl kinase-activated β -catenin in *Slit2*- and *Wnt9a*-overexpressing BPs but did not observe a change in phosphorylated β -catenin. We also overexpressed a dominant-negative Robo1. In some dominant-negative Robo1 overexpressing ears, we observed a reduction in ganglion size; however, this affect did not reliably replicate. These data suggests that Slit-Robo signaling could be involved in neuroblast delamination and/or migration.

RNA sequencing results indicate that *Contactin 6 Cntn6* transcripts increased by 1.5 fold when *Wnt9a* was overexpressed. Contactins are cell adhesion molecules that have been previously shown to impact neurite outgrowth and innervation. In the auditory field, clinical studies have also shown that patients diagnosed with autism who also have mutations in *Cntn5* and *Cntn6* are more likely to exhibit increased sensitivity to sound. Based on RNA sequencing in the embryonic day (E)6 chicken ear, *Cntn6* has low levels of expression in controls. We attempted to examine the spatial expression of *Cntn6* but found that *in situ* hybridization is not sensitive enough to detect low levels of *Cntn6* in control or *Wnt9a*-overexpressing BPs.

Class III Semaphorin secreted ligands are known to repel neurites expressing Neuropilin (Nrp) and/or Plexin (Plxn) receptors. *Sema3D* and *Nrp2* were downregulated in the presence of exogenous *Wnt9a*; however, the spatial expression of these transcripts did not support their role in establishing or maintaining radial innervation patterns. There is, however, a growing body of literature supporting that Sema signaling also has alternative roles in development such as

synaptogenesis, boundary formation, and vasculogenesis. To evaluate these options during inner ear development, we used *in situ* hybridization or immunohistochemistry to map the expression of *Sema3D*, *Sema3F*, *Nrp1*, *Nrp2*, and *PlxnA1* in the chicken inner ear from E5 to E10. The resulting expression patterns in either the otic epithelium or its surrounding mesenchyme suggest that Sema signaling could be involved in each of the varied functions reported for other tissues. *Sema3D* expression flanking the sensory tissue in vestibular organs suggests that it may repel *Nrp2*- and *PlxnA1*-expressing neurites of the vestibular ganglion away from nonsensory epithelia, thus channeling them into the sensory domains at E5-E8. Expression of Sema signaling genes in the sensory hair cells of both the auditory and vestibular organs on E8–E10 may implicate Sema signaling in synaptogenesis. In the nonsensory regions of the cochlea, *Sema3D* in the future tectum vasculosum opposes *Nrp1* and *PlxnA1* in the future cuboidal cells; the abutment of ligand and receptors in adjacent domains may enforce or maintain the boundary between them. In the mesenchyme, *Nrp1* colocalized with capillary-rich tissue. *Sema3D* immediately flanks this *Nrp1*-expressing tissue, suggesting a role in endothelial cell migration towards the inner ear. In summary, Sema signaling may play multiple roles in the developing inner ear.

To better understand innervation patterns in the avian BP, we also examined the developing efferent innervation patterns from E11 to E17 using NeuroVue lipophilic tracer dye. Our data suggest that efferents have already begun to penetrate the sensory epithelium at E11 and that efferents arrive to the ipsilateral BP earlier than the contralateral BP. By E12, many efferents appear to send back branches out to short HCs. At E15, many efferents appear to have reached the abneural edge of the BP, are innervating the hyaline cells, and are projecting apically.

In summary, this work suggests that Slit and Sema signaling are not involved in establishing radial innervation patterns but may have alternative roles in inner ear development. Additionally, while efferents appear to arrive to the ipsilateral BP sooner than the contralateral BP, both ears send projections across the radial axis and back branch around the same time.

CHAPTER 1. INTRODUCTION

1.1 The anatomy of the avian inner ear

1.1.1 The vestibular system

The avian inner ear houses two systems: the vestibular system and the auditory system. The vestibular system is responsible for detecting orientation and angular acceleration in the head and consists of seven sensory organs: three cristae (anterior, lateral, and posterior) and four maculae (utricle, neglecta, saccular, and lagenar). Each of the cristae are located within the ampulla at the base of the semicircular canals. The utricular macula (UM), macula neglecta, and saccular macula (SM) are located in the vestibular compartment. The lagenar macula (LM) is located at the distal tip of the cochlear duct (CD) (Fig. 1.1 A). The detection of sensory information in each of these vestibular organs is reliant upon mechanosensory hair cells (HCs) that are innervated by neurites from the vestibular ganglion, a component in the eighth cranial ganglion (Lewis *et al.*, 1985).

1.1.2 The auditory system

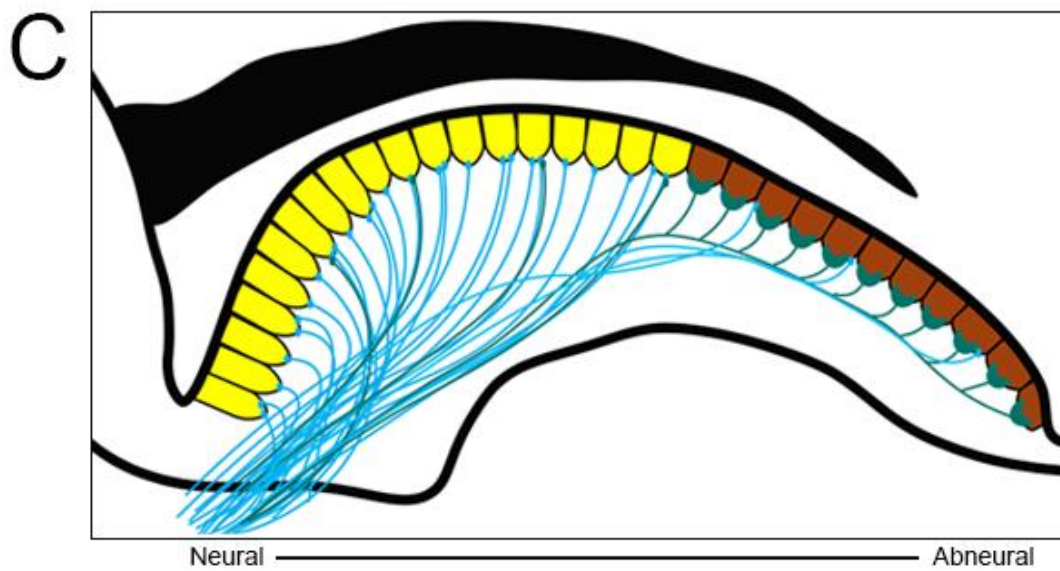
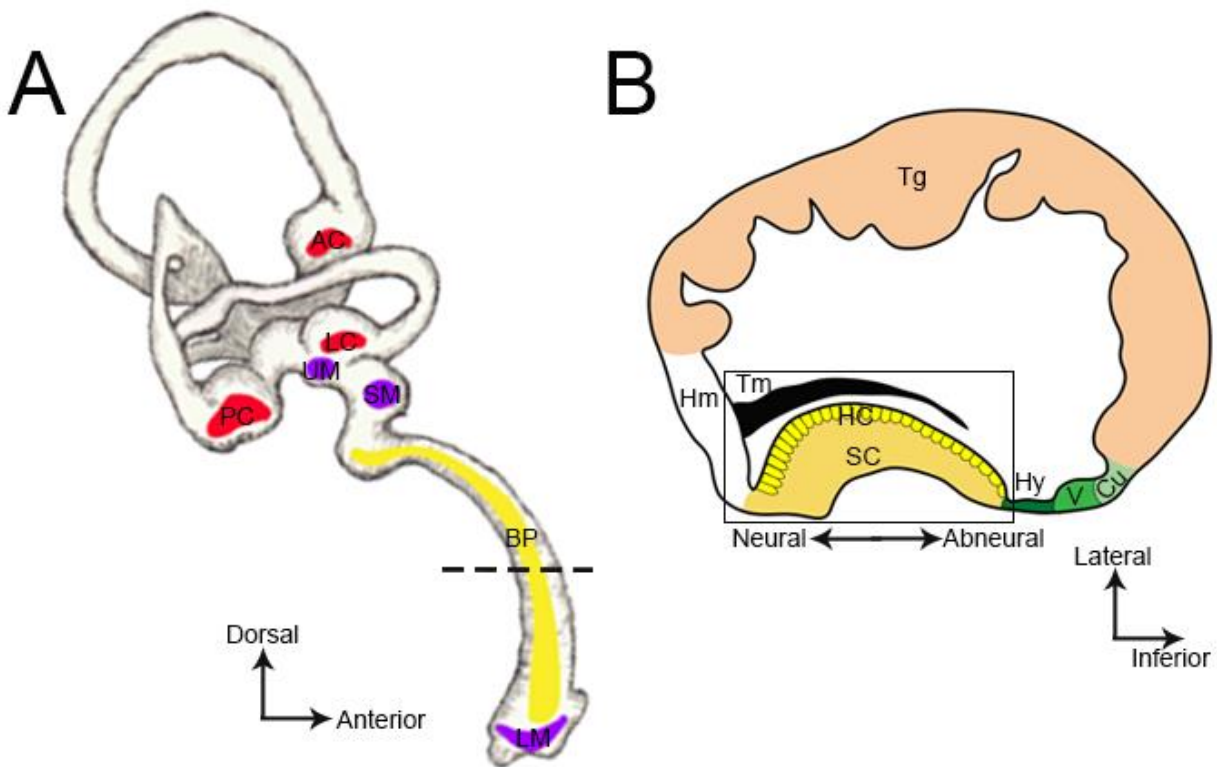
The auditory system is responsible for detecting sound and consists of a single organ: the basilar papilla (BP). Located within the CD, the avian BP is homologous to the mammalian organ of Corti (oC) (Fig. 1.1 A). Much like the vestibular organs, the detection of sensory information is dependent upon mechanosensory HCs innervated by neurites from a subset of neurons in the eighth cranial ganglion referred to as the cochlear ganglion which is homologous to the mammalian spiral ganglion. Along the radial axis of the BP, hair cells are organized in a single row above the nuclei of the supporting cells (SCs) (Fig. 1.1 B). On the neural side of the radial axis, tall HCs (homologous to mammalian inner HCs) are primarily innervated by afferent neurons (neural-side identity). On the abneural side, short HCs (homologous to mammalian outer HCs) are primarily innervated by efferent neurons (abneural-side identity) (Fig. 1.1 C) (Lewis *et al.*, 1985; Takasaka & Smith, 1971; Tanaka & Smith, 1978).

1.1.3 Nonsensory domains of the cochlear duct

In addition to the sensory domain, the CD is made up of several nonsensory tissue domains that also play essential roles in the detection of sound. On the superior edge of the avian CD, homogeneous cells anchor the tectorial membrane (Fig. 1.1 B) (Chandler, 1984; Tanaka & Smith, 1978). While the precise function of the tectorial membrane has been controversial, it has been suggested that it is important in enhancing cochlear amplification (Goodyear & Richardson, 2018). The lateral wall of the CD makes up the tegmentum vasculosum (Fig. 1.1 B), the presumed homolog of the mammalian stria vascularis (Cotanche & Sulik, 1982; Ishiyama *et al.*, 1970). This nonsensory tissue domain is responsible for maintaining the ionic composition of the endolymph and thus is important for maintaining endocochlear potential (Kuijpers, 1970; Schneider *et al.*, 1987). On the inferior edge of the CD, hyaline cells, vacuole cell, and cuboidal cells are located (Fig. 1.1 B) (Oesterle *et al.*, 1992). Hyaline cells contain contractile actin, myosin, and α -actinin proteins and are innervated by efferent neurons, suggesting that these cells play a role in modulating the stiffness of the basilar membrane (Cotanche *et al.*, 1992; Drenckhahn *et al.*, 1991; Oesterle *et al.*, 1992). Gap junctions present in the hyaline and cuboidal cells suggest another role in transporting recycled potassium back to the tegmentum vasculosum for endolymph maintenance (Nickel *et al.*, 2006).

Figure 1.1 Anatomy of the avian inner ear

(A) A diagram of a mature chicken inner ear highlights the vestibular and auditory compartments. The vestibular cristae are in red and the maculae are in purple. The auditory BP is shown in yellow. The dashed line depicts the location of the cross section through the CD shown in (B). This cross section represents the distinct nonsensory and sensory tissue domains of the CD. The nonsensory domain at the superior edge of the CD (white) consists of homogeneous (Hm) cells anchoring the tectorial membrane (Tm). The nonsensory domain at the inferior edge of the CD (green) consists of hyaline (Hy) cells (dark green), vacuole (V) cells (medium green), and cuboidal (Cu) cells (pale green). The tegmentum vasculosum (Tg) (peach) makes up the lateral wall of the CD. The sensory domain (yellow) consists of a single row of HCs (bright yellow) and SCs (dark yellow). (C) A close up of the sensory domain depicts two distinct HC identities that are organized along the radial axis (neural to abneural). The neural-side identity consists of tall HCs (yellow) which are primarily innervated by afferent neurons (light blue). The abneural-side identity consists of short HCs (brown) that are primarily innervated by efferent neurons (dark teal).



1.2 Chicken inner ear development and innervation

The inner ear arises from the otic placode. At embryonic day (E)2 (HH 12) the placode begins to invaginate to form the otic cup, and at HH 16-17 the otic cup closes to form the otocyst (Hemond & Morest, 1991; Meier, 1978). From the otocyst, the membranous labyrinth forms and the vestibular and auditory compartments of the inner ear begin to form at E4. For the various vestibular organs, the prosensory patches emerge from E3 (HH19) to E6 (HH29) (Knowlton, 1967). The prosensory domain of the auditory BP emerges at E4 (HH 23) (Wu & Oh, 1996). On E8 the pool of progenitor cells that make up the prosensory domain of the BP differentiate into SCs and HCs and on E11 HCs begin to differentiate into tall HCs and short HCs (Cohen & Cotanche, 1992; Cohen & Fermin, 1978).

As the otic epithelium develops, the cochleovestibular ganglion is formed. At E2-3.5 (HH 13-21) neuroblasts delaminate and migrate medially from the otic epithelium. These neuroblasts give rise to the neurons of the cochleovestibular ganglion (Adam *et al.*, 1998; Carney & Couve, 1989; D'Amico-Martel & Noden, 1983; Hemond & Morest, 1991). At E4 and E6, neurites from the cochleovestibular ganglion extend out toward the vestibular and auditory organs, respectively (Von Bartheld *et al.*, 1991; Whitehead & Morest, 1985b). For the vestibular organs, afferents synapse onto HCs at E6 and efferents at E10 (Ginzberg & Gilula, 1980; Meza & Hinojosa, 1987). In the BP, afferents begin to form synapses with HCs at E9 and efferents at E14 (Rebillard & Pujol, 1983; Whitehead & Morest, 1985b). Efferent innervation is described in detail in chapter 7.

1.3 Molecular regulators of innervation in the inner ear

A version of this chapter section has been accepted for publication in *Synapse*:

Coate, T. M., **Scott, M. K.**, Gurjar, M. C. (2018). Current concepts in cochlear ribbon synapse formation: a view from the postsynaptic side.

The development of the neural- and abneural-side identities and their innervation patterns has been a topic of recent interest. The expression of many axon guidance factors has been reported in the developing inner ear and cochleovestibular ganglion. Many of these axon guidance factors are poised to influence innervation and development of cochleovestibular ganglion neurites (Coate &

Kelley, 2013). Some of these axon guidance factors have been studied in bird or mammal for their influence on innervation patterns in the inner ear.

1.3.1 Molecular regulators of vestibular innervation

Axon guidance factors have been previously investigated for their roles in innervation of the inner ear. The neurotrophins are one such set of factors that have been shown to impact innervation of vestibular sensory organs in the mouse. Specifically, this includes brain-derived neurotrophic factor (BDNF) and neurotrophin (NT)-3 and their tyrosine kinase (Trk) receptors. In the mouse, BDNF and NT-3 are expressed in the vestibular organs while NT-3 is expressed in the auditory organ. The cochleovestibular ganglion neurons express both TrkB and TrkC receptors (Farinas *et al.*, 2001). While much of the work examining the roles of these neurotrophins in the inner ear strongly supported their importance in neuron survival, their role in axon pathfinding was initially unclear (Agerman *et al.*, 2003; Coppola *et al.*, 2001; Ernfors *et al.*, 1995).

To further examine the role of neurotrophins in axon guidance, Tessarollo and colleagues used endogenous BDNF null mice where BDNF was misexpressed under NT-3 promoter control (*NT-3^{tgBDNF}; BDNF^{-/-}*). In these mice at E13.5, vestibular afferents projected towards the posterior crista (PCr) but failed to reach it. These vestibular afferents extended in multiple directions or sent aberrant projections to the base of the cochlea. In some cases, some fibers from the SM projected to the base of the cochlea as well. Additionally, the lateral crista (LCr) and anterior crista (ACr) received more projections than wildtype mice. At birth, these mice also showed aberrant projections extending beyond the sensory epithelium of the vestibular organs where low levels of NT-3 are typically expressed. These data suggest that the appropriate expression patterns of NT-3 and BDNF are essential for proper innervation of the vestibular organs and may prevent vestibular afferents from projecting to the cochlea (Tessarollo *et al.*, 2004).

Another group of molecular regulators of vestibular innervation are the class 3 Semaphorin (Sema) secreted ligands and their Neuropilin (Nrp) receptors. Gu and colleagues created a knock in mouse for a Nrp1 receptor insensitive to Sema3. In these mice, aberrant projections were observed in the vestibular compartment. These defects included: 1) projections running from the ACr and LCr; 2) projections extending beyond the vestibular compartment to project into the superficial skin; 3) projections extending from the UM to the PCr; and 4) projections looping around the base of the cochlea (Gu *et al.*, 2003). Sema3E is expressed in the semicircular canals

(Miyazaki *et al.*, 1999) and plexin (Plxn) A1 and PlxnA3 are expressed in the cochleovestibular ganglion (Murakami *et al.*, 2001). It is possible that Sema3E repels Plxn and Nrp expressing vestibular ganglion neurites from the canals, preventing them from projecting into the skin; however, further investigation is required to determine the specific ligands and coreceptors that interact with Nrp1.

Another example of a molecular regulator of vestibular innervation can be found in the chicken embryo. A detailed survey of the expression of Slits (secreted repulsive cue) and their transmembrane receptors, roundabouts (Robos) indicated that *Slit/Robo* expression is poised to influence innervation of the inner ear. Specifically, *Slit2* flanks the innervated sensory domain of the three cristae at HH 25-37 while *Robo1* is expressed in the vestibular ganglion. Additionally, when projection towards the cristae begins (HH17), *Robo2* was expressed in the cochleovestibular ganglion while *Slit1* and *Slit2* were expressed in the medial otic epithelium (Battisti & Fekete, 2008). To explore their function, Slit1 and Slit2 were misexpressed in the cristae by electroporating plasmids carrying myc-tagged human SLIT1 or SLIT2 genes into the otocyst at HH15-18. When either Slit1 or Slit2 were misexpressed, fewer neurites were observed innervating the ACr; however, neurites were unresponsive to ectopic Slits in the PCr. Based on these results, the authors proposed a model by which ACr afferents are prevented from projecting posteriorly by Slits expressed in the medial otic epithelium. PCr afferents, unresponsive to the Slit, pass the Slit-expressing otic epithelium to project posteriorly (Battisti *et al.*, 2014).

1.3.2 Molecular regulators of cochlear innervation

1.3.2.1 Axon guidance factors regulate afferent innervation to inner hair cells

Classic axon guidance factors that influence radial innervation of the mammalian oC include EphrinA (Efna)5, a membrane-bound ligand, and one of its receptors, EphA4. During periods of innervation and refinement in the oC, EphA4 is expressed by type I afferents that project to the inner HCs while Efna5 is expressed by the outer HCs as well as a subset of type I afferents. To investigate the impact of EphA4/Efna5 signaling on radial innervation, Defourny and colleagues examined Efna5^{-/-} cochleae and found they exhibited increased numbers of peripherin-negative (type I) fibers and decreased numbers of peripherin-positive (type II afferents that project to the outer HCs) fibers at post-natal day (P)14 (Defourny *et al.*, 2013). Complementing this, Efna5^{-/-}

cochleae, compared with wild type controls, showed fewer presynaptic inner HC ribbon bodies and proportionally higher outer HC ribbon bodies. This radial shift of afferent innervation to the outer HCs is maintained in three-month-old *Efna5*^{-/-} mice and was accompanied by reduced peak 1 amplitudes in response to subthreshold click stimuli in auditory brainstem responses (ABRs) (Defourny *et al.*, 2013). Similar effects were observed in the ABRs of *EphA4*^{-/-} mice (Miko *et al.*, 2008), further supporting that *EphA4* is acting as the receptor for *Efna5*. These data support a model in which *EphA4* on the plasma membrane of the growth cones of type I afferents are repelled by *Efna5* present on the surface of outer HCs. This model is further supported by growth cone collapse assays in which the size of growth cones in type I afferents was reduced when cultured in the presence of *Efna5*, while type II afferent growth cones were unchanged relative to controls (Defourny *et al.*, 2013).

Another classic axon guidance factor shown to impact radial innervation in the mouse oC is the secreted ligand *Sema3F* and its receptor, *Nrp2*. *Sema3F* is expressed in the lateral compartment of the oC which houses the outer HCs. *Nrp2* localizes to type I and type II afferents during periods of HC innervation. To test the hypothesis that *Sema3F* in the lateral compartment inhibits type I projections to the outer HCs, Coate and colleagues examined peripheral afferent fibers in *Nrp2*^{-/-}, *Nrp2*^{+/-}, and *Sema3f*^{-/-} mice. Compared to wildtype, *Nrp*^{-/-}, *Nrp*^{+/-}, and *Sema3f*^{-/-} mice (in some cases mutant mice were crossed with *Neurog1*^{CreERT2}; *R26R*^{tdTom} to visualize a subset of afferents) showed ectopic projections to the outer HCs by P0. Interestingly, and in contrast with the *Efna5*/*EphA4* work mentioned above, both *Nrp2*^{+/-} and *Sema3f*^{-/-} cochleae showed no significant differences in numbers of ribbon bodies, ABRs, or numbers of type II projections (Coate *et al.*, 2015). The authors speculated that early innervation errors could be corrected by synaptic pruning events, which normally occur after birth.

Given that *EphA4* and *Efna5* have been shown to inhibit type I innervation of the outer HCs and that those effects are maintained at older ages (P14 and 3 months; Defourny *et al.* 2013), one possibility is that these other molecules are able to correct the innervation errors in the *Nrp2*^{+/-} and *Sema3f*^{-/-} mice. These data support a model whereby *Nrp2*-expressing type I afferents are repelled from the *Sema3F*-expressing lateral compartment and then preferentially innervate inner HCs. Interestingly, type II afferents also express *Nrp2*, yet they still project into the lateral compartment. Given how *Nrps* form receptor complexes with various co-receptors and the composition of these complexes can impact the resulting intracellular signaling events and function (Zhou *et al.*, 2008),

one possible explanation is that a Nrp2 co-receptor is expressed by type I afferents, but not by the type II. While one candidate co-receptor, neuronal cell adhesion molecule (NrCAM), has already been ruled out (Harley *et al.*, 2018), other co-receptors such as Plexin (Plxn)A1 and PlxnA3 are indeed expressed by the spiral ganglion neurons (Coate *et al.*, 2015; Katayama *et al.*, 2013; Murakami *et al.*, 2001) and remain candidate co-receptors. PlxnA3 protein was shown to be enriched in type I afferents (Coate *et al.*, 2015), but functional studies remain to be performed.

1.3.2.2 Molecular regulators of afferent innervation to the outer hair cells

While guidance molecules (summarized above) have been identified that restrict a subset of afferents (type I in mouse) to the medial side of the oC, less is known about the molecular cues that regulate the projections of type II afferents. Whereas type I afferents project to the inner HCs, type II afferents must project past the tunnel of Corti to the lateral compartment and do so starting around E15.5 in mouse. At E16.5, the type II spiral ganglion neurons make a 90° turn and begin projecting toward the base of the cochlea. As these fibers continue to project toward the base, they track along the basal surface of a row of outer HCs and send branches to outer HCs to synapse with them. One type II fiber can form synapses with at least 10-15 outer HCs (Berglund & Ryugo, 1987; Koundakjian *et al.*, 2007) and it has been estimated the initiation of an action potential in a type II afferent requires transmitter release by at least six outer HCs (Weisz *et al.*, 2014).

Recently, it was discovered by Ghimire and colleagues that planar cell polarity (PCP) proteins are involved in this curious turning of the type II spiral ganglion neurons. Van Gogh like (VANGL2) and other PCP proteins, frizzled class receptor (Fzd)3, cadherin epidermal growth factor laminin G seven-pass G-type receptor (Celsr)1, and Celsr3 are expressed by spiral ganglion neurons, SCs, and HCs. High-resolution imaging indicates VANGL2 localizes to the basolateral walls of the SCs. *Vangl2*^{-/-}, *Frzd3*^{-/-}, and *Celsr1*^{-/-} mice all showed type II turning errors relative to littermate controls. Through an elegant series of conditional knockout models, the authors demonstrated VANGL2 operates non-autonomously: loss of *Vangl2* in SCs causes turning errors, whereas loss of *Vangl2* in spiral ganglion neurons does not (Ghimire *et al.*, 2018).

Based on these results, the authors suggested two alternative models. In a “direct” model, *Frzd3*-expressing growth cones encounter VANGL2 on the basolateral wall of the inner pillar cell, which stabilizes that side of the growth cone and steers it toward the base. In an “indirect” model, the authors suggest classic axon guidance mechanisms (repulsion, attraction, or a combination of

the two) could act downstream of VANGL2 and channel axon growth toward the base (Ghimire *et al.*, 2018).

Another regulator of type II projection and innervation is the homeobox gene *Prox1*. *Prox1* expression has been reported in the developing inner ear of several species including zebrafish (Glasgow & Tomarev, 1998), chicken (Stone *et al.*, 2003), and mouse (Birmingham-McDonogh *et al.*, 2006). In the mouse oC, *Prox1* is expressed in the SCs and in the outer HCs as early as E14.5 and continues through E17.5. At E17.5 *Prox1* is also detected in the spiral ganglion neurons. Fritzsich and colleagues conditionally knocked out *Prox1* using *Prox1^{flox/flox}; Tg(Pax-Cre)* and *Prox1^{flox/flox}; Tg(Nes-Cre)* mice. In both these strains, type II afferents extend past the tunnel of Corti but then turn randomly towards the apex or base of the cochlea. In the *Prox1^{flox/flox}; Tg(Nes-Cre)* mice, *Prox1* expression is abolished in the spiral ganglion neurons but continues to be expressed in the SCs and outer HCs. Given that similar type II turning defects were observed in both strains, this suggests that type II turning is not dependent upon *Prox1* in the SCs or HCs but is dependent upon its expression in the spiral ganglion neurons (Fritzsich *et al.*, 2010).

Another factor that impacts type II innervation is roof plate-specific spondin (*Rspo2*). *Rspo2* is a secreted protein that positively regulates canonical Wnt signaling (Kim *et al.*, 2008). In the developing cochlea at E14.5 through P0 *Rspo2* is expressed in the medial nonsensory tissue (greater epithelial ridge). When Mulvaney and colleagues examined *Rspo2* null mice at E18.5, they found only a few type II fibers turning abnormally turning towards the apex with most type II fibers turning towards the base; however, fibers entering at the base of the cochlea had not bundled into three distinct tracts. At this timepoint, the fibers at the base looked similar to the fibers at the less developed mid base in control animals, suggesting a possible developmental delay in type II afferent organization. The type II fibers were also disorganized relative to controls in the mid base and apex as well. It is also important to note that the *Rspo2* null mice also had an extra row of outer HCs and it is possible that type II disorganization is a secondary effect of the extra row of outer HCs (Mulvaney *et al.*, 2013).

1.4 Significance and study objectives

In the mammalian inner ear, damaged HCs cannot regenerate. This damage leads to hearing loss. Molecular therapies are currently being tested for their ability to induce regeneration of HCs (Devarajan *et al.*, 2013; Maiorana & Staecker, 2005). One strategy for identifying candidate genes

for molecular therapies is to identify and study genes involved in HC development and innervation. Genes identified during development provide a foundation for future HC regeneration studies which has the potential to lead to treatments for hair cells loss and damage. The objectives of this dissertation primarily focus on identifying and examining the molecular regulators that are necessary to establish and/or maintain appropriate innervation of HCs in the inner ear.

Once such gene that influences innervation is *Wnt9a*. *Wnt9a* transcripts are endogenously expressed on the neural edge of the BP (Sienknecht & Fekete, 2008). Data from Dr. Donna Fekete's lab supported that when *Wnt9a* is overexpressed across the radial axis, an increase in cells taking on the neural-side identity at the expense of the abneural-side identity occurs (Fig. 1.2 A). In this abneural-to-neural conversion, the following are observed: 1) an increase in the width of the BP; 2) an increase in tall HC numbers; 3) an increase in afferent innervation; and 4) disruption of efferent arrangement (Fig. 1.2) (Munnamalai *et al.*, 2017).

Based on these data, we hypothesized that *Wnt9a* was instructive for HCs to take on the neural-side identity by influencing proliferation, differentiation, and axon guidance through downstream effectors. This hypothesis was examined with the following objectives: 1) complement the *Wnt9a* overexpression experiments with *Wnt9a* knock-down experiments using shRNA (Fig. 1.2 C, right column); 2) identify genes acting downstream of *Wnt9a* using ribonucleic acid (RNA) deep sequencing to compare the transcriptomes of control and *Wnt9a*-overexpressing BPs (fig. 1.2 C, middle row); 3) determine if axon guidance factors identified by RNA sequencing are asymmetrically expressed and influence radial innervation patterns. Given that the timing and targets (short HCs or tall HCs) of ipsilateral and contralateral efferent projections to the BP are poorly understood in birds, an additional objective was to describe ipsilateral and contralateral efferent projections at various time points.

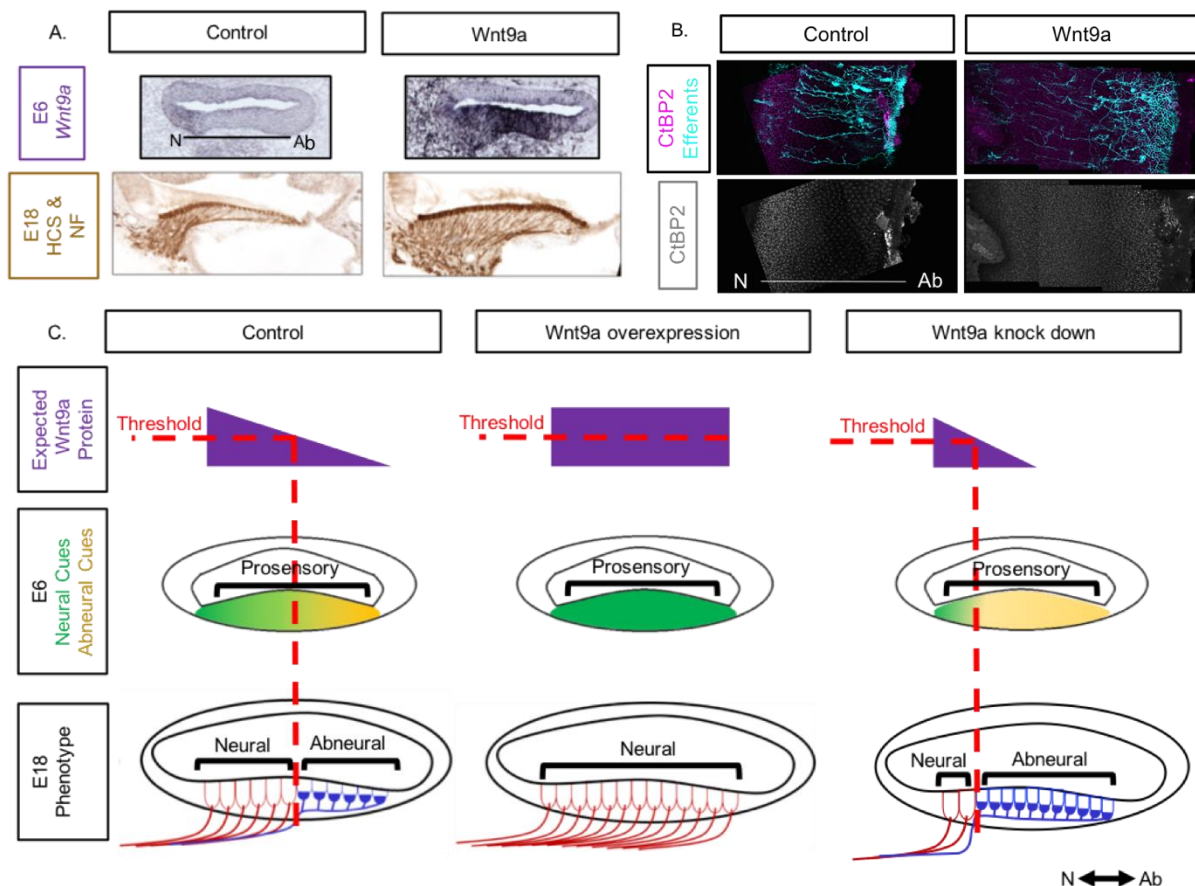


Figure 1.2 Hypothesis

(A) E6 cross sections were labeled for *Wnt9a* transcripts (top) while E18 cross sections were labeled for hair cells (with HCS antibody) and Neurofilament (NF) (bottom) in control and *Wnt9a* overexpressing BPs. When *Wnt9a* is overexpressed, an increase in cells taking on the neural-side identity (tall HCs innervated by afferents) as well as an increase in the width of the BP. Supporting this, (B) we see an increase in afferent pre-synaptic components shown by the C-terminal-binding protein 2 (CtBP2, magenta) immunolabel. We additionally see a disruption of the arrangement of efferents (cyan) labeled with lipophilic tracer dye. Based on this evidence, (C) we hypothesized that *Wnt9a* promotes the neural side identity (red, tall HC and afferents, bottom row). The expected protein gradients for *Wnt9a* are shown in top row (purple). We predicted that axon guidance factors attractive to afferents or repulsive to efferents would be present on the neural side of the BP (green). We expected that these factors would increase in the presence of exogenous *Wnt9a* and decrease when *Wnt9a* is knocked down. Additionally, we predicted that axon guidance factors that are repulsive to afferents or attractive to efferents would be expressed on the abneural side (yellow). It was expected that these factors would decrease when *Wnt9a* was overexpressed and increase when *Wnt9a* was knocked down. The data in A and B have been published in Munnamalai *et al.* (2017).

The findings of these objectives are described in detail in chapters 3-7 of this dissertation. Briefly, one main finding of this dissertation is that shRNA is an ineffective method of knocking down transcripts in the chicken cochlea at the desired times and places. Additionally, axon guidance factors, *Slit2* and *Sema3D*, as well as cell-adhesion molecule, Contactin-6 (*Cntn6*), are differentially expressed in control and *Wnt9a*-overexpressing BPs but they likely have alternative functions other than, or in addition to, axon guidance in the inner ear.

CHAPTER 2. MATERIALS AND METHODS

2.1 Plasmid design and construction

2.1.1 Design and construction of tools for *Wnt9a* knock down

To complement *Wnt9a*-overexpression experiments in the chicken BP previously done by the Fekete lab, three small interfering RNAs (siRNAs) were designed and constructed by Qing Zhou and Donna Fekete to knock down *Wnt9a*. Each of the three siRNAs targeted a unique coding region in the *Wnt9a* transcript (Table. 2.1). These siRNAs are referred to as si*Wnt9a*-1, si*Wnt9a*-2, and si*Wnt9a*-3 throughout this dissertation. The siRNA targets were selected using the Biotechnology and Biological Sciences Research Council's ChickEST Database (http://www.chick.manchester.ac.uk/cgi-bin/chickEST.cgi?show_assembled_seq=037781.1). Each of these siRNAs had previously been inserted into a microRNA (miRNA) operon expression cassette (MOEC) that folds into a short-hairpin RNA (shRNA). This MOEC has been previously described by Das *et al.* (2006) (Fig. 2.1 A). This chapter section (2.1.1) and figure 2.1 describe the insertion of the shRNA into an artificial intron and the subsequent insertion of that resulting artificial intron into several delivery vectors.

Table 2.1 Target sequences for shRNAs

siRNA	Target Sequence
si <i>Wnt9a</i> -1	5'-AAGGACTACGGATCTTGTCTA-3'
si <i>Wnt9a</i> -2	5'-AAGAGAGGTTTCAAGGAGACG-3'
si <i>Wnt9a</i> -3	5'-AAGCTATGTTGAGACATAAGC-3'

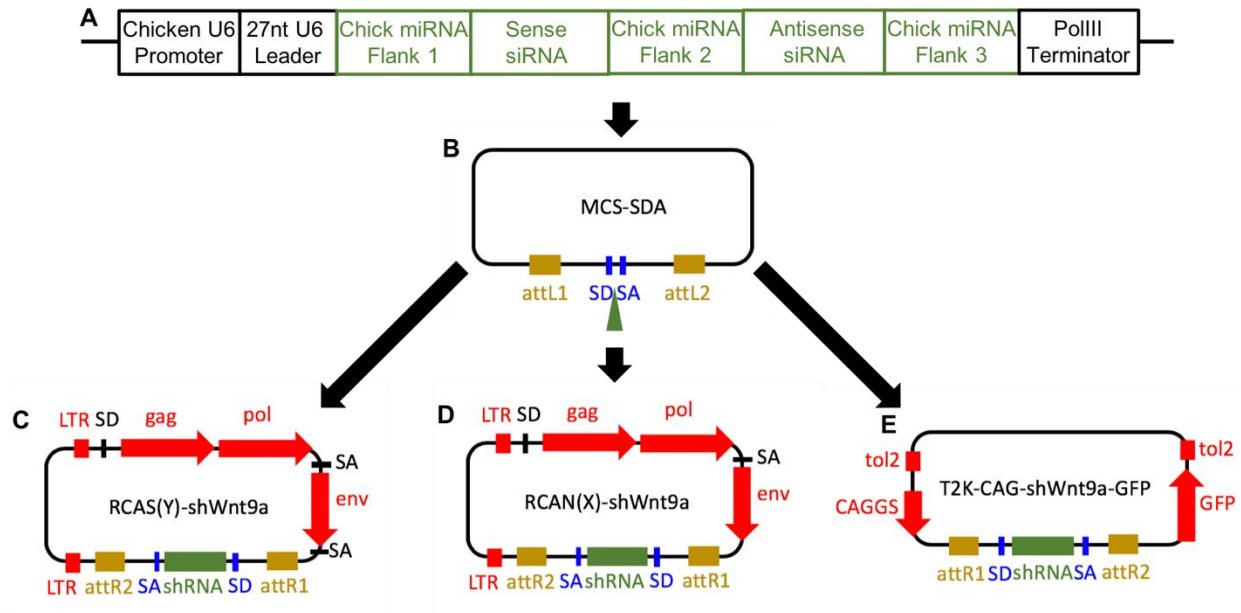


Figure 2.1 Inserting shRNA into expression vectors using Gateway

(A) The MOEC contains the short-hairpin sequence and carries the *siWnt9a* sequence at the siRNA insertion site. The MOEC was truncated at the U6 promoter and Polymerase (pol) III terminator before it was inserted into the shuttle vector. The shRNA (A, green) was inserted into the shuttle vector (B, MCS-SDA) in between the splice donor (SD) and slice acceptor (SA) sites (blue). Gateway compatible sites (attL1 and attL2, yellow) allowed for the insertion of the SD/SA flanked shRNA into the expression vectors via Gateway recombination. (C) The RCAS(Y) retroviral vector contains the long terminal repeats (LTR, red) which drives the expression of the group-specific antigen (gag), pol, and envelope (env) viral genes (red) as well as the expression the inserted shRNA (green). Gateway recombination occurs at the Gateway sites (attR1 and attR2, yellow). Similar to RCAS(Y), (D) RCAN(X) retroviral vector contains viral sequences and shRNA genes driven by LTR and recombination occurs at the Gateway sites. Unlike RCAS(Y), RCAN(X) does not have a SA occurring after the env sequence. (E) The Tol2 (T2K) vector contains Tol2 sites (red) that facilitate the transposase-mediated integration into the subjects genome. A green fluorescent protein (GFP) reporter (red) and the shRNA are driven by the CAG β -actin promoter (CAGGS, red). Similar to the viral vectors, Gateway recombination occurs at the Gateway sites.

2.1.1.1 Artificial intron

The MCS-SDA shuttle vector (Fig. 2.1 B) contains splice donor (SD) and a slice acceptor (SA) sites. The vector was used to insert the shRNA into this artificial intron which has been previously used to express miRNAs (Stoller *et al.*, 2013; Zhang *et al.*, 2015) in the chicken inner ear. We expect that the hairpin created by the shRNA is processed into a siRNA that is antisense to a unique region of the *Wnt9a* transcript by the miRNA processing machinery.

The siRNAs has been previously inserted into the RFPRNAiC plasmid containing the MOEC used by Das *et al.* (2006) by Qing Zhou (Fekete lab rotation student). To ensure that the U6 promoter in the MOEC did not interfere with transcription via the promoters present in the expression plasmids (Fig. 2.1 C-E), the MOEC was truncated after the U6 promoter and before the PolIII terminator, and the sequences in between were retained (Fig. 2.1 A). Polymerase chain reaction (PCR) was used to amplify the MOEC sequence containing the *siWnt9as* out of the RFPRNAiC plasmid. The primers were designed to avoid including the U6 promoter or the Polymerase (pol) III terminator and to add a XhoI site at both the 5' and 3' ends. The PCR was run using a Phusion® High Fidelity deoxyribonucleic acid (DNA) polymerase kit (New England BioLabs). The resulting PCR product for each shRNA was inserted into the MSC-SDA shuttle vector.

To insert the amplified shRNAs into the shuttle vector, the shuttle vector was cut at the XhoI site in between the SD and SA sites. Calf Intestinal Alkaline Phosphatase (Invitrogen) was used to remove 5' phosphatases from the cut shuttle vector. The shRNA was ligated into the shuttle vector using T4 DNA ligase kit and protocol (New England BioLabs). Using this method, *shWnt9a-3* was successfully inserted into the artificial intron; however, multiple attempts for *shWnt9a-1* and *shWnt9a-2* resulted in insertion into the artificial intron in the incorrect orientation. For these shRNAs, In-Fusion (ClonTech®) cloning was used to insert them into the artificial intron.

Primers for In-Fusion cloning were designed using the guidelines in the In-Fusion cloning manual. Briefly, the 3' end of the primers were specific to the ends of the MOEC to be amplified. Similar to previous attempts, the primers were designed to amplify the fragment of the MOEC after the U6 promoter and before the PolIII terminator. The 5' end of the primers consisted of 15 or more bases homologous to the insertion site in the MCS-SDA plasmid and would be used in the In-Fusion reaction to insert the amplified fragment into the plasmid. Full length In-Fusion primers are listed in Table 2.2. A Phusion® High Fidelity DNA polymerase kit (New England BioLabs) and PCR protocol were used to amplify the shRNAs out of the RFPRNAiC plasmid. To insert the resulting PCR fragment into the artificial intron in the shuttle vector, the In-Fusion reaction was done using the In-Fusion kit and protocol (ClonTech®).

Table 2.2 Primers used to amplify the MOEC

Primer Name	Primer Sequence
RFPRNAic_NoU6_Xho_F	5'-GCCTCGAGGTACCATAAAGTGC GTCCC-3'
RFPRNAic_NoU6_Xho_R	5'-CGCTCGAGCTTACCGTGCTGACAACCG-3'
MCS_MOEC_InFusion_F	5'-TAATCTAGAGGATCCCTCGAGAGGTACCATAAAGTG CGTCCCGGCT-3'
MCS_MOEC_InFusion_R	5'-AGGTACCAGTTAGTACTCGAGAGCTTACCGTGCTGA CAACCGCA-3'

2.1.1.2 RCAS(Y)-*siWnt9a*

The RCAS(Y) (replication-competent avian sarcoma-leukosis virus long terminal repeat with a splice acceptor) retroviral plasmid has Gateway compatible sites to facilitate cloning from a Gateway shuttle vector (Loftus *et al.*, 2001) (Fig. 2.1 C). In this plasmid, transcription of inserted genes and of the viral genes group-specific antigen (gag), pol, and envelope (env) are driven by the strong promoter in the 5' viral long terminal repeats (LTRs) and processed through the spliced message. Gateway recombination using a Gateway LR Clonase II kit was done to insert the artificial intron containing the *shWnt9a* from the shuttle plasmid into the RCAS(Y) plasmid.

2.1.1.3 RCAN(X)-*siWnt9a*

RCAN(X) (replication-competent avian sarcoma-leukosis virus long terminal repeat no splice acceptor) is also an avian retroviral vector; however, it does not have the extra envelope splice acceptor site that RCAS(Y) has. This plasmid also contains Gateway recombination sites and was kindly provided by Sheri Holmen (Van Andel Research Institute) (Bromberg-White *et al.*, 2004). Gateway recombination was done using a Gateway LR Clonase II kit to insert the artificial intron containing shRNAs into the RCAN(X) and was performed by Ankita Thawani (Fekete Laboratory).

2.1.1.4 *Tol2-siWnt9a*

The pT2K-CAG-EGFP plasmid has been previously used by our lab to express miRNAs in the chicken inner ear (Zhang *et al.*, 2015). It and its transposase plasmid (p-CAG-T2TP) were kindly

provided by Yoshiko Takahashi (University of Tokyo, Japan). The Tol2 vector, when used in conjunction with the p-CAG-T2TP plasmid, uses transposable elements to integrate inserted genes and a green fluorescent protein (GFP) reporter flanked by Tol2 sites into the host genome (Kawakami, 2007).

This plasmid was not originally Gateway compatible and a Gateway cassette was inserted using an XbaI site upstream of GFP. Before this could be done, a second XbaI site in the backbone was removed using a QuickChange II XL site directed mutagenesis kit (Agilent). Primers for this procedure were designed to mutate the XbaI sequence from 5'-TCTAGA-3' to 5'-TCCAGA-3' and full primer sequences can be found in Table 2.3.

Table 2.3 Primers for site directed mutagenesis of pT2K-CAG-GFP

Primer Name	Primer Sequence
pT2K-CAG-GFP-t98c_as	5'-GTGGCGGCCGCTCTGGAACTAGTGGATCTG-3'
pT2K-CAG-FP-t98c	5'-CAGATCCACTAGTTCCAGAGCGGCCGCCAC-3'

To insert the Gateway cassette into pT2K-CAG-GFP, the plasmid was cut with XbaI and the ends of the vector were blunted using a Quick Blunt™ kit (New England BioLabs). 5' phosphatases were removed using Calf Intestinal Alkaline Phosphatase (Invitrogen). The Gateway cassette was then inserted into the plasmid using T4 DNA ligase (New England BioLabs). The Gateway sites were then used to insert the artificial intron carrying sh*Wnt9a* using a Gateway LR Clonase II kit.

2.1.2 Design and construction of tools for Sema3D overexpression

To create a tool for the overexpression of Sema3D, In-Fusion Cloning (ClonTech®) was used to amplify the Sema3D gene from complementary deoxyribonucleic acid (cDNA) made from E6 chicken BPs and insert it into the RCAS(A) retroviral plasmid. The resulting plasmid is shown in figure 2.2.

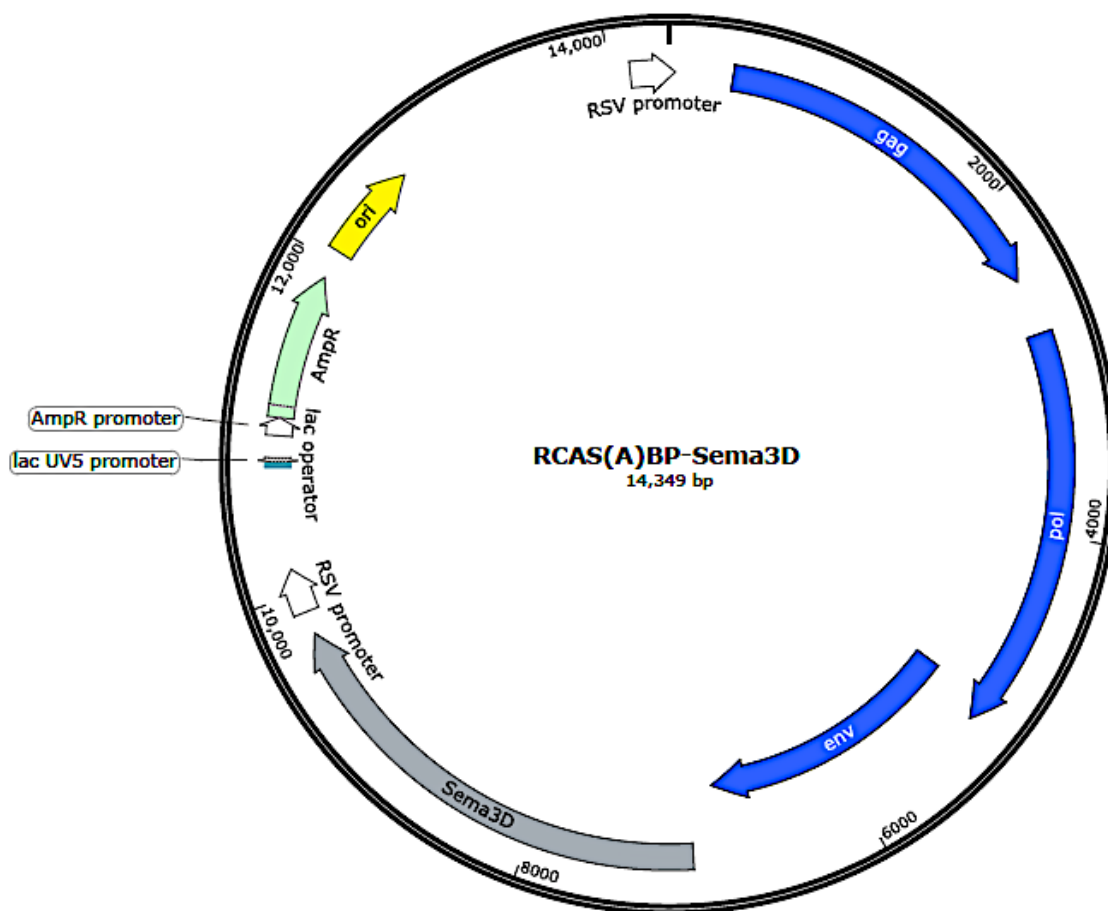


Figure 2.2 RCAS-Sema3D

The RCAS-Sema3D plasmid contains the viral genes, gag, pol, and env, shown in blue. The inserted Sema3D gene is shown in grey. The Rous sarcoma virus (RSV) promoters (which is part of the long-terminal repeat, LTR) and other promoters are shown in white. This plasmid confers resistance to ampicillin and carbenicillin (pale green). The origin of replication (yellow) and lactose operon (light blue) are shown.

First, primers were designed using the guidelines from the In-Fusion Cloning manual. The 3' end of the upstream (F or forward) primer was made up of 18-25 bases specific to Sema3D. This portion of the primer was important for amplifying Sema3D out of chicken cDNA; therefore, the melting temperature and GC-content were carefully considered with respect to the PCR protocol to be used. The 5' end of the primer was made up of a base sequence complementary to the RCAS plasmid where Sema3D would be inserted. This portion of the primer was important for joining the PCR product to the plasmid. A comparable strategy was used to design the downstream (R or reverse) primer. A *Cla*I restriction site was added in between the 5' and 3' portions of both primers.

This resulted in the flanking of Sema3D with ClaI restriction sites for diagnostic purposes. The complete primer sequences can be found in table 2.4.

Table 2.4 Primers used for In-Fusion Cloning of RCAS(A)-Sema3D

Primer Name	Primer Sequence
IF-RCAS(A)BP-Sema3D_F	5'-GTACCACTGTGGCATCGATGAATTCCGGCCTCC-3'
IF-RCAS(A)BP-Sema3D_R	5'-GGCCCGTACATCGCATCGATCGTAGCCTCAGGC TGT-3'

The RCAS(A) DNA plasmid was linearized at the insertion site with the ClaI restriction enzyme. The linearized plasmid was purified with a QIAquick® PCR Purification kit (Qiagen). The Sema3D gene was amplified from cDNA made from dissected E6 cochlear ducts. PCR was conducted using Phusion polymerase and the PCR product was gel purified using a Purelink® Quick Gel Extraction kit. The In-Fusion reaction inserted the PCR product into the linearized RCAS(A) plasmid. Once the plasmid was Maxi-prepped, the virus was created. The virus preparation protocol is described in detail in section 2.2.

2.1.3 Design and construction of *in situ* probe DNA templates

To make a DNA template for RNA probes antisense to Cntn6, Sema3D, and Sema3F, fragments of these genes were amplified out of cDNA from E6 chicken cochlear ducts and inserted into the pCR™2.1-TOPO® vector using TOPO® TA Cloning®. The following descriptions detail how this was accomplished.

Primers were designed to amplify the desired sequence out of cDNA. For all three genes, primer sequences were chosen such that the amplicons were unique to the gene of interest. For Sema3D and Sema3F, we used previously published primer sequences that had been used by another group to make *in situ* probe template (Bao & Jin, 2006; Jin *et al.*, 2006). For Cntn6 and Sema3F, the T3 promoter sequence was added to the 5' end of the reverse primer. This was to ensure that if the PCR fragment inserted into the TOPO vector in the incorrect orientation, the resulting plasmid could still be used to transcribe antisense probe using the inserted T3 promoter instead of the T7 promoter present in the TOPO backbone. Table 2.5 includes the primer sequences, the NCBI reference number, and the nucleotides in the amplicon.

Table 2.5 Primers for amplifying probe template out of cDNA

Primer Name	Primer Sequence	Gene, amplicon	Reference
Cntn6_F	5'-CTCACTGACAAAGAAAATCAAACAC GACA-3'	XM_4944703.3, 1343-1912	N/A
Cntn6_T3_R	5'-GGGAATTAACCCTCACTAAAGGGGCC CTTTTGTTCAGGC-3'	XM_4944703.3, 1343-1912	N/A
Sema3D_F	5'-TGGACTACTTTTCTGAAAGCCAG-3'	NM_205373.1, 1031-1792	Bao & Jin (2006)
Sema3D_R	5'-GGCACAGTATGGGTCTCT-3'	NM_205373.1, 1031-1792	Bao & Jin (2006)
Sema3F_F	5'-GATGACAAACTCTACTTCTTCTTCC GGG-3'	NM_204258.1 721-1440	Jin et al. (2006)
Sema3F_T3_R	5'-GGGAATTAACCCTCACTAAAGGATC TCCTCCAGCATCAGCTC-3'	NM_204258.1 721-1440	Jin et al. (2006)

To amplify the probe template out of the cDNA, a PCR reaction using Taq polymerase (New England BioLabs) was performed. Taq polymerase adds a single deoxyadenosine overhang to the 3' end of PCR products. The pCR-TOPO2.1 vector is supplied linearized at the insertion site and has a single deoxythymidine overhang at its 3' ends. Topoisomerase is covalently bound to the deoxythymidine overhangs in the vector and facilitates the ligation of the PCR product with the TOPO vector. Once ligation is complete, the topoisomerase is released from the vector.

Sema3D was inserted into the TOPO vector in the correct orientation on the first attempt. To transcribe probe antisense to the Sema3D messenger RNA (mRNA), the plasmid is linearized using the BamHI restriction enzyme and RNA probe is transcribed using T7 RNA polymerase (Fig. 2.3; Table 2.9). Given that Sema3F and Cntn6 did not insert into the plasmid in the correct orientation on the first set of attempts, the T3 promoter was inserted into the TOPO vector along with the Sema3F or Cntn6 probe template using TOPO cloning described above. To transcribe probe from pCR-TOPO-Sema3F, it must be cut with BamHI and transcribed using T3 RNA polymerase (Fig. 2.4; Table 2.9). For pCR-TOPO-Cntn6, antisense probe can be transcribed as

well as sense negative control probe. For the antisense probe, the plasmid is cut with NotI and transcribed with T3 polymerase. For sense probe, the plasmid is cut with BamHI and transcribed with T7 polymerase (Fig. 2.5; Table 2.9).

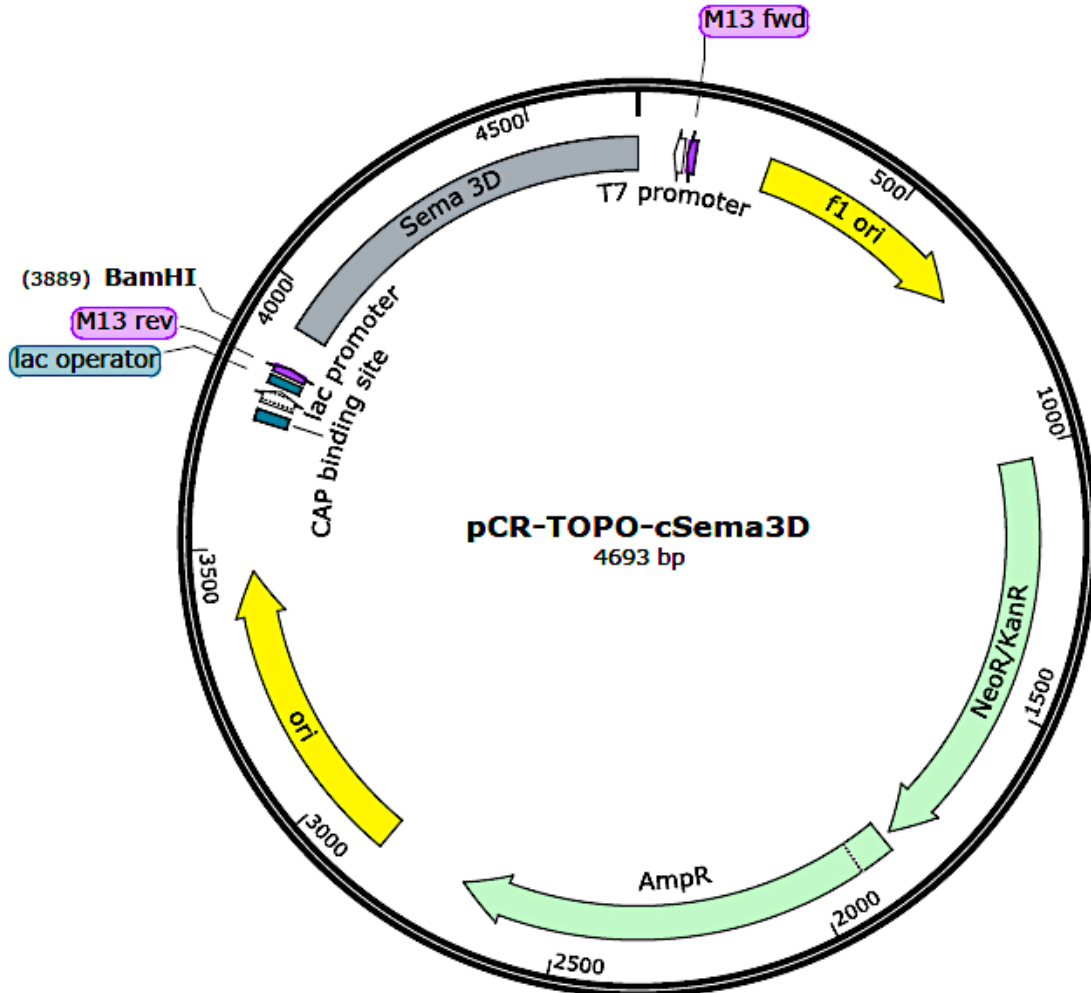


Figure 2.3 Sema3D DNA template for *in situ* probe

When the plasmid is cut using the BamHI restriction enzyme, the T7 RNA polymerase promoter (white) can be used to transcribe antisense RNA probe from the Sema3D DNA template (grey). This plasmid contains M13 forward and reverse primer binding sites for sequencing (purple). This plasmid confers resistance to neomycin, kanamycin, Geneticin®, ampicillin, and carbenicillin (green). Replication origins are shown in yellow and the lactose operon is shown in blue.

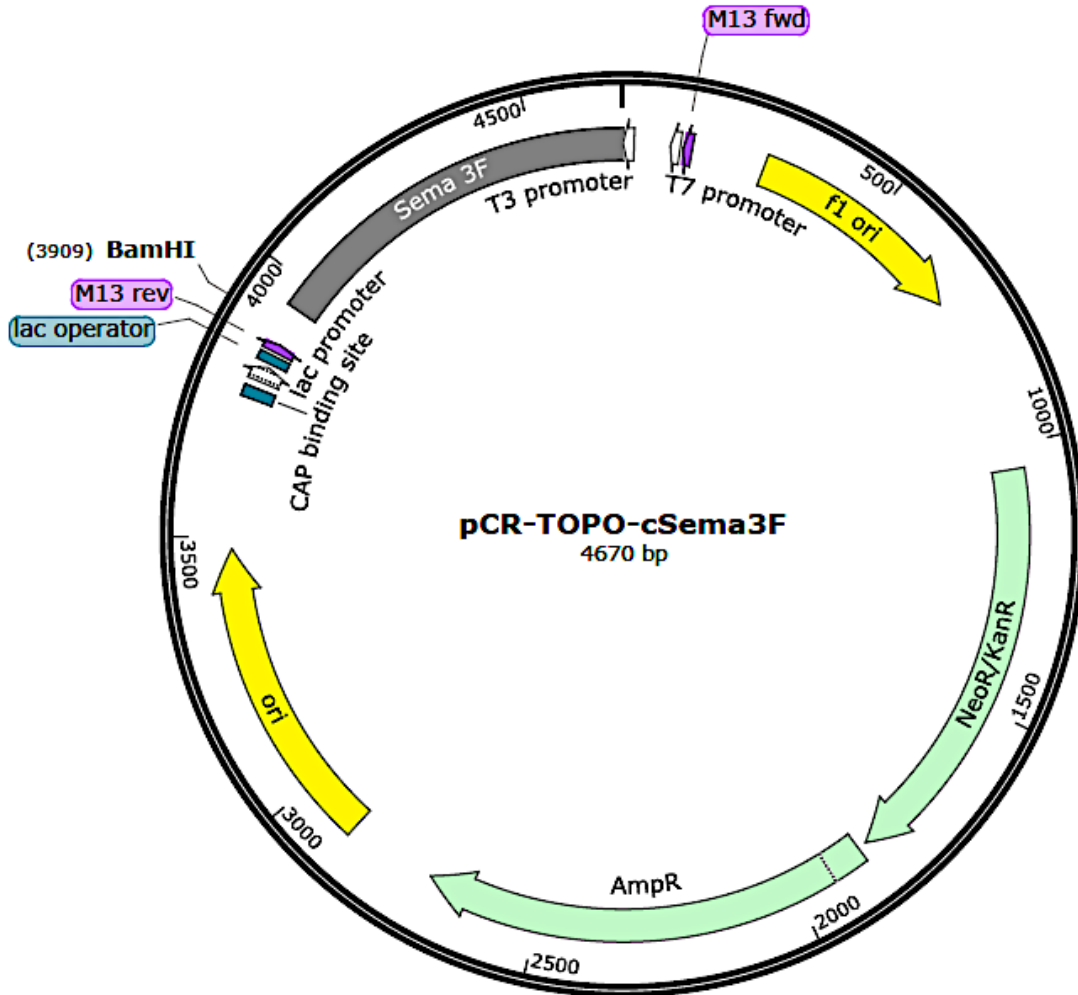


Figure 2.4 Sema3F DNA template for *in situ* probe

When the plasmid is cut using the BamHI restriction enzyme, the T3 RNA polymerase promoter (white) can be used to transcribe antisense RNA probe from the Sema3F DNA template (grey). This plasmid contains M13 forward and reverse primer binding sites for sequencing (purple). This plasmid confers resistance to neomycin, kanamycin, Geneticin®, ampicillin, and carbenicillin (green). Replication origins are shown in yellow and the lactose operon is shown in blue.

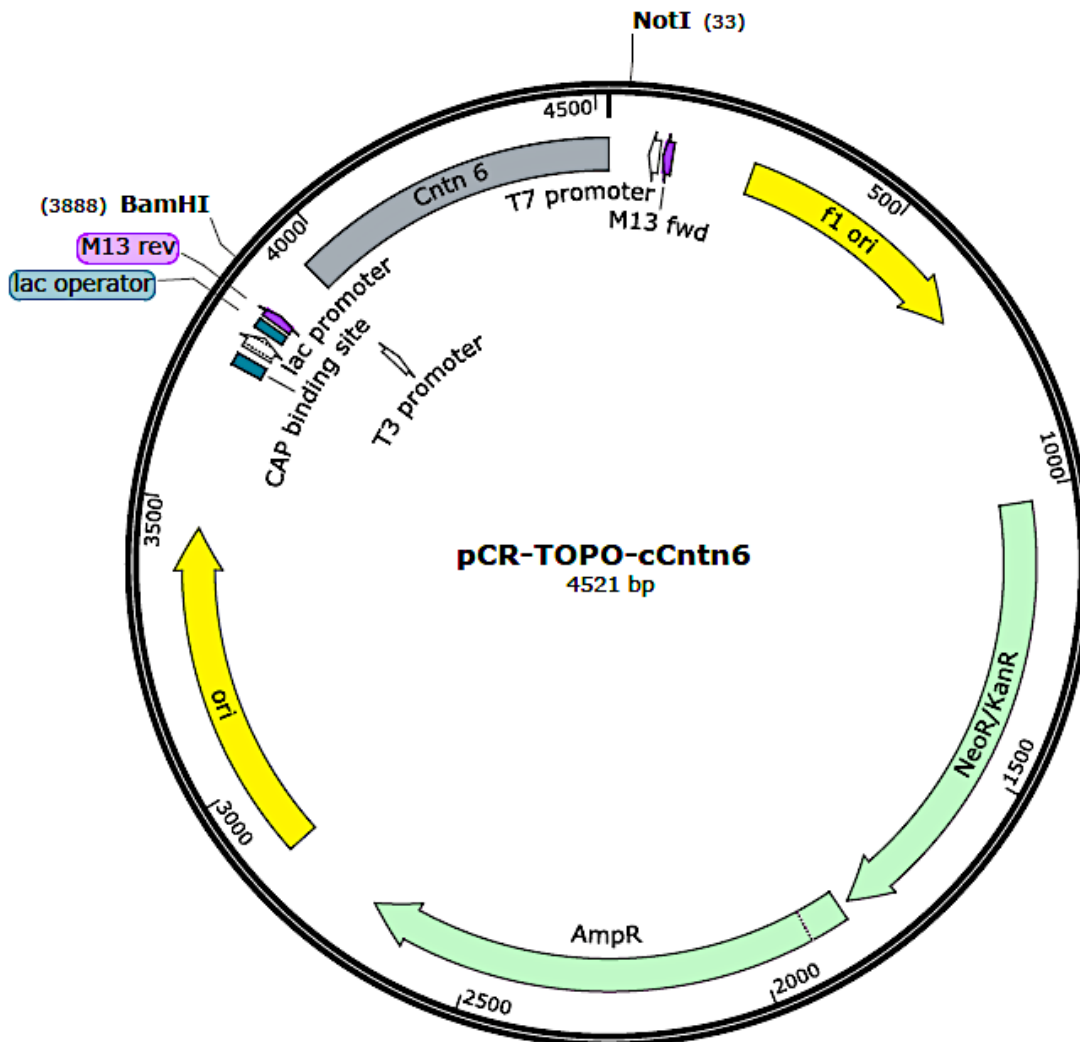


Figure 2.5 Cntn6 DNA template for *in situ* probe

When the plasmid is cut using the NotI restriction enzyme, the T3 RNA polymerase promoter (white) can be used to transcribe antisense RNA probe from the Sema3F DNA template (grey). When the plasmid is cut using BamHI, the T7 RNA polymerase promoter can be used to transcribe sense probe as a negative control probe. This plasmid contains M13 forward and reverse primer binding sites for sequencing (purple). This plasmid confers resistance to neomycin, kanamycin, Geneticin®, ampicillin, and carbenicillin (green). Replication origins are shown in yellow and the lactose operon is shown in blue.

2.2 Virus preparation and injection

2.2.1 Virus preparation

To create concentrated viral particles to inject into the chicken otocyst, UMNSAH/DF-1 chicken fibroblasts were transfected with the retroviral plasmid carrying the gene or shRNA of

interest. Retroviral expression plasmids used to make the viruses tested in this dissertation can be found in table 2.6. Ankita Thawani prepared the RCAN(X)-sh*Wnt9a* virus that was tested in this dissertation. RCAS(A) and RCAS(A)-*Wnt9a* have been previously used by Hartmann and Tabin (2001) and (Später *et al.*, 2006).

Table 2.6 Retroviral plasmids

Retroviral plasmids used to make virus		
RCAS(Y)-sh <i>Wnt9a-1</i>	RCAN(X)-sh <i>Wnt9a-1</i>	RCAS(A)
RCAS(Y)-sh <i>Wnt9a-2</i>	RCAN(X)-sh <i>Wnt9a-2</i>	RCAS(A)- <i>Wnt9a</i>
RCAS(Y)-sh <i>Wnt9a-3</i>	RCAN(X)-sh <i>Wnt9a-3</i>	RCAS(A)-Sema3D

The protocols used for virus preparation have been previously described by (Morgan & Fekete, 1996). Briefly, 10 µg of DNA was precipitated in 2M CaCl₂ in HEPES buffered saline (HBS; 20 mM HEPES and 150 mM NaCl in reverse osmosis (RO) water) for 45 minutes at room temperature. The media (Dulbecco's Modified Eagle Media supplemented with 1mM L-glutamine, 1 mM penicillin-streptomycin, 10% fetal calf serum, and 1% chicken serum) was removed from DF-1 cells and the precipitated DNA was added to the cells. After 20 minutes of exposure to the DNA, the DNA was left on the cells and media was added. The cells were then incubated for 4 hours at 37 °C. Afterward, the media was removed and a 90 second glycerol shock was done at 37 °C with 15% glycerol in HBS. The cells were rinsed with media twice. Media was added back and cells were placed back in the incubator to grow. Cells were grown to approximately 90% confluency and split to expand the number of cells. The final number of plates was dependent on the amount of virus needed for future experiments. The day before the virus concentration, the standard media was replaced with a half-volume of Nu-Serum supplemented media (Dulbecco's Modified Eagle Media supplemented with 1mM L-glutamine, 1 mM penicillin-streptomycin, 10% Nu-Serum).

To harvest and concentrate the virus, the media supplemented with Nu-Serum was pooled from each plate and filtered with a 0.45 µm filter. Two 1 ml samples of filtered unconcentrated virus were stored at -80 °C and would be titered later to check the efficiency of concentration. The remainder of the unconcentrated virus was transferred to tubes and spun with an S28 rotor with swinging buckets at 20,000 revolutions per minute (RPM) for 2 hours and 15 minutes at 4 °C.

After centrifugation, the supernatant was poured off leaving behind less than 200 μ l of supernatant per tube. The pelleted virus was resuspended in the remaining supernatant by trituration every 5 to 10 minutes for 1 hour on ice. The concentrated virus from each tube was then pooled, aliquoted into cryovials, and stored in liquid nitrogen.

To titer the virus, the unconcentrated and concentrated virus was thawed and a stepwise serial dilution of virus into media was performed. For the unconcentrated virus, the dilution was performed out to a 10^{-5} dilution. The 10^{-3} , 10^{-4} , and 10^{-5} dilutions were used to infect cells for titer. For concentrated virus, the dilution series was done out to 10^{-8} . The 10^{-5} , 10^{-6} , and 10^{-7} dilutions were used to infect cells for titer. 1 ml of each of the dilutions listed above was added to a 3.5 cm diameter well of DF-1 cells and incubated at 37 °C for 4 hours. Leaving the diluted virus in the wells, another 1 ml of fresh media was added to each well and the cells were incubated for another 48 hours.

The media was then removed from the cells and a chromogenic immunolabel (described in detail in chapter 2.9.2) was done using a primary antibody that detects the 3C2 epitope of Avian Myoblastosis Virus core protein (DHSB Cat #AMV-3C2). Once the immunolabeling was complete, the number of virus-positive clusters (presumed to reflect single virus infection events) in each well were counted. Cell counts for duplicated wells receiving the same dilution were averaged and that number was divided by the dilution factor to get the titer.

2.2.2 Virus injection

Fertilized chicken embryos from specific pathogen-free eggs (Charles River) were incubated at 37° to 39 °C in a humidified incubator; the start of the incubation is defined as E0. At E2, 2 to 3 ml of albumin was pulled from a hole made on the narrow end of the egg. A window in the shell was opened on the side of the egg that was facing up in the incubator. The hole and window were sealed with tape and placed back into the incubator.

The next day (E3), an aliquot of virus was thawed and 2 μ l of 0.25% Fast-Green dye was added to help visualize the virus during and after the injection. The tape over the window was removed and embryos were staged according to a standardized scheme (Hamburger & Hamilton, 1951). The amnion was opened over the otocyst and virus was injected into the right otocyst using a pulled glass pipet and a Picospritzer® II (Parker Instrumentation). Several drops of Chick Ringer's solution (123.2 mM NaCl, 1.56 mM CaCl₂, 4.96 mM KCl, and 0.81 mM Na₂HPO₄ in RO water,

pH 7.4) were added to keep the embryo moist. The window was resealed with tape and the embryo was placed back into the incubator until harvest.

2.3 Electroporation

White Leghorn chicken embryos (Purdue University Farms) were incubated at 37 to 39 °C in a humidified incubator. At E2, albumin was pulled and the eggs were windowed. Electroporation of plasmid DNA was performed on otic cups (HH 11-12) or otocysts (HH 14-17). Prior to electroporation, embryos were staged according to Hamburger and Hamilton (1951).

Concentrated plasmids (3 to 5 µg/µl) were mixed with 0.2% Fast-Green dye and 0.2% sucrose. For Tol2 plasmids, pCAG-T2TP transposase plasmid was mixed with the Tol2 expression plasmid in a molar ratio of 0.75 to 1. Given the pEF-Slit2 plasmid did not contain a reporter gene, it was co-electroporated with pEF1-GFP. Expression plasmids used in electroporations described in this dissertation are listed in table 2.7.

Table 2.7 Expression plasmids used in electroporation

Expression plasmid	Source of plasmid	Co-electroporated with
pT2K-CAG-sh <i>Wnt9a</i> -1-GFP	See chapter 2.1.1	pCAG-T2TP
pT2K-CAG-sh <i>Wnt9a</i> -2-GFP	See chapter 2.1.1	pCAG-T2TP
pT2K-CAG-sh <i>Wnt9a</i> -3-GFP	See chapter 2.1.1	pCAG-T2TP
pEF1-GFP	Battisti <i>et al.</i> (2014)	pEF1-hSlit2 or none
pEF-hSlit2	Battisti <i>et al.</i> (2014)	pEF-GFP
p-CAG-Robo1(DN)-GFP	Hammond <i>et al.</i> (2005)	none

A small incision was made in the amnion and the amnion Chick Ringer's solution was dripped over the hole. This inflated the amnion away from the surface of the embryo, making it easier to open without touching the embryo. The right otic cup or otocyst was then injected with DNA using a Picospritzer® II (Parker Instrumentation) and a pulled glass pipet.

The placement of the negative tungsten electrode and the positive platinum electrode depended on the age of the embryo at electroporation, the electrodes used, and the target organ. For the experiments in this dissertation, the CD was usually the target organ. For electroporations at the otic cup stage (HH 11-12), the DNA needed to be driven medially. Electrodes were placed parallel

to the embryo with the negative electrode on the embryo's right side and the positive on the left (Fig. 2.6 A) as previously described by Chrysostomou *et al.* (2012). For otocyst stages (HH 14-18), the negative electrode was placed over the top of the right otocyst while the positive electrode was slipped under the embryo next to the left otocyst (Fig. 2.6 B). In some cases, a negative tungsten needle was placed in the otocyst and a positive platinum paddle was placed ventrally (Fig. 2.6 C) (Sho Ohta, personal communication).

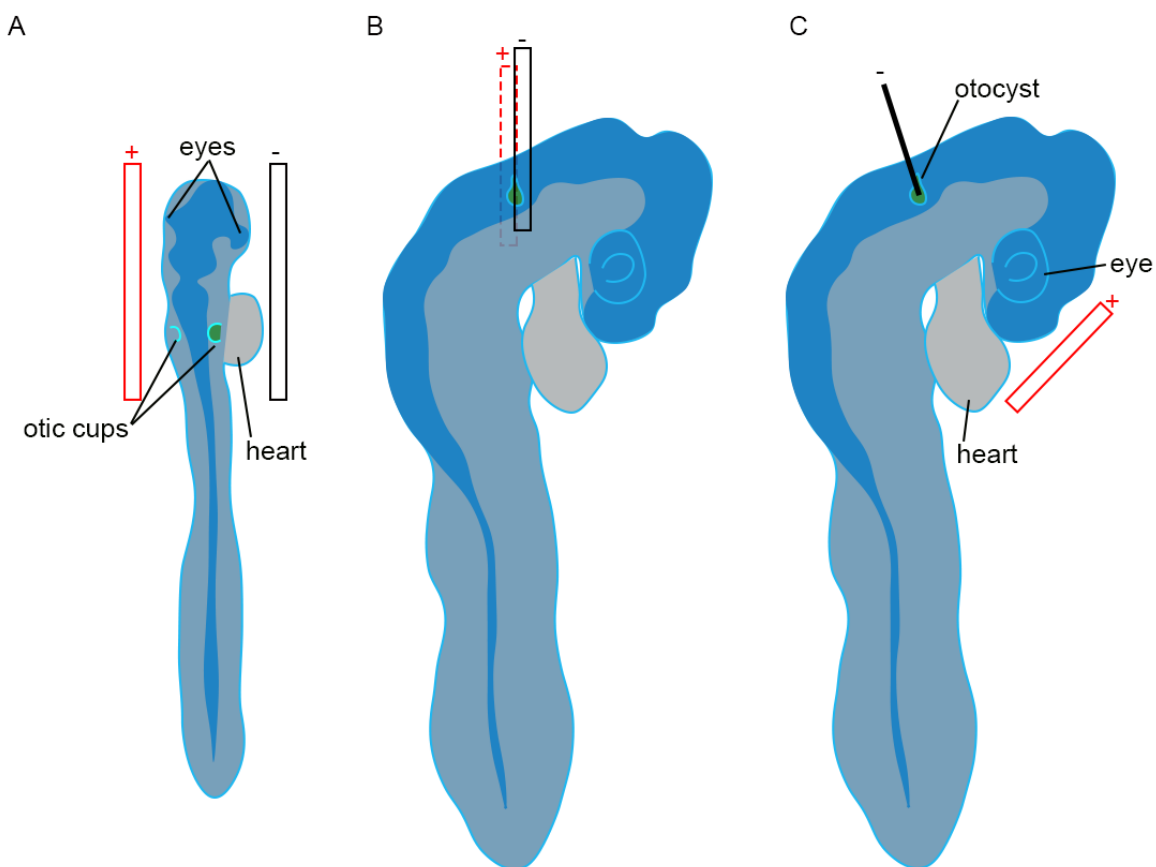


Figure 2.6 Electrode placement

Electrode placement varied depending on the age electroporated and the electrodes used. Electrode placements shown above often target the BP. For each image, the neural tube is shown in dark blue. The developing eyes and ears are outlined in light blue and injected right ears are filled in green. The heart is light grey. In each case, the injected DNA (green) is driven towards the positive (red) electrode. Negative electrodes are black. (A) An otic cup electroporation at HH 12, just as the head is starting to turn. Electrodes are placed on either side of the embryo. (B) An otocyst electroporation at HH 17. The negative electrode is placed over the otocyst while the positive electrode is below the embryo. (C) A negative needle electrode is inserted into the HH 17 otocyst and DNA is driven towards a positive paddle.

Once electrodes were placed, the electroporation was performed using a TSS20 Ovodyne electroporator and an EP1 current amplifier (Intracel). When electrodes were placed on both sides of the embryo (Fig. 2.6 A, B), two 50 millisecond, 10 volt pulses spaced 10 milliseconds apart were delivered to the otic cup or otocyst. When the negative tungsten needle was placed in the otocyst (Fig. 2.6 C), five 25 millisecond, 8 volt pulses spaced 975 milliseconds apart were delivered.

After electroporation, a few drops of Chick Ringer's solution were applied to keep the embryo moist and the window was sealed with tape. Embryos were returned to the incubator until they were harvested. The techniques used in this protocol have been previously described in detail by Freeman *et al.* (2012) and Stoller and Fekete (2016).

2.4 Blood vessel infusion

Blood vessel infusions with fluorescent ink were performed as previously described by Takase *et al.* (2013). Ink was extracted from a highlighter pen (Sharpie yellow 1912767) and diluted 1:2 in phosphate buffer saline (PBS). A Picospritzer® II (Parker Instrumentation) was used to inject approximately 2-3 μ l of diluent through a pulled glass capillary tube (10-20 mm outer diameter) and into the vitelline artery of E5-E10 chicken embryos. The ink was given 1-2 minutes to spread through the circulatory system and the quality of the infusion was checked under a fluorescent dissection microscope (Leica MZFL III).

2.5 Tissue preparation

Virus infected, electroporated, ink-infused, and untreated embryos were sacrificed at an age range of E3-E18. Tissue and sample preparation were dependent upon the experimental protocol for which the tissue would be used (Fig. 2.7). At E10 and younger, embryos were removed from the egg and the vasculature connecting the embryo to the yolk and allantois was cut. The embryo was then placed in PBS, staged according to Hamburger and Hamilton (1951) and decapitated. For embryos older than E10, embryos were removed from the egg but remained attached to the yolk and allantois, and subjected to trans-cardial perfusion of PBS followed by chemical fixative. All embryos processed for RNase-free protocols (RNA sequencing, real-time quantitative PCR (RT-qPCR), and *in situ* hybridization) were handled using RNase-zapped, baked, and/or autoclaved tools as well as diethyl pyrocarbonate (DEPC) treated reagents.

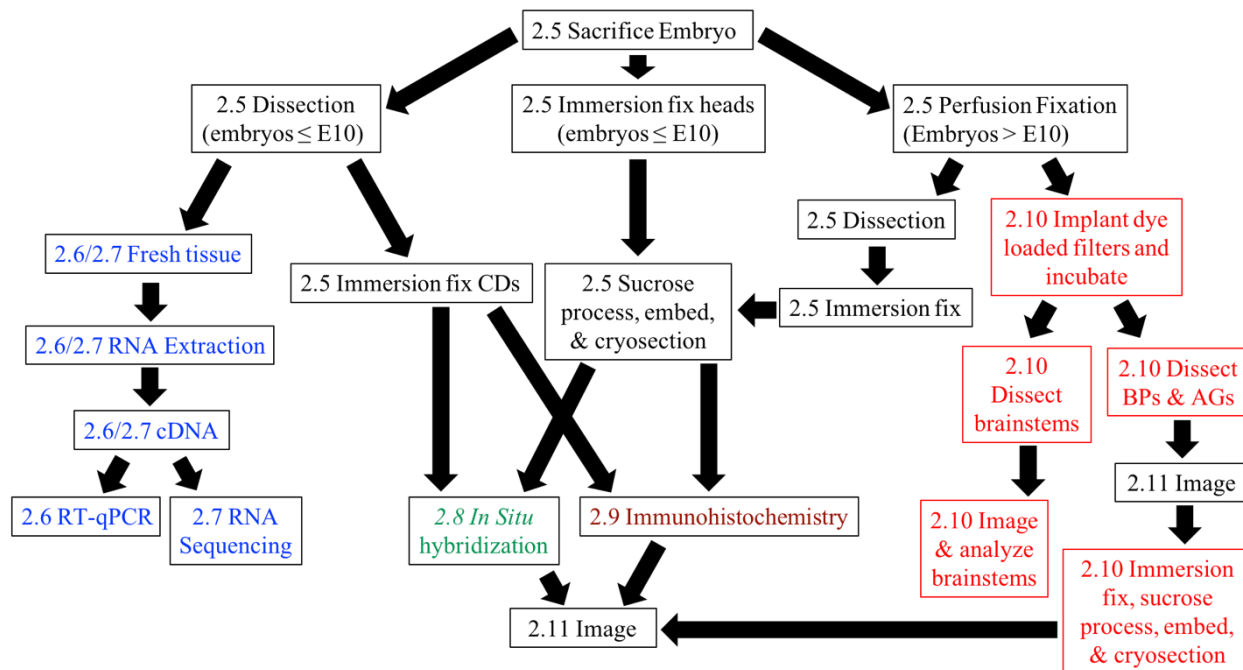


Figure 2.7 Tissue preparation

The tissue preparation is specific to the experimental protocol that was used. Black boxes represent procedures that are shared across multiple protocols and are described in chapters 2.5 and 2.11. Blue boxes represent procedures that are specific to RT-qPCR and RNA sequencing protocols. These protocols are described in chapters 2.6 and 2.7. Green and brown boxes represent *in situ* hybridization and immunohistochemistry, respectively. Details on these protocols can be found in chapters 2.8 and 2.9. Red boxes are specific to the efferent labeling protocol and are described in chapter 2.10.

2.5.1 Whole mount preparation

For whole mount preparations for *in situ* hybridization or immunohistochemistry on E10 embryos or younger, CDs were dissected from the head and otic capsule. Isolated CDs were immersed in 4% paraformaldehyde (PFA) and were placed in 4 °C for overnight fixation. The tissue was then washed in PBS prior to starting the *in situ* or immunohistochemistry protocol.

2.5.2 Cryosectioning

For cryosectioned tissue preparations, the heads, brainstems, or dissected BPs were immersed in 4% PFA and fixed overnight at 4 °C. Tissue was then washed in PBS for a minimum of 1 hour and cryoprotected in ascending concentrations of sucrose solutions (10%, 20%, and 30% sucrose in PBS). For lipophilic dye-treated or RNase-free samples, the tissue was run through all three sucrose solutions in 24 hours. For all other samples, the tissue was immersed in each sucrose

solution for 24 hours. For RNase-free samples, tissue was embedded in Tissue Freezing Media™ (General Data Company, Inc.). For all other samples, tissue was embedded in 300 bloom gelatin (7.5% gelatin, 15% sucrose, 0.05% sodium azide in PBS). The embedded tissue was frozen on a metal stand in liquid nitrogen and frozen tissue blocks were stored at -80 °C until they were sectioned. Using a cryostat set to -22 °C to -24°C, 15 µm horizontal cross sections were cut and collected onto Superfrost® Plus Slides (Fisherbrand®). Depending on the age of the embryo, two to four alternate series of sections were collected from one embryo. This allowed for multiple experiments to be performed on the same embryo. Sections were stored at -20 °C until use.

2.5.3 Perfusion fixation

Embryos older than E10 were fixed via trans-cardiac perfusion. Embryos' limbs were pinned to a dissection pad to expose the abdomen. A longitudinal incision was made into the peritoneal and thoracic cavities. An incision was made in the right atrium and a needle attached to a peristaltic pump (MasterFlex Easy-Load II, Cole-Parmer Instrument Company) via a Tygon tube was placed into the left ventricle. For embryos younger than E14, a 25-gauge needle was used. For embryos E14 and older, a 19-gauge needle was used. PBS was perfused through the circulatory system at a rate of 40 RPM for embryos younger than E14 and 50 RPM for embryos E14 and older for 1 minute. 4% PFA was then perfused for 5 minutes. The embryo was staged according to Hamburger and Hamilton (1951) using toe length and then decapitated. In PBS, the mandible, tympanic membranes, and columella (middle ear) bones were removed. The head was then stored in 4% PFA until they were used for efferent labeling or the BPs were extracted for labeling.

2.6 Real-time quantitative polymerase chain reaction

DF-1 cells were dissociated from the culture dish with 500 µl of cold TRIzol™ or freshly dissected CDs were placed into 500 µl of cold TRIzol™ Lysis Reagent (Invitrogen) immediately after being isolated. Four to eighteen CDs were pooled into one 500 µl tube of TRIzol™. The TRIzol™ samples were homogenized and an acidic Phenol-Chloroform extraction was used to isolate RNA. Isopropanol and ethanol washes were used to further purify and concentrate the RNA. Any residual DNA was removed with RQ1 deoxyribonuclease (Promega) and the RNA sample was further purified using an RNeasy® kit (Qiagen).

cDNA was reverse transcribed from the RNA samples using Oligo(dT) primers (ThermoFisher) and Superscript® III reverse transcriptase (Invitrogen). For shRNAs, the reverse transcription primers were used from table 2.8 in place of Oligo(dT) primers. RT-qPCR was performed on a LightCycler® 96 (Roche) using FastStart Essential DNA Green (Roche). *Gapdh* was used the housekeeping gene. All the primers used in this dissertation are listed in table 2.8.

Table 2.8 Primer sequences for RT-qPCR

Target Gene	Primer Sequence
<i>GAPDH</i>	Forward: 5'-TTGGCATTGTTGAGGGTCTT-3' Reverse: 5'-GTGGACGCTGGGATGATGTT-3'
<i>cWnt9a</i>	Forward: 5'-CGCCGCCTACTTCGGGCTGA-3' Reverse: 5'- TTCTCCAGCTTCAGGCGGTCACAG-3'
<i>siWnt9a-1</i>	Forward: 5'-GCGGCGGTAGACAAGATCCGTA-3' Reverse: 5'-GTGCAGGGTCCGAGGT-3' Reverse Transcription of shRNA: 5'-GTCGTATCCAGTGCAGGGTCCGAGGTATTCGCACTGGATACGAC AAGGAC-3'
<i>siWnt9a-2</i>	Forward: 5'-GCGGCGCGTCTCCTTGAAACC-3' Reverse: 5'-GTGCAGGGTCCGAGGT-3' Reverse Transcription of shRNA: 5'-GTCGTATCCAGTGCAGGGTCCGAGGTATTCGCACTGGATACGACA AGAGA-3'
<i>siWnt9a-3</i>	Forward: 5'-GCGGCGGGCTTATGTCTCAACA-3' Reverse: 5'-GTGCAGGGTCCGAGGT-3' Reverse Transcription of shRNA: 5'-GTCGTATCCAGTGCAGGGTCCGAGGTATTCGCACTGGATACGACA AGCTA-3'

Table 2.8 continued

<i>cSema3F</i>	Forward: 5'-GAGACAGAGGAGCTGATGCTGGA-3' Reverse: 5'-GCACAGGCTTCTCCATACACGTCA-3'
<i>cEfn5</i>	Forward: 5'-ACCGCTACGCCGTCTACTGGA-3' Reverse: 5'-CACGGGATGGCTCGGCTGACTC-3'

2.7 RNA deep sequencing

As previously described in chapter 2.2, right otocysts were injected with RCAS(A)-*Wnt9a* retrovirus on E3. In the control group, E3 right otocysts were injected with RCAS(A) parent virus. At E6, right CDs were extracted and the SM, LM, and cochleovestibular ganglion were removed. Fresh CDs were placed into 700 µl of cold QIAzol™ Lysis Reagent (Invitrogen) immediately after dissection. 24 CDs were pooled into one tube of 700 µl QIAzol™. Three of these biological replicates were collected for both experimental and control groups. For each run, tissue collections were done by three lab members (myself, Ankita Thawani, and Donna Fekete) simultaneously and then pooled.

QIAzol™ samples were homogenized and total RNA, including small RNAs, were extracted using a miRNeasy® kit (Qiagen). The Purdue sequencing facility checked the RNA quality, constructed cDNA libraries, and conducted the sequencing. An Agilent Technologies Bioanalyzer was used to validate quality of the RNA samples with an RNA Integrity Number (RIN) of less than or equal to eight. A TruSeq Stranded kit (Illumina) was used to create the cDNA libraries. Illumina HiSeq2500 with paired-end reads and at least 60 million reads per sample were used to sequence the transcriptome.

Nadia Atallah, from the Purdue Center for Cancer Research, performed our bioinformatics analysis. Sequencing reads were aligned to the Galgal4 Ensembl *Gallus gallus* genome using Tophat2 (Kim *et al.*, 2013). Three statistical packages, Cufflinks (Roberts *et al.*, 2011; Trapnell *et al.*, 2013; Trapnell *et al.*, 2012; Trapnell *et al.*, 2010), DeSeq2 (Love *et al.*, 2014), and EdgeR (Robinson *et al.*, 2010) were used to calculate the number of reads for each transcript and identify differentially expressed genes using a false discovery rate of 5%. The complete RNA sequencing data set is available on the Gene Expression Omnibus database (accession # GSE95295).

2.8 *In situ* hybridization

Alkaline phosphatase *in situ* were performed on whole mount and sectioned tissue to determine the spatial patterns of expression of mRNAs. RNAScope *in situ* were done along with a hematoxylin stain to examine the expression of mRNAs of Semaphorin receptors.

2.8.1 Making probes for alkaline phosphatase *in situ* hybridization

For alkaline phosphatase *in situ*, digoxigenin (DIG)-labeled RNA probes were transcribed from DNA probe templates. Information on the DNA probe templates used in this dissertation can be found in table 2.9.

Table 2.9 DNA Templates for RNA Probe

Probe Template Name	Restriction Enzyme	Polymerase
pCR2.1-TOPO-cSema3D	BamHI	T7
pCR2.1-TOPO-cSema3F	BamHI	T3
pCR2.1-TOPO-cCntn6	NotI	T3
pBSKS-cWnt9a	NcoI	T3
pKS-cSer1	HindIII	T7
pBSKS-cSlit2	XhoI	T3
pBSKS-cRobo1	BamHI	T7
pBSKS-cRobo2	XhoI	T3

First, the DNA probe template was linearized using the appropriate restriction enzyme as indicated by the plasmid map and/or instructions. The linearized DNA template was then purified using a phenol-chloroform extraction. Ethanol washes were used to precipitate the DNA. The DNA pellet was dried and, depending on the size of the pellet, was resuspended in 10-20 μ l of sterile water.

The transcription reaction was run using 300 ng of purified linearized DNA template, T7 or T3 polymerase (Promega), 1X transcription buffer (Promega), 8 mM Dithiothreitol (Promega), 1X DIG RNA labeling mix nucleoside 5'-triphosphates (Roche), and RNaseOUT™ recombinant ribonuclease inhibitor (ThermoFisher Scientific). The reaction was incubated at 37 °C for 1 hour and 40 minutes. The DNA template was then degraded using ribonuclease-free deoxyribonuclease (Promega) incubated at 37 °C for 20 minutes. DIG-labeled RNA was precipitated using 0.13M LiCl in ethanol, incubated at -20 °C overnight, and pelleted via centrifugation. The pellet was washed once with 100% ethanol and once with 70% ethanol. After decanting the supernatant and air-drying the DIG-labeled RNA pellet, it was resuspended in 25 μ l of Tris-

Ethylenediaminetetraacetic acid (EDTA). DIG-labeled RNA probe was stored at -80 °C until it was diluted in hybridization buffer.

2.8.2 Alkaline phosphatase *in situ* hybridization on whole mount tissue

Dissected CDs were fixed in 4% PFA. To disrupt the lipids, a series of ethanol and xylene washes were done. First CDs were washed in ascending concentrations of ethanol (50%, 70%, 90%, and 95% ethanol in RO water). CDs were washed for 5 minutes in each ethanol solution. Three 15 minute washes were done in 100% ethanol and CDs were washed in 100% ethanol overnight. The following day, two 5 minute washes were done in xylene followed by three 5 minute washes in ethanol. CDs were then incubated in pre-hybridization buffer (50% formamide, 10% dextran sulfate, 1X Denhardt's solution (1% Bovine Serum Albumin, 1% Ficoll, and 1% Polyvinylpyrrolidone), 2% Roche blocking reagent (proprietary), 0.05% Tween20, 0.2 M NaCl, 8.9 mM Tris HCl, 1.1 mM Tris base, 5 mM NaH₂PO₄, 5 mM Na₂HPO₄, 5 mM EDTA, 1 mg/ml yeast tRNA in DEPC water) for 1 hour at 68-70 °C. Then CDs were incubated in hybridization buffer (0.2 µg/ml DIG-labeled probe in pre-hybridization buffer) for 2 days at 68-70 °C.

Following hybridization, the following washes were done in order at room temperature: 1) three 30 minute washes in 0.1% Tween20 in DEPC water; 2) three 30 minute washes in 1X saline-sodium citrate (SSC) buffer and 0.1% Tween20 in DEPC water; and 3) three 10 minute washes in 0.1% Tween20 in Tris-buffered saline (TBS). Samples were then blocked against nonspecific binding for 30 minutes in blocking solution (10% heat inactivated goat serum (HINGGS) and 0.1% Tween20 in PBS). Probes were detected by incubating the sample in a 1:2000 dilution of anti-DIG alkaline phosphatase fab fragments (Roche) diluted in blocking solution at 4 °C overnight.

Samples were then washed in 0.1% Tween20 in PBS throughout the next 24 hours. Afterwards, samples were washed three times for 30 minutes each in alkaline phosphatase buffer (5 M NaCl, 2 M Tris pH 9.5, 1 M MgCl₂, 0.01% Tween20 in water). Samples were then incubated with BM Purple alkaline phosphatase substrate (Roche) in the dark until the probe's signal was easily visualized by a purple color change in the tissue.

2.8.3 Alkaline phosphatase *in situ* hybridization on sectioned tissue

Sectioned tissue was fixed in 4% PFA for 10 minutes and then washed in PBS. Tissue was digested with 1 µg/µl ProteinaseK for 10 minutes, fixed again for 10 minutes in 4% PFA, and then

washed in PBS. Treatment with 0.1M triethanolamine and 0.25% acetic anhydride acetylated positively charged amino groups in the tissue, decreasing background binding of the negatively charged RNA probe. Tissue was then permeabilized with 0.1% triton in PBS for 30 minutes and then incubated in pre-hybridization buffer (50% formamide, 10% dextran sulfate, 1X Denhardt's solution, 1 mg/ml yeast tRNA, 0.2 M NaCl, 8.9 mM Tris HCl, 1.1 mM Tris base, 5 mM NaH₂PO₄, 5 mM Na₂HPO₄, 5 mM EDTA in DEPC water) for 2 hours at room temperature. The slides were then moved into hybridization buffer (1 µg/ml probe in pre-hybridization buffer) and incubated overnight at 72 °C.

After hybridization of the DIG-labeled probe to the transcripts present in the tissue, the tissue was washed in 2X SSC for 30 minutes at 72 °C and then again in 0.2X SSC for 1 to 2 hours at 72 °C. Two 5 minute washes in 0.1% Tween20 in PBS were done and then nonspecific binding was blocked with 2% Roche blocking reagent, 10% fetal bovine serum (FBS), and 0.1% Tween20 in PBS for 1 hour at room temperature in a humidified chamber. Slides were incubated in anti-DIG alkaline phosphatase fab fragments (Roche) diluted 1:3500 in the previous blocking buffer overnight at room temperature to detect the probe.

The next day, tissue was washed three times in 0.05% Tween20 in PBS for 10 minutes each, before equilibration in B2 Buffer (100 mM Tris pH 9.5, 100 mM NaCl, 50 mM MgCl₂ in water) for two 10 minute washes. The probe was visualized by incubating the tissue with BM Purple alkaline phosphatase substrate (Roche) or Sigma Fast™ nitro-blue tetrazolium and 5-bromo-4-chloro-3'-indolyphosphate p-toluidine salt (NBT/BCIP) in a humidified chamber at room temperature in the dark. In most cases, a strong signal was detected in less than 8 hours of incubation. In some cases, if the signal was weak after 8 hours, the incubation was continued overnight at 4 °C.

Once the blue/purple signal was clearly visible, the slides were removed from the NBT/BCIP developing solution and washed two times for 10 minutes in 0.05% Tween20 in PBS. Slides were soaked in alkaline phosphatase stop solution (100 mM Tris pH 7.5 and 1 mM EDTA in water) and then washed in PBS. Cover slips were mounted with Fluoromount-G® mounting media (Southern BioTech) or tissue was dehydrated in ethanol and hemoD and coverslipped with toluene-based liquid mounting media.

This protocol was previously described by Sanchez-Calderon *et al.* (2004) and Sienknecht and Fekete (2008).

2.8.4 RNAScope *in situ* hybridization on sectioned tissue

For *in situ* against *Nrp1* (Cat #501181), *Nrp2* (Cat #501191), and *PlxnA1* (Cat #506111) we used RNAScope® 2.5 HD Detection Red protocol and reagents (Advanced Cell Diagnostics). Probes were also ordered from Advanced Cell Diagnostics (see catalog numbers listed above).

All 40 °C incubations were performed in a Hybaid OmniSlide hybridization oven. Tissue was first washed with PBS and then incubated at room temperature with hydrogen peroxide for 10 minutes. Slides were then rinsed in RO water and then submerged into boiling 1X target retrieval buffer for 5 minutes. Slides were washed twice with RO water, once with 100% ethanol, and then allowed to dry at room temperature. Tissue was treated with a Protease Plus kit (Advanced Cell Diagnostics) for 15 to 30 minutes at 40 °C. Pre-warmed probe was applied and incubated for 2 hours at 40 °C.

Once the probe was hybridized, the signal amplification steps were performed using the RNAScope amplification kit (Advanced Cell Diagnostics). Two 2 minute washes in 1X RNAScope buffer were done at room temperature and then amplification (AMP)1 solution was applied to the slides and incubated for 30 min at 40 °C. Slides were washed in RNAScope buffer as previously described and then incubated with AMP2 at 40 °C for 15 minutes. Slides were washed in RNAScope buffer. AMP3 was applied and incubated at 40 °C for 30 minutes. Slides were washed in RNAScope buffer and incubated with AMP4 for 15 minutes at 40 °C. After washing with RNAScope buffer again, AMP5 was applied and the slides were moved to a humidified chamber at room temperature. For strongly expressed transcripts, such as *PlxnA1*, a 15 minute AMP5 incubation was used. All other probes, a 30 minute AMP5 incubation was done. Slides were washed and AMP6 was applied and incubated for 15 minutes at room temperature.

After another RNAScope buffer wash, a 1:60 dilution of FastRED-B diluted in FastRED-A was applied to detect the signal. Slides were incubated at room temperature for 10 minutes in the dark. Two washes in RO water were done and then the tissue was counterstained with 50% Hematoxylin (American MasterTech) for 2 minutes to label the cell nuclei. Tissue was washed in RO water until the glass slides were clear and the tissue was purple. The tissue was then treated with 0.02% ammonium hydroxide in RO water until the tissue turned blue. After washing with RO water, the tissue was dried at 60 °C for 15 minutes or until completely dry. Slides were dipped in xylene and coverslips were mounted with EcoMount (Fisher Scientific).

2.9 Immunohistochemistry

2.9.1 Immunofluorescence

Sectioned tissue dried onto slides was post-fixed with 4% PFA for 10 minutes and washed in PBS. A dip in 0.05% Tween20 in PBS allowed for better spreading of blocking buffer in the subsequent step. Nonspecific binding was reduced using blocking solution (5% goat serum or 5% horse serum, 0.05% sodium azide, and 0.05% Tween20 in PBS) for one hour in a humidified chamber at room temperature. To detect the antigen(s) of interest, primary antibody was diluted in blocking solution and applied to the slides. Slides were incubated in a humidified chamber for 1 hour at room temperature or overnight at 4 °C. Tissue was washed in PBS and dipped in 0.05% Tween20 in PBS. Fluorophore-conjugated secondary antibodies were diluted 1:500 in blocking solution and applied to slides to detect the primary antibody. Slides were incubated in the dark in a humidified chamber for 1 hour at room temperature. In some cases, slides were washed and counterstained with 1 µM TO-PRO3 in PBS to detect double-stranded DNA (dsDNA). TO-PRO3 was incubated for 15 to 30 minutes at room temperature in the dark. Protecting the slides from light exposure, the tissue was washed in PBS and cover slipped with Fluoromount-G® (Southern BioTech), 4',6-diamidino-2-phenylindole (DAPI) Fluoromount-G® (Southern BioTech), or Vectashield® antifade mounting medium (Vector Laboratories).

2.9.2 Chromogenic immunohistochemistry

In most experiments, chromogenic labeling using 3, 3'-diaminobenzidine (DAB) was performed on previously unlabeled tissue or cells. In some cases, however, DAB was used to label neurofilament associated protein or viral protein after an *in situ* hybridization.

The sample was post-fixed with 4% PFA for 10 minutes, washed with PBS, and dipped in 0.05% Tween20. Nonspecific binding was reduced with blocking solution (5% goat serum or 5% horse serum, 0.05% sodium azide, and 0.05% Tween20 in PBS). The blocking step was performed in a humidified chamber for 1 hour at room temperature. To detect the antigen of interest, the appropriate antibody was diluted in blocking solution and incubated in a humidified chamber. The primary antibody step was performed at room temperature for 1 hour or at 4 °C overnight. The sample was washed in PBS and endogenous peroxidases were saturated with 0.3% hydrogen peroxide in ice cold methanol for 30 minutes. After another PBS wash, the primary antibody was

detected with a biotinylated secondary antibody diluted 1:250 in blocking solution. This step was conducted in a humidified chamber for 1 hour at room temperature. The tissue was washed and dipped in 0.05% Tween20 in PBS. The signal was amplified with a Vectastain® Avidin-Biotin Complex (ABC) horseradish peroxidase kit (Vector Laboratories) prepared 45 minutes prior to use. The sample was treated with ABC for 1 hour at room temperature in a humidified chamber. Samples were washed with PBS and washed with 50 mM Tris pH 7.5. Peroxidase activity was detected with 0.5 mg/ml DAB and 0.06% hydrogen peroxide in 50 mM Tris pH 7.5; this development step typically lasted no longer than 20 minutes. Samples were washed in 50 mM Tris 7.5 and then washed in PBS. At this point, labeled cells and tissue could be observed. For tissue sections, slides were coverslipped. In some cases, cover slips were mounted using Fluoromount-G® mounting media (Southern BioTech). Other times, sectioned tissue was dehydrated in ethanol and HemoD and covered with toluene-based liquid mounting media and a coverslip followed by sealing with nail polish.

2.10 Efferent labeling

Perfusion-fixed embryos stored in 4% PFA at 4 °C were further dissected to expose the dorsal surface of the brain and rostral brainstem. Skin, fat, and muscle were trimmed away from the dorsal head and neck. The skull was cut down the midline from the olfactory bulb down to the rostral brain stem. From there, the dorsal skull, cerebral hemispheres, and the cerebellum were removed. The dura mater was opened at the midbrain and hindbrain and a NeuroVue® Red lipophilic tracer dye-loaded filter was implanted into one side of the pons to target the efferent cell bodies (Fig. 2.8 A-B). Filters were cut into rectangles or isosceles trapezoids (Fig. 2.8 C) and the size of the filter was based on the age of the embryo (table 7.1).

The heads with implants were incubated in 2% or 4% PFA. The incubation time (1-6 weeks) and temperature (37 °C or 55 °C) was set based on the age of the embryo and the BP (ipsi- or contralateral relative to the implant). After the appropriate incubation time, ipsi- and contralateral BPs and cochlear ganglia were extracted and imaged. In some cases, when efferents were strongly labeled after imaging the whole mount, BPs were embedded.

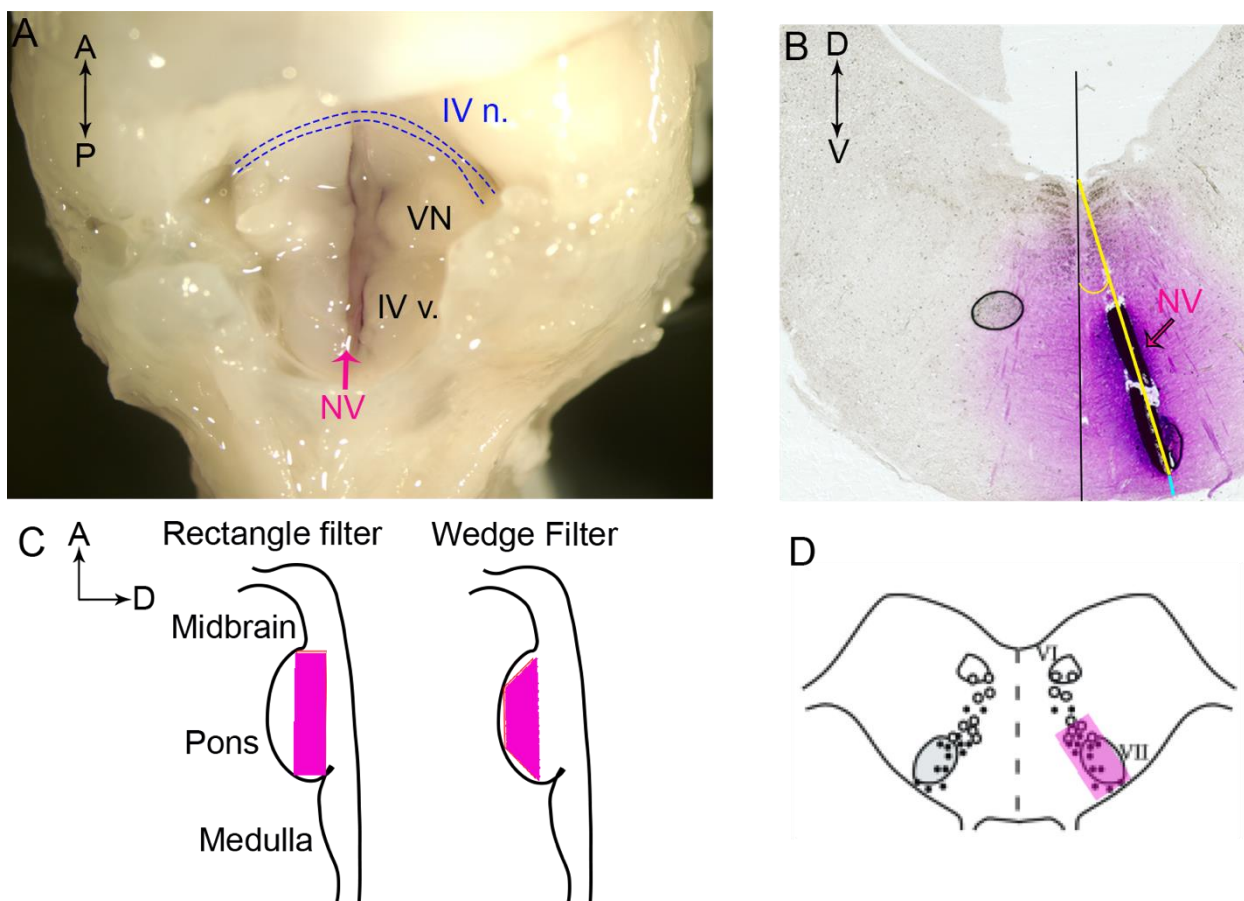


Figure 2.8 NeuroVue filter implants

(A) The cerebellum was removed to expose the dorsal surface of midbrain, pons, and medulla. The filter was placed parallel to the midline below the IVth cranial nerve (IV n., outlined in dotted blue lines). In the example shown here, bilateral implants were inserted along the entire anterior-to-posterior axis of the pons (0-100% A-P). The magenta arrow indicates the left NeuroVue implant. (B) A cross section of a hindbrain shows the location of the NeuroVue implant (magenta arrow) relative to the midline (black line). The angle of the filter (yellow) and the depth of the filter from the ventral edge (cyan line) were measured using ImageJ. (C) A lateral view of the midbrain and hindbrain with the cerebellum removed illustrates the approximate location of the filters. Wedge shape filters (magenta, right) were preferred over rectangle (magenta, left) shaped filters as they could be pushed further ventrally into the pons. (D) Previous work has shown the location of the auditory (closed circles) and vestibular efferents (open circles) relative to the facial brachial motor nucleus (VII) and the abducens motor nucleus (VI). The goal was to implant the filter (magenta rectangle) at an angle and depth appropriate to target the auditory efferent cell bodies. Image A was provided by Donna Fekete. Image D was modified from Simmons (2002). Abbreviations: A, anterior; D, dorsal; IV v, fourth ventricle; P, posterior; V, ventral; VN, vestibular nucleus.

Brainstems with the implant were extracted, embedded, cryosectioned, and imaged. To determine what combination of variables (incubation time/temperature, filter size/shape, and filter

placement) resulted in the most successful labeling of efferents in the BP and cochlear ganglion, NIH ImageJ software was used to analyze the filter angle and depth of the filter (Fig. 2.8 B & D). A detailed list of the variables that were recorded and analyzed can be found in tables 7.1 and 7.2.

NeuroVue lipophilic tracer dyes have been previously used to detect auditory and vestibular efferents and afferents in the mouse inner ear (Duncan *et al.*, 2011; Fritzsche *et al.*, 2005).

2.11 Microscopy

All brightfield images were taken using a Nikon Eclipse E800 photomicroscope with a SPOT Flex digital camera or a SPOT Insight CMOS camera. Fluorescent images were taken on the Nikon Eclipse with one of the cameras listed above or a Nikon Eclipse 90i confocal microscope. On the Nikon photomicroscope, images of cross sections of the CD were usually taken using the 20X lens and images focusing on only the prosensory/sensory domain were taken with a 40X or 60X lens. Whole mount CDs were usually imaged using a 10X lens. On the Nikon confocal microscope, cross sections of the CD were usually imaged using a 20X lens. Images focusing on the prosensory/sensory domain used a 60X lens. For NeuroVue labeled whole mounts, cochlear ganglia were imaged using a 20X lens and BPs were imaged with a 40X and/or 60X lens. For images of sectioned BPs, images were taken at approximately 25%, 50%, and 75% along the total length of the BP. Images in the subsequent chapters of sectioned BPs were taken at approximately 50% along the total BP length, unless stated otherwise in the figure legend.

CHAPTER 3. WNT9A OVEREXPRESSION AND KNOCKDOWN IN THE CHICKEN BASILAR PAPILLA

Data from this chapter have been published:

Munnamalai, V., Sienknecht, U. J., Duncan, R. K., **Scott, M. K.**, Thawani, A., Fantetti, K. N., Atallah, N. M., Bieseimer, D. J., Song, K. H., Luethy, K., Traub, E., Fekete, D. M. (2017). Wnt9a can influence cell fates and neural connectivity across the radial axis of the developing cochlea. *The Journal of Neuroscience*, 1554-1517.

3.1 Wnt signaling and inner ear development

The Wnt family of proteins are secreted ligands that bind to Frizzled transmembrane receptors. The ligands, receptors, co-receptors, and available intracellular signaling components influence the signaling pathways through which each Wnt can signal, and thus the functional outcome of signaling (Dale, 1998; Huelsken & Birchmeier, 2001; van Amerongen & Nusse, 2009). In the canonical pathway, binding between a Wnt and its receptor indirectly causes the stabilization of β -catenin, which then translocates to the nucleus and regulates transcription (Clevers & Nusse, 2012; Huelsken & Birchmeier, 2001). The other signaling pathways involve intracellular calcium release (Kohn & Moon, 2005; Slusarski *et al.*, 1997) or activation of RhoA (Dale, 1998; Mlodzik, 2002) and can impact the actin cytoskeleton and PCP. Wnt signaling can also impact patterning, cell fate specification, morphogenesis, and proliferation (Huelsken & Birchmeier, 2001; Munnamalai & Fekete, 2013).

Wnt signaling has multiple roles in inner ear development (Munnamalai & Fekete, 2013). Previous work in the developing chicken BP (Jacques *et al.*, 2014), zebrafish lateral line (Jacques *et al.*, 2014), and mouse organ of Corti (Jacques *et al.*, 2012; Munnamalai & Fekete, 2016) support that Wnt/ β -catenin signaling upregulates the proliferation of cells within the prosensory domain and biases the types of hair cells that differentiate. Similarly, overexpression of activated β -catenin in the chicken BP induces ectopic patches of vestibular hair cells in the basilar papilla (Stevens *et al.*, 2003). These studies, however, do not evaluate the effects (either direct or indirect) of Wnts on afferent and efferent innervation of the BP.

A detailed survey of the spatial and temporal expression patterns of Wnt ligands, their receptors and inhibitors in the developing chicken inner ear showed that *Wnt9a* (previously known as Wnt14) was expressed along the neural edge of the BP from E4 through E12 (Sienknecht & Fekete,

2008, 2009)(Fig. 1A). Given that Wnts are secreted ligands, it was predicted that Wnt9a ligand was present in a gradient highest on the neural side and lowest on the abneural side of the BP. During these time points, proliferation (Katayama & Corwin, 1989), differentiation (Cohen & Cotanche, 1992; Cohen & Fermin, 1978; Cotanche & Sulik, 1983), and innervation (Whitehead & Morest, 1985a) are occurring in the chicken BP.

Based on this, it was hypothesized that a gradient of Wnt9a ligand was instructive for the neural-side identity and was involved in patterning and innervation along the radial axis of the BP. Other work from the Fekete lab complementing the experiments described in this dissertation found that when *Wnt9a* was overexpressed in the BP, an increase in width along the radial axis of the BP was observed along with an increase in the number of cells that take on the neural-side identity at the expense of those taking on the abneural-side identity (Fig. 1.2). Complementing this, an increase in ribbon bodies (pre-synaptic components of the afferent synapses) was observed in the BP as well as a disruption in efferent organization. Given that E4 cochleovestibular ganglion neurites had been previously shown to be unresponsive to Wnt9a and other Wnts (Fantetti, 2011; Fantetti *et al.*, 2011), it was unlikely that Wnt9a was acting directly as a guidance factor for afferents. Instead, we predicted that Wnt9a acts upstream of an axon guidance cue, which can influence radial innervation by upregulating cues attractive to afferents on the neural side or downregulating cues repulsive to afferents on the abneural side (Fig. 1.2 C). This work and the work described in the subsequent sections of this chapter were published in *The Journal of Neuroscience* (Munnamalai *et al.*, 2017).

3.2 Knock down of Wnt9a using small-interfering RNA

As previously described, we hypothesized that *Wnt9a* present on the neural side of the BP is instructive for the neural-side identity through diffusion of the encoded protein across the sensory epithelium (Fig. 1.2 C). Previous work in the Fekete lab had shown an increase in tall HCs and afferent innervation across the radial axis of the BP when *Wnt9a* was overexpressed (Fig. 1.2). To complement these experiments, we attempted to knock down *Wnt9a* using siRNAs. We expected an increase in the abneural-side identity at the expense of the neural-side identity (Fig. 1.2).

To knock down *Wnt9a*, we inserted siRNAs designed to target coding regions of the *Wnt9a* transcript into a MOEC; the insert should fold into a shRNA that would then be processed by miRNA biogenesis machinery (Dicer and Drosha) into a siRNA. We tested RCAS(Y) and

RCAN(X) avian retroviruses as well as Tol2-mediated gene transduction technology for their ability to deliver these shRNAs to the developing inner ear. Detailed descriptions of the construction of the shRNAs and each of these delivery strategies are found in chapter 2.

3.2.1 Delivery of si*Wnt9a* using viral-mediated gene transduction

We attempted to use avian retrovirus to deliver siRNA to knock down *Wnt9a*. For the results discussed in this section, information on replicates can be found in figure 3.1 legend. The results suggest that both of the viral-mediated gene transduction methods, RCAS(Y) and RCAN(X), failed to induce robust knock down *Wnt9a* in both *in vivo* and *in vitro* experiments. *In situ* hybridization of strongly infected (indicated by 3C2 immunolabels) whole mount (Fig. 3.1) and sectioned (Fig. 3.1 B) BPs showed little to no reduction of *Wnt9a* transcripts. Similarly, RT-qPCR results for RCAS-si*Wnt9a* did not show a reduction in *Wnt9a* levels in infected DF-1 chicken fibroblasts (Fig. 3.1 C).

A modest knockdown of *Wnt9a* transcripts was observed in DF-1 cells infected with RCAN-si*Wnt9a*-2; however, this reduction was not observed in BPs infected with RCAN(X)-si*Wnt9a*-2 (Fig. 3.1 C). This discrepancy could be due to the fact that cDNA transcribed from CDs was from the six pooled CDs. If any of the pooled CDs were not strongly infected, this could have lessened the observed effect of the knock down. In the RT-qPCR experiments for siRNA infected CDs, we also used primers designed to amplify the si*Wnt9as* (table 2.8) (Varkonyi-Gasic *et al.*, 2007). With these primers, the amplification curves produced from the RT-qPCR do show that the si*Wnt9as* were expressed for each of the conditions we tested (data not shown). Given that the primers used to reverse transcribe cDNA for this experiment were designed to reverse transcribe small RNAs (Varkonyi-Gasic *et al.*, 2007), we speculate that this detected the siRNA and not just the genomic viral RNA. We speculate that either the viral transcripts were not processed into functional siRNAs or that the siRNAs produced were not able to effectively knock down *Wnt9a*.

In addition to examining E6 and E7 BPs for reductions in *Wnt9a*, we also examined E16 BPs for changes in HC morphology and innervation. In support of the results from *in situ* hybridization and RT-qPCR, no change in phenotype was observed at E16 (Fig. 3.1 D). This could be due to the presence of other molecules that are functioning redundantly to ensure a robust normal phenotype or that RCAS(Y) and RCAN(X) retroviruses carrying si*Wnt9a* are ineffective tools to knock down *Wnt9a*.

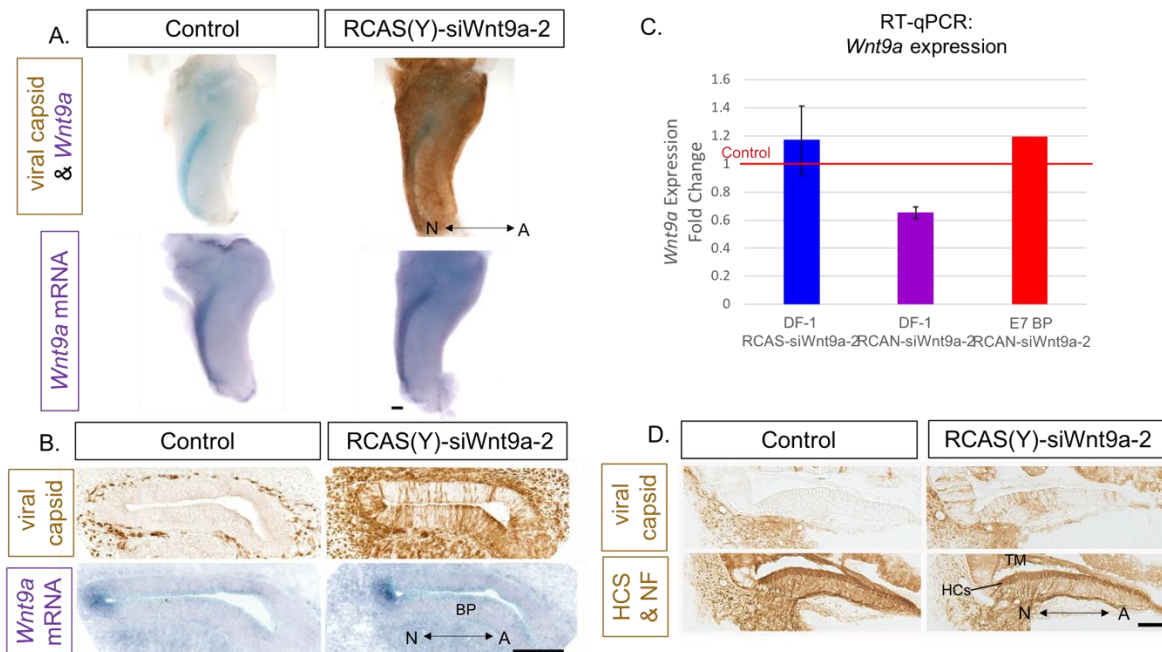


Figure 3.1 *Wnt9a* knock down using retrovirus to deliver siRNA

RCAS(Y) and RCAN(X) retroviruses were used to deliver siWnt9a to the BP. Because the results for each siWnt9a were similar, the results depicted in this figure are for siWnt9a-2 only. The methods depicted in this figure were used to analyze results for siWnt9a-1, -2, and -3. (A) E6 infected and control CDs were dissected and labeled for *Wnt9a* transcripts (bottom) followed by an immunolabel for viral capsid protein (3C2, top). Little to no knock down was observed for each siRNA. Replicates: RCAS-siWnt9a-2, n= 3; RCAS-siWnt9a-3, n=1. Scale bar = 100 μ m. (B) Infected embryos were harvested at E6 and sectioned. Infected right ears were compared to uninfected, control left ears. Alternate sections were labeled for viral capsid protein (top) and *Wnt9a* transcripts (bottom). There was no obvious reduction in *Wnt9a* for any of the siRNAs tested. Replicates: RCAS(Y)-siWnt9a-1, n=3; RCAS(Y)-siWnt9a-2, n=18; RCAS(Y)-siWnt9a-3, n=9. Scale bar = 200 μ m. (C) RT-qPCR was also used to detect *Wnt9a* transcripts after retroviral delivery of siWnt9a to chicken fibroblasts (DF-1) *in vitro* or inner ears *in vivo*. While a modest knock down was observed in DF-1 chicken fibroblasts infected with RCAN-siWnt9a-2, no knock down was observed in E7 BPs infected with the same virus. Biological replicates: DF-1 RCAS(Y)-siWnt9a-1, -2, -3, n=3; DF-1 RCAN(X)-siWnt9a-2, n=3; BP RCAN(X)-siWnt9a-2, n=1. (D) We also examined the phenotype of hair cell morphology and afferent innervation in control and infected E16 BPs. While the *Wnt9a* expression domain appeared to be infected, we did not observe a change in hair cell morphology or afferent innervation for any of the siWnt9as tested. Replicates: RCAS (Y)-siWnt9a-2, n=2; RCAN-siWnt9a-2, n=3. Scale bar = 100 μ m.

3.2.2 Delivery of siWnt9a using tol2 transposase-mediated gene transduction

After obtaining little evidence that the RCAS-siRNA delivery strategy was able to knockdown *Wnt9a* in embryos, we explored an alternative approach that should also integrate the transgene into the DNA, where it would then transcribe siRNAs. This approach utilizes Tol2 transposase to

insert siRNA-encoding plasmids that carry Tol2 terminal repeat sequences. We created *Wnt9a*-siRNA expression vectors based on the Tol2-CAG-GFP plasmid. Using electroporation to deliver the Tol2 and transposase plasmids to the otic cup or otocyst, it was challenging to target the neural edge of the BP where *Wnt9a* is expressed. Many embryos were electroporated in order to get a few replicates with successful targeting to the *Wnt9a*-expression domain. In the instances where the *Wnt9a* domain was targeted, as indicated by GFP localization shown in figure 3.2 A and B (top), little to no reduction in *Wnt9a* was observed (Fig. 3.2 B, middle). Serrate (*Ser1*) transcripts increase in the presence of exogenous *Wnt9a* at E7 (Munnamalai *et al.*, 2017); therefore it was expected that *Ser1* would decrease if *Wnt9a* was knocked down. We observed minimal to no reduction in *Ser1* protein or mRNA (Fig. 3.2 A & B, bottom). We therefore concluded that Tol2-CAG-GFP plasmid carrying si*Wnt9a* was an unreliable tool to knock down *Wnt9a* or that other molecules present serve a redundant function as *Wnt9a*.

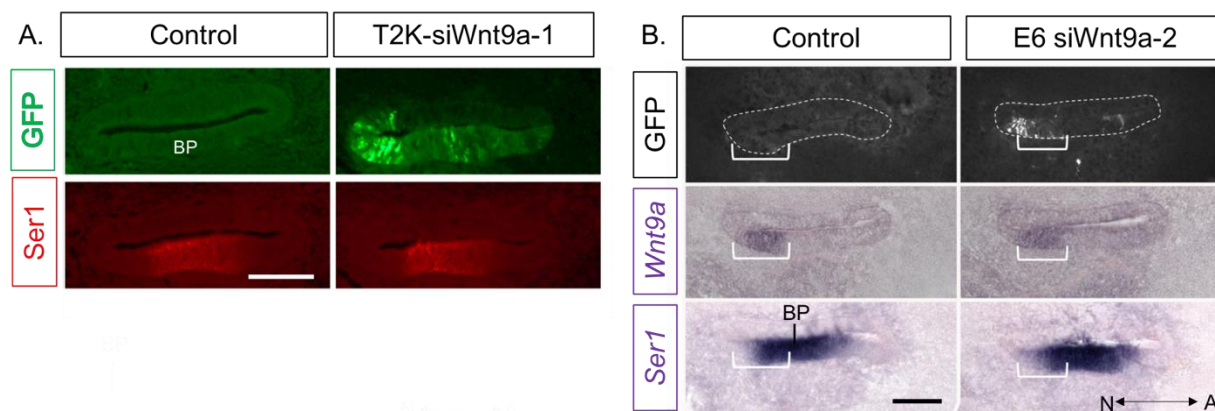


Figure 3.2 *Wnt9a* knock down using Tol2-mediated gene transduction

Cells that have integrated the si*Wnt9a* and GFP into their genome can be detected with an anti-GFP antibody (A & B, top). In cells where the *Wnt9a* expression domain has been targeted, little to no reduction of *Wnt9a* transcripts is observed (B, middle). No change in *Ser1*, a gene downstream of *Wnt9a*, is detected using immunofluorescence or *in situ* (A & B, bottom). Images are from an E7 embryo. Replicates: T2K-CAG-si*Wnt9a*-3, n=1; T2K-CAG-si*Wnt9a*-2, n=4. Scale bars = 100 μ m.

3.3 RNA deep sequencing in *Wnt9a*-overexpressing BPs

RNA deep sequencing was performed comparing BPs infected with RCAS(A)-*Wnt9a* and RCAS(A) parent virus (see Chapter 2 for details on experimental methodology). The results identified axon guidance genes summarized in figure 3.3. *Sema3F* and *Efna5* had been previously

shown to influence radial innervation in the mouse (Coate *et al.*, 2015; Defourny *et al.*, 2013); however, RNA sequencing results did not report a significant difference in expression levels between the experimental and control groups (Fig. 3.3 A). When we attempted to validate these RNA sequencing results using RT-qPCR, we observed a reduction for both genes in the presence of exogenous *Wnt9a*. Despite the fact that all replicates showed a reduction in expression, there was a lot of variability between each replicate (Fig. 3.3 B). We attempted to validate other genes using RT-qPCR as well (data not shown) but observed high variability between replicates each time. This high variability between biological replicates is discussed in chapter section 3.4.

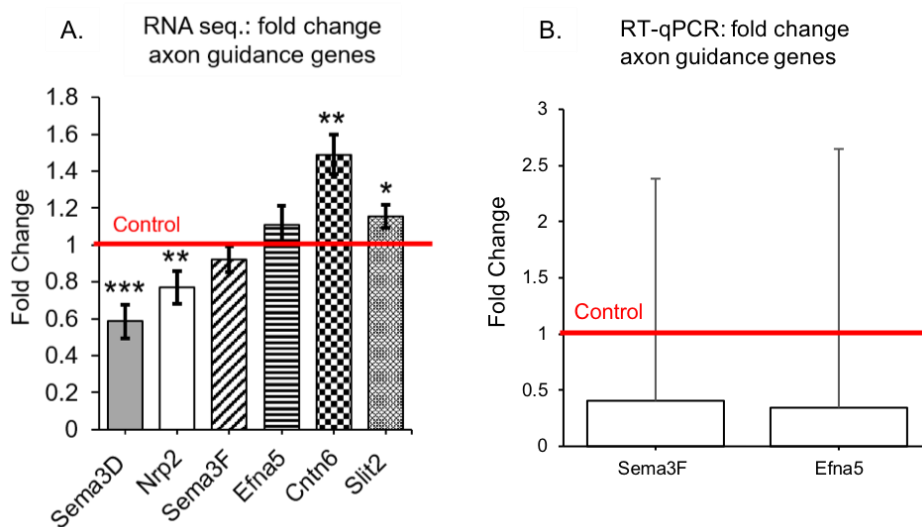


Figure 3.3 Differentially expressed axon guidance factors

(A) RNA deep sequencing of RCAS(A)-*Wnt9a* and RCAS(A) control BPs identified axon guidance genes such as *Sema3D*, *Nrp2*, *Cntn6*, and *Slit2* that were differentially expressed between the control and experimental groups (n=3). Two genes previously shown to influence radial innervation in the mouse cochlea, *Sema3F* and *Efna5*, were not differentially expressed in our RNA sequencing data set (B); nonetheless they appeared to be down regulated by *Wnt9a* overexpression using RT-qPCR. For RT-qPCR experiments, each replicate (n=2) showed a reduction in *Sema3F* and *Efna5* but to varying degrees. This resulted in a large standard error. *P<0.005, **P<1X10⁻¹⁵, ***P<1X10⁻¹⁵.

RNA sequencing results also identified differentially expressed genes that have been previously shown to impact axon guidance in other literature (literature reviewed in Chapters 4-6); however, these genes had not been previously examined for their impact of radial innervation in the inner ear. To determine how these genes downstream of *Wnt9a* impact radial innervation and inner ear development, we examined the spatial expression of several of these genes and, in

some cases, attempted to overexpress them. The results of these experiments are described in the subsequent chapters.

Another transcript we validated using *in-situ* hybridization was *Ser1*. *Ser1* is a Wnt target gene that is expressed across the prosensory domain of the BP. Prior to performing RNA sequencing, *Ser1* had been shown to increase in the presence of ectopic *Wnt9a* in the E7 chicken BP by Vidhya Munnamalai (Fekete Lab) using *in situ* hybridization (n=3-5 embryos). Unexpectedly, RNA sequencing indicated that *Ser1* was unchanged between controls and *Wnt9a*-overexpressing E6 BPs. In accordance with our RNA-sequencing results, *Ser1 in situs* and immunolabels at E6 performed by myself and Vidhya Munnamalai showed little to no increase in *Wnt9a*-infected BPs compared to controls (n=4-7 embryos). This suggests that *Ser1* is not upregulated in response to ectopic *Wnt9a* until E7.

A summary of more differentially expressed genes can be found in Munnamalai *et al.* (2017). Additionally, the complete data set for RNA sequencing can be found at the Gene Expression Omnibus database (GEO accession # GSE95295).

3.4 Discussion

3.4.1 si*Wnt9a* is ineffective to knock down *Wnt9a* in the chicken inner ear

Despite the fact that RCAS(Y) and RCAN(X) avian retroviruses carrying si*Wnt9a* were able to successfully infect the BP *in vivo* and DF-1 cells *in vitro* (Fig. 3.1), these viruses were unsuccessful in producing a robust knock down of *Wnt9a* in the chicken BP or DF-1 cells. In the RCAS virus, we were concerned that the splice acceptor after the *env* gene could interfere with the splicing of the artificial intron, thus we also attempted shRNA deliver using the RCAN virus. The RCAN retrovirus is similar to RCAS but lacks a splice acceptor after the *env* gene (Fig. 2.1 D) and had previously been used to deliver small non-coding RNAs to knock down genes necessary for the replication of Marek's disease virus and herpes virus of turkeys (Bromberg-White *et al.*, 2004; Chen *et al.*, 2008). These data suggest that RCAN(X) is capable of delivering small non-coding RNAs.

We additionally attempted to use Tol2 transposase-mediated gene transduction to deliver siRNAs. When we were able to target the *Wnt9a*-expression domain using electroporation, we did not observe a robust decrease in *Wnt9a* or *Ser1* (downstream of *Wnt9a*). T2K-CAG-GFP plasmids

had been previously used to successfully overexpress miRNAs by Zhang *et al.* (2015). This suggests that Tol2 plasmids are able to deliver small non-coding RNAs.

Both retroviral and Tol2 transposase methods of gene transduction had been previously used to deliver small noncoding RNAs. Infection and RT-qPCR data for the viruses and GFP localization for Tol2 plasmids suggest that both of these delivery methods were functioning properly and that shRNA was likely being transcribed. We speculate that either transcripts from the artificial intron were not processed into functional siRNAs or that the siRNAs were produced but were unable to knock down *Wnt9a*.

3.4.2 RNA deep sequencing identified axon guidance genes downstream of *Wnt9a*

RNA sequencing of RCAS(A)-*Wnt9a* and RCAS(A) parent virus infected BPs identified axon guidance genes (Fig. 3.3 A) and other genes (Munnamalai *et al.*, 2017) downstream of *Wnt9a*. We hypothesized that axon guidance genes that decreased in the presence of exogenous *Wnt9a* would be expressed on the abneural side of the BP and function in repelling afferents or attracting efferents. Conversely, we expected that axon guidance factors that increased in the presence of exogenous *Wnt9a* would be expressed on the neural side of the BP and function in attracting afferents or repelling efferents (Fig. 1.2). To test this, we examined the expression patterns of these genes and in some cases attempted to overexpress these genes. These experiments are described in the subsequent chapters.

We attempted to validate differentially expressed genes from the RNA sequencing data set using RT-qPCR. In the RT-qPCR experiments, we observed large variability between replicates, making it difficult to use this method to validate results. In some cases, there were even discrepancies between RNA sequencing and RT-qPCR results. The variability between replicates in RT-qPCR experiments as well as the discrepancies between RNA sequencing results and RT-qPCR could be due to differences in experimental methodology. For RNA sequencing each biological replicate was made up of 24 pooled BPs to insure adequate amounts of total RNA, including small RNAs. For RT-qPCR, we did not examine small RNAs and less RNA per sample was required. In some cases, as few as four BPs were pooled in each replicate. Infection and *Wnt9a* expression levels can vary in each embryo. A single biological replicate consisting of many BPs (RNA sequencing) with varying levels of infection may result in less variability between biological replicates when compared to biological replicates consisting of fewer BPs (RT-qPCR).

The collection and preparation of one biological replicate (24 pooled BPs) for RNA sequencing required the effort of three investigators (myself, Donna Fekete, and Ankita Thawani) for a full day. Given the time and manpower to collect these samples, we elected not to pool this many BPs for RT-qPCR experiments. We instead validated RNA sequencing data using *in situ* hybridization on RCAS(A)-*Wnt9a* infected BPs. These data are described in chapters 4-6 of this dissertation and in Munnamalai *et al.* (2017).

CHAPTER 4. EXPRESSION AND MISEXPRESSION OF SLIT2 LIGAND AND ROUNDABOUT RECEPTOR

4.1 Slit-Robo Signaling and Inner Ear Development

Slit secreted ligands are most commonly known for their repulsive axon guidance effects on Robo transmembrane receptor-expressing neurites (Brose *et al.*, 1999; Dickson & Gilestro, 2006). In the mouse oC, Slit2 is secreted from the nonsensory medial wall (the spiral limbus and the greater epithelial ridge) while Robo receptors are present in the cochlear ganglion. In wild type mice, cochlear ganglion neurites extend projections peripherally to innervate the oC while the cell bodies remain in the ganglion. In *Slit2*^{-/-} and *Robo1*^{-/-}; *Robo2*^{-/-} mice, some cochlear ganglion neurons extend projections to the oC while other neuronal cell bodies migrate beyond the cochlear ganglion to reside closer to the cochlear epithelium (Wang *et al.*, 2013). These data support the idea that Slit/Robos are important for confining cochlear ganglion neuronal cell bodies to the cochlear ganglion.

In the chicken inner ear and cochleovestibular ganglion, the expression of *Slits* and *Robos* were previously reported by Holmes and Niswander (2001) and Battisti and Fekete (2008); however, expression patterns across the radial axis are unclear from these data. In the chicken embryo, another study found that the afferent neurites that project towards and eventually innervate the anterior cristae are repelled when Slits are ectopically expressed; however, no evidence was found that cochleovestibular ganglion neurites responded to purified Slit proteins when they were cultured *in vitro* in the presence of purified Slit protein (Battisti *et al.*, 2014). This suggests that the majority of cochleovestibular ganglion neurites, such as those that innervate the BP, are most likely unresponsive to Slit. Since *Slit2* does not appear to influence the outgrowth of the majority of cochleovestibular ganglion neurites, it may have another function in the BP.

RNA sequencing experiments show that *Slit2* transcripts are modestly increased by 1.2 fold when *Wnt9a* is over-expressed (Fig. 3.3 A). Slit-Robo signaling has previously been shown to activate β -catenin signaling. This occurs when the binding of Slit to Robo induces the binding of Robo-associated Abelson (Abl) kinase to N-cadherin associated β -catenin. This results in the phosphorylation of β -catenin at tyrosine⁴⁸⁹ (PY⁴⁸⁹- β -catenin), dissociation of β -catenin from N-cadherin, and subsequent nuclear localization of β -catenin (Rhee *et al.*, 2007; Rhee *et al.*, 2002).

Preliminary data from our lab suggested a radial gradient across the BP (high neurally) of PY^{489} - β -catenin (Fig. 4.1). This suggested the possibility that *Slit2* may contribute to β -catenin signaling in the BP. In addition to this, Slit/Robo signaling has been shown to suppress proliferation and influence cellular morphology (decrease process length and branching) in cortical interneurons (Andrews *et al.*, 2008). This suggested that it could also be involved in regulating proliferation or morphology of cells in the BP. We hypothesized that *Slit2* may influence radial identity of the BP by increasing the activity of the transcription factor TCF through this non-canonical Abl-mediated activation of β -catenin.

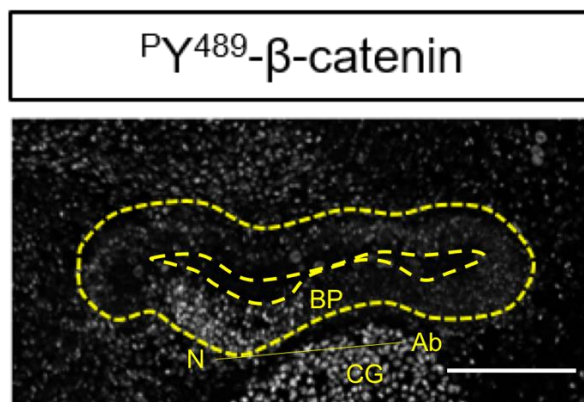


Figure 4.1 Slit activated β -catenin in the BP

An immunolabel for phosphorylated β -catenin in the normal BP indicates that it localizes to the neural side of the BP and in the ganglion. The CD is outlined in yellow. This image was provided by Ankita Thawani. Abbreviations: Ab, abneural; CG, cochlear ganglion; N, neural.

4.2 Expansion of *Slit2* expression domain in the presence of ectopic *Wnt9a*

To validate the 1.2-fold increase in *Slit2* reported by the RNA sequencing, we used *in situ* hybridization to examine the spatial expression pattern of *Slit2* in control and RCAS(A)-*Wnt9a* infected BPs (Fig. 4.2). In control BPs, we found two distinct *Slit2* domains: one located on the neural edge of the BP overlapping with the *Wnt9a* domain, and another on the nonsensory abneural wall of the CD. Both domains have minimal to no overlap with Ser1 (marker for the prosensory domain) suggesting that they both occur in the nonsensory tissue of the CD. When *Wnt9a* is overexpressed, we did not observe an upregulation in *Slit2* expression. Instead, it appears that the 1.2-fold increase is due to an expansion in the *Slit2* domain as a result of an overall increase in the total width of the BP. Therefore, *Slit2* is likely not acting downstream of *Wnt9a*.

To determine if β -catenin activation was impacted by the increased size of the *Slit2* domain, we also examined PY489 - β -catenin in control and RCAS(A)-*Wnt9a* BPs. We did not observe a change in the localization of PY489 - β -catenin (Fig. 4.2). Also, of note, in two of our three replicates, the gradient (high neurally) of PY489 - β -catenin on the control sides was not as distinct as what was observed in figure 4.1. This antibody required an antigen retrieval step by boiling slides in citric acid. The strength of the antibody labeling may be highly impacted by the efficiency of this step.

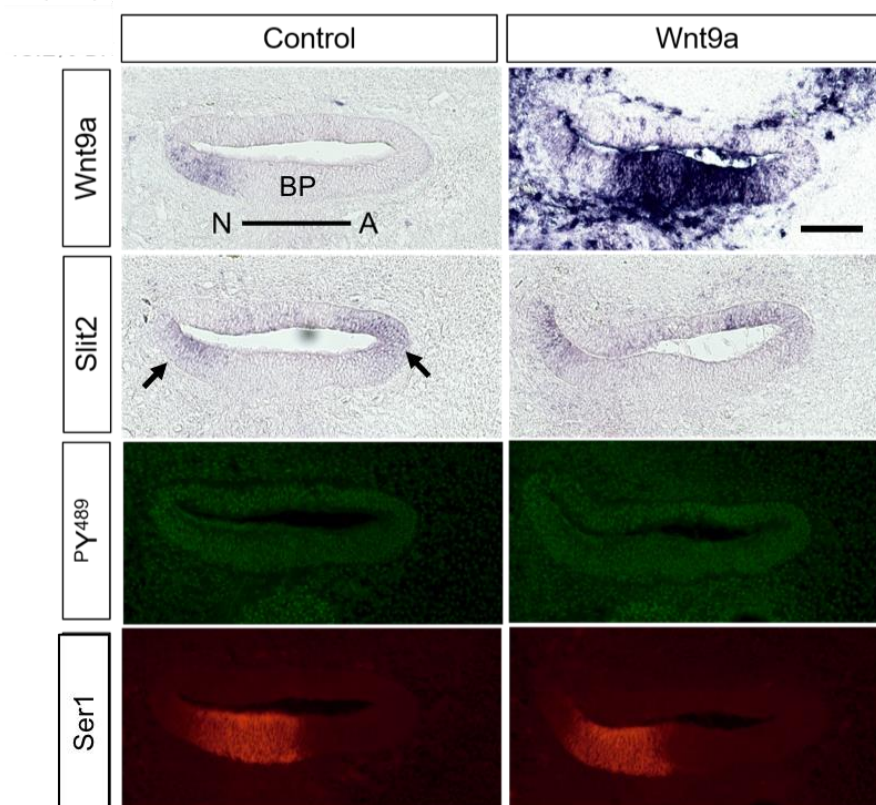


Figure 4.2 *Slit2* expression in the presence of ectopic *Wnt9a*

When *Wnt9a* is overexpressed (right), the width of the BP expands along the radial axis when compared to control uninjected BPs (left). As a result, the *Slit2* domains present on neural (N) edge of the BP and on the posterior nonsensory wall of the CD increase in size. Based on this data, it does not appear that *Slit2* is upregulated in response to *Wnt9a* overexpression. In addition, there are no discernable changes in PY489 - β -catenin or Ser1 when comparing controls to RCAS(A)-*Wnt9a* CDs. Images are from alternate sections of a HH stage 29 (E6) embryo. N=3. Scale bar = 100 μ m.

4.3 Radial expression of *Slit2* and *Robos*

Although *Slit2* does not appear to act downstream of *Wnt9a* (Fig. 4.2), new insights into *Slit2* expression in the chicken CD were gained by examining radial cross sections. We additionally examined radial expression of *Robo1* and *Robo2*. These data are presented in figure 4.3.

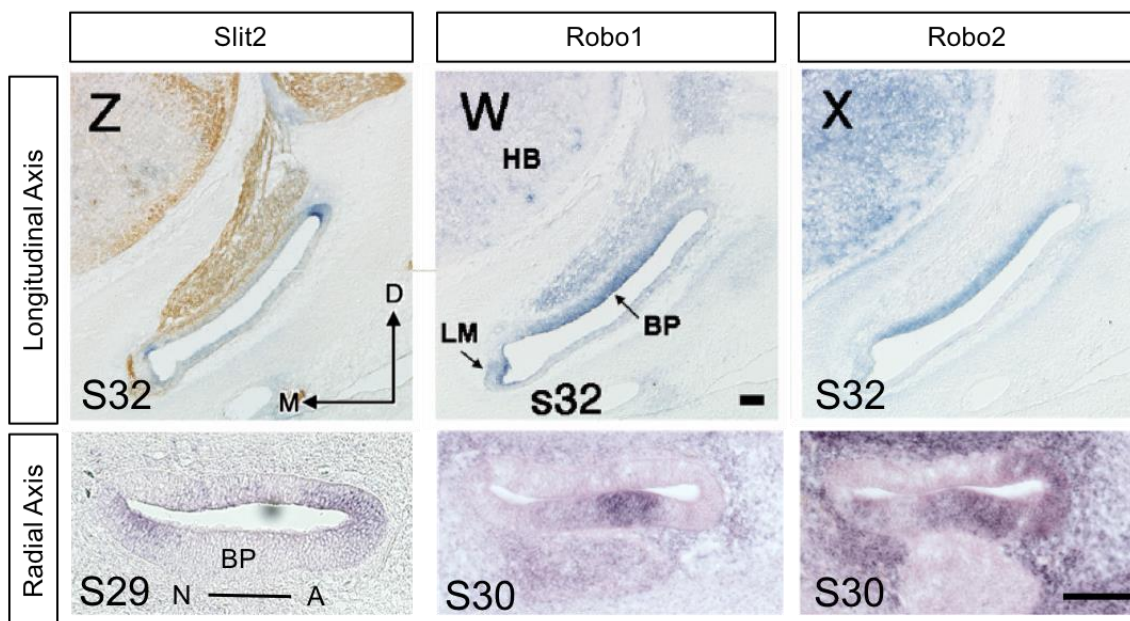


Figure 4.3 Expression of *Slit2*, *Robo1*, and *Robo2*

Images of longitudinal cross sections are from Battisti and Fekete (2008) and show expression for HH stage 32 (E 7.5). Scale bar = 100 μ m (top). Radial cross sections show expression data for HH stage 29-30 (E 6.5). Scale bar = 100 μ m (bottom). Expression is shown for *Slit 2* (left), *Robo1* (middle), and *Robo2* (right).

Slit2 in situ hybridization on longitudinal cross sections had identified *Slit2* in the LM and SM but not in the CD (Battisti & Fekete, 2008). Radial cross sections identify *Slit2* expression domains on the neural and abneural nonsensory walls of the CD. For *Robo1*, longitudinal cross sections showed transcripts in the BP and in the cochlear ganglion (Battisti & Fekete, 2008). Our data from radial cross sections concur with this, but also show graded *Robo1* expression highest on the abneural side. Longitudinal cross sections also show *Robo2* expressed in the BP (Battisti & Fekete, 2008); however, a radial view also shows graded *Robo2* expression highest on the abneural side and *Robo2* in the abneural nonsensory wall of the CD.

4.4 Misexpression of *Slit2* in the CD

To determine the function of *Slit2* expressed in the nonsensory CD, we misexpressed hSlit2 by co-electroporating pEF-hSlit2 and pEF-GFP plasmids into the inner ear. Despite robust localization of GFP across the prosensory domain of the BP, we did not observe any changes in the ganglion (Fig. 4.4, NF), innervation of the BP (Fig. 4.4, NF), activated β -catenin localization (Fig. 4.4, ^PY⁴⁸⁹), or proliferation (Fig. 4.4, PH3). Similar to β -catenin localization in figure 4.2, we did not see a distinct gradient of ^PY⁴⁸⁹ β -catenin in any of our replicates. This made it difficult to assess the effect of exogenous Slit2 on β -catenin activation. We attempted to examine innervation and hair cell morphology at older ages; however, due to the transient expression of the plasmid, GFP expression was weak or absent in older ages, making it difficult to assess the success of the electroporation.

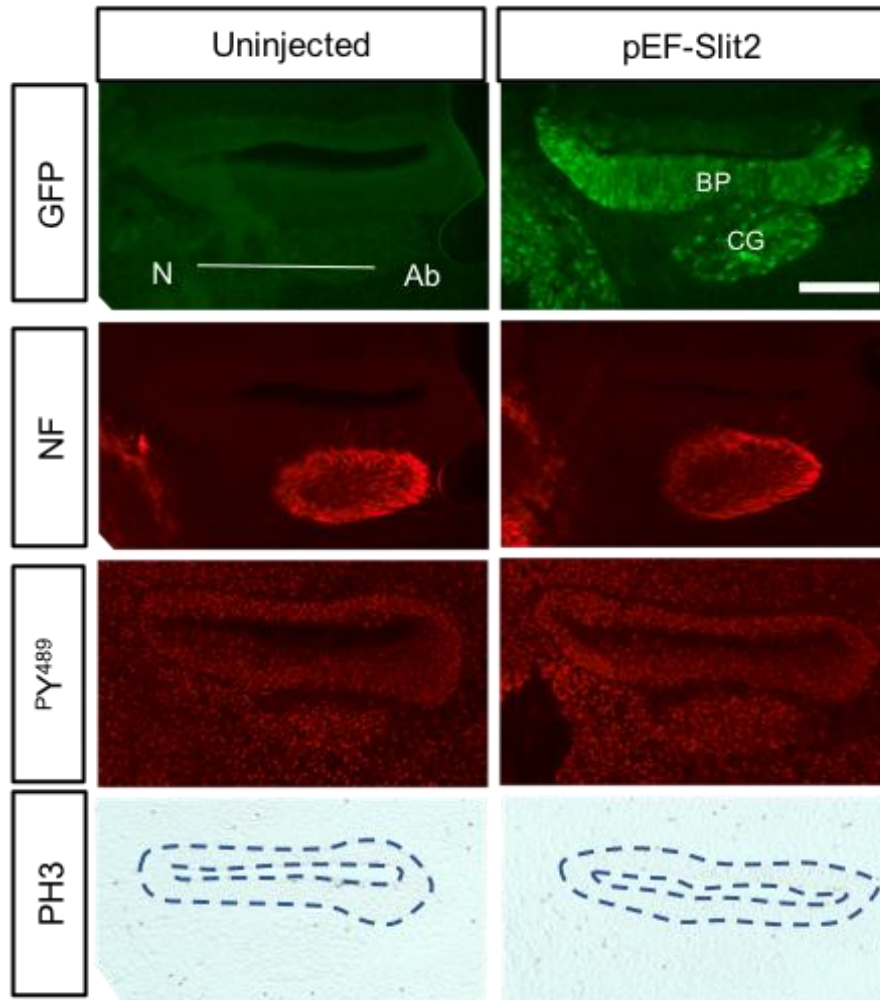


Figure 4.4 Misexpression of Slit2

pEF-hSlit2 and pEF-GFP plasmids were co-electroporated into right ears to misexpress Slit2 (right). Left ears were unelectroporated controls (left). Cells targeted by the electroporation are positively labeled for GFP. The cochlear ganglion and its neurites are indicated with neurofilament associated protein (NF) in red. ^PY⁴⁸⁹-β-catenin (^PY⁴⁸⁹) labels for activated β-catenin in the red. Phosphohistone3 (PH3) indicates proliferating cells in brown. Dotted blue lines outline the CD in brightfield images. Images are from alternate sections of an E6 embryo. N=3. Scale bar = 100 μm.

4.5 Misexpression of dominant-negative Robo1 in the CD

To determine the function of Robo1 receptor expressed in the prosensory domain of the BP and ganglion, we electroporated pCAG-Robo1(DN)-GFP into the inner ear. This plasmid carried a dominant-negative Robo1 where the intracellular domain of the single pass membrane-bound receptor was truncated and replaced with GFP, preventing it from signaling intracellularly

(Hammond *et al.*, 2005). When embryos were harvested and examined at E3 or E4, GFP was easily visualized; however, embryos harvested after this time point had weak or no visible GFP. This made it difficult to assess the success of the electroporation or determine the cells targeted by the electroporation. It is also possible that the dominant-negative Robo1 was only expressed at early ages. Although we could not assess GFP at later ages, we did observe a reduction in ganglion size at E6 in two out of the seven right electroporated ears (Fig. 4.5).

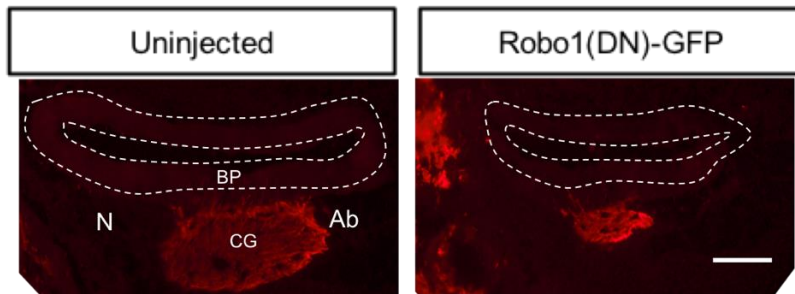


Figure 4.5 Misexpression of dominant-negative Robo1

pCAG-Robo1(DN)-GFP plasmid carrying a dominant-negative Robo1 was electroporated into the inner ear. Neurofilament-associated protein is labeled in red to visualize the cochlear ganglion and its neurites. We observed a reduction in ganglion size in 2 out of 7 embryos. Images are from an E6 embryo. Scale bar = 100 μ m.

4.6 Discussion

Given that *Slit2* expression levels do not increase in the presence of ectopic *Wnt9a*, it seems unlikely that *Slit2* is acting downstream of *Wnt9a*. The *Slit2* domains do appear to expand slightly in *Wnt9a* overexpressing CDs (fig. 4.2). We suspect that this and the 1.2-fold increase in *Slit2* reported in the RNA sequencing data are due to an increase in width that occurs in the presence of ectopic *Wnt9a* (Munnamalai *et al.*, 2017).

In situ hybridization showed that *Slit2* is expressed in the CD flanking the prosensory domain, while *Robo1* and *Robo2* are expressed in an abneural-to-neural gradient in the prosensory domain. Given that Slit can have repulsive effects on Robo-expressing neurons, it is tempting to speculate that *Robo1*-expressing cochlear ganglion neurites are channeled into the prosensory domain by repulsive *Slit2* cues in the flanking nonsensory tissue; however, Battisti *et al.* (2014) has shown that vestibulocochlear ganglion neurites do not respond to Slits in culture. The expression patterns also suggested that, while *Slit2* likely does not act downstream of *Wnt9a*, graded *Robo* expression in the prosensory domain and *Slit2* in the nonsensory CD suggest that Slit-Robo signaling could be involved in radial patterning of the BP. Given that Slit-Robo signaling had previously been

shown to influence migration of cochlear ganglion neurons (Wang *et al.*, 2013) and proliferation (Andrews *et al.*, 2008), we hypothesized that *Slits* and *Robos* expressed in the CD may be involved establishing or maintaining the ganglion or help balance proliferation in the BP.

Contrary to this hypothesis, we did not observe any changes in proliferation in the presence of ectopic Slit2 or any changes in activated β -catenin. We did not look for changes in hair cell morphology as this occurs at timepoints after the transient GFP reporter had faded. When a dominant-negative Robo1 was misexpressed we did see a reduction in ganglion size observed in some ears. This suggests that Robo1 may play a role in neuroblast delamination and migration to the ganglion. Battisiti and Fekete (2008) showed that Robo1 is expressed in the anteroventral otic epithelium, where the neuroblasts delaminate, and faintly in the ganglion at E2. *Slits1*, 2, and 3 are also expressed in the otic epithelium during the period when neuroblasts delaminate and migrate. It is possible that Slits in the epithelium repel Robo-expressing neuroblasts away from the epithelium. Given that we were unable to assess GFP, we are uncertain if the five unaffected embryos had good uptake of the plasmid in the otic epithelium or if this is an artifact of electroporation. Smaller ganglion sizes were not observed in embryos electroporated with other plasmids.

Further testing is required to elucidate the role of Slit-Robo signaling in the BP. Misexpression with a tool designed to induce long-term overexpression, such as RCAS retrovirus or Tol2 plasmids, will be required to better understand how *Slit2*, *Robo1*, and *Robo2* impact inner ear development.

CHAPTER 5. EXPRESSION OF CONTACTIN-6 IN THE BASILAR PAPILLA

5.1 Contactins

Contactins are glycosylphosphatidylinositol (GPI)-anchored cell adhesion molecules belonging to the immunoglobulin superfamily that can bind to Notch, other contactins, and cell adhesion molecules such as NrCAM, NCAM, and L1 (Shimoda & Watanabe, 2009). Contactins have been shown to induce neurite outgrowth in dorsal root ganglion neurons cultured *in vitro* (Gennarini *et al.*, 1991). In the retina, *Cntn2* targets subpopulations of retinal dendrites to the appropriate sublamina in inner plexiform layer (Yamagata & Sanes, 2012).

In the auditory system, patients diagnosed with autism spectrum disorder who carried mutations in CNTN5 or CNTN6 were more likely to have increased sensitivity to sound (hyperacusis) (Mercati *et al.*, 2017). *Cntn5* (also known as NB-2) was shown to be expressed throughout the auditory brainstem of rats (Ogawa *et al.*, 2001; Toyoshima *et al.*, 2009a) and mice (Li *et al.*, 2003). When *Cntn5* knockout mice were examined, a decrease in neural excitability was observed in the inferior colliculus compared to wildtype mice after pure-tone stimulation (Li *et al.*, 2003). *Cntn5* knockout mice also had decreased glutamatergic neurons in the medial nucleus of the trapezoid body, lateral superior olive, and ventral cochlear nucleus compared to wildtype controls and displayed increased auditory brainstem response wave latencies (Toyoshima *et al.*, 2009b).

RNA-sequencing results reported that *Cntn6* transcripts increased by approximately 1.5-fold (Fig. 3.3) when *Wnt9a* was overexpressed. While *Cntn5* expression has been reported in the auditory brainstem of postnatal mice, *Cntn6* (also known as NB-3) had not been extensively studied in the inner ear. We hypothesized that *Cntn6* would be expressed on the neural side of the BP and serve as an attractant, survival, or adhesive factor for neurites projecting to the neural side of the BP.

5.2 Low levels of *Cntn6* expression in the chicken inner ear

When we examined the spatial expression of *Cntn6* using *in situ* hybridization, we had trouble detecting *Cntn6* transcripts in both the control and *Wnt9a*-overexpressing BPs (Fig. 5.1). When

examining the transcript counts from our RNA sequencing results, we found an average of 147 transcripts in the BP when *Wnt9a* was overexpressed. *Cntn6* was barely expressed in the control BPs (average of 61 transcripts).

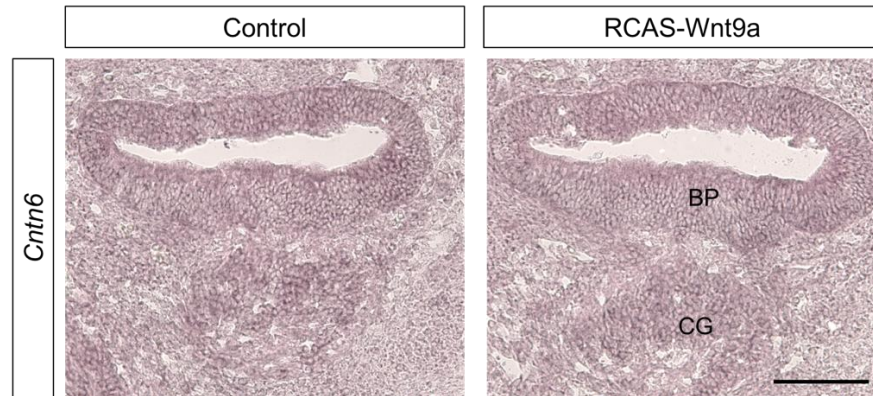


Figure 5.1 Low levels of *Cntn6* in *Wnt9a*-overexpressing and control BPs

In situ hybridization does not appear sensitive enough to detect endogenous expression of *Cntn6* or elevated levels of *Cntn6* after *Wnt9a* overexpression. Images are from an E6 embryo. N=2. Scale bar = 100 μ m.

5.3 Discussion

Given the low number of transcript copies detected by RNA sequencing even in the presence of ectopic *Wnt9a*, this method of *in situ* hybridization was not sensitive enough. So few transcripts are unlikely to make a large impact on patterning and innervation in the BP.

CHAPTER 6. CLASS 3 SEMAPHORINS AND THEIR RECEPTORS IN THE INNER EAR

A version of this chapter has been accepted for publication in the *Journal of Comparative Neurology*:

Scott, M. K., Yue, J., Biesemeier, D. J., Lee, J., Fekete, D. M. (2018). Expression of Semaphorins and their receptors in the developing chicken inner ear.

6.1 Semaphorin signaling

Semaphorins are most commonly known as axon guidance factors. There are eight classes of Semaphorins and each class has different affinities for different receptors; this adds diversity to Sema signaling and function. While RNA sequencing data indicate that there are multiple families for Semaphorins present in the BP at E6 (Munnamalai *et al.*, 2017), the work described in this chapter focuses on class 3 Semaphorins. Previous work in the mouse has shown that *Sema3F* plays a role in innervation in the inner ear during development (Coate *et al.*, 2015) and that *Sema3A* may be involved in maintaining innervation after birth (Salehi *et al.*, 2017). While *Sema3D* has not previously been examined for its role in inner ear development, it was shown to decrease in the presence of ectopic *Wnt9a* in our RNA sequencing data (Munnamalai *et al.*, 2017) (Chapter 3). Class 3 Semaphorins are secreted ligands and typically bind to a Neuropilin (Nrp) receptor and recruit a PlexinA (PlxnA) receptor to create an active holoreceptor (Zhou *et al.*, 2008). RNA sequencing data indicated that *Nrp1*, *Nrp2*, and *PlxnA1* were expressed in the E6 BP. Of these receptors, only *Nrp2* was differentially expressed between *Wnt9a*-overexpressing and control BPs (Munnamalai *et al.*, 2017) (Chapter 3). While class 3 Semaphorins are most commonly known for their repulsive effect on receptor expressing neurites, a growing body of literature supports that they play other roles in development as well, during processes such as vasculogenesis and synaptogenesis (Yazdani & Terman, 2006). Alternative functions of Sema signaling are described in detail in the discussion section of this chapter.

To gain a better understanding of the roles of Sema signaling in the embryonic inner ear of the chicken, we examined the expression of *Sema3D*, *Nrp* and *PlxnA1* genes in the auditory and vestibular compartments, as well as changes in *Sema3D* and *Nrp2* levels in response to *Wnt9a*-overexpression. We additionally examined *Sema3F*, as it has previously been shown to influence innervation in the mammalian auditory organ (Coate *et al.*, 2015). The expression patterns

described leave open the possibility that *Sema* signaling may serve various roles in innervation, synaptogenesis, vasculogenesis, and boundary formation within the inner ear, any of which may impact either hearing or vestibular disorders, including Meniere's disease.

In the sections below, molecular expression patterns within the developing inner ear were visualized with several labeling methods. We used an alkaline-phosphatase-based *in situ* hybridization protocol to map *Sema3D* and *Sema3F* transcripts in purple and DAB-based immunohistochemistry to co-label axons (neurofilament-associated protein) in brown. The *Nrp1* receptor was visualized by immunofluorescence in the red channel, along with *Tuj1* immunofluorescence to co-label for neurites in the far-red (false-colored blue) and a yellow fluorescent-dye (depicted in green) that was used to fill the vasculature in live embryos. Transcripts for *Nrp2* and *PlxnA1* were visualized with RNA-Scope probes using a magenta histochemical processing protocol and a purple hematoxylin counterstain. Immunohistochemistry (brown label) was used to map retrovirus-infected cells. The expression data in the sections below have been submitted for publication in the *Journal of Comparative Neurology*.

6.2 Changes in Semaphorin signaling genes in response to *Wnt9a* overexpression

The RNA sequencing data set comparing *Wnt9a*-overexpressing BPs with control BPs indicated that *Sema3D* and *Nrp2* transcripts were downregulated in the presence of exogenous *Wnt9a* at E6 (Munnamalai *et al.*, 2017). *In situ* hybridization was used to validate the RNA sequencing data and to examine the spatial expression of these transcripts (Fig. 6.1). We predicted that *Sema3D* would be expressed on the abneural side of the BP, where it would be poised to repel *Nrp2*-expressing afferents (Fig. 1.2 C). Contrary to this, *Sema3D* transcripts were not restricted to the abneural side but rather were expressed across the prosensory domain in control sections (Fig. 6.1 C). *Nrp2* transcripts were expressed in the cochlear ganglion, but were also expressed on the abneural side of the prosensory epithelium in control sections (Fig. 6.1 E). In accordance with the RNA sequencing data, both *Sema3D* and *Nrp2* transcripts expressed in the prosensory epithelium at E6 were nearly abolished when *Wnt9a* was over expressed (Fig. 6.1 D & F).

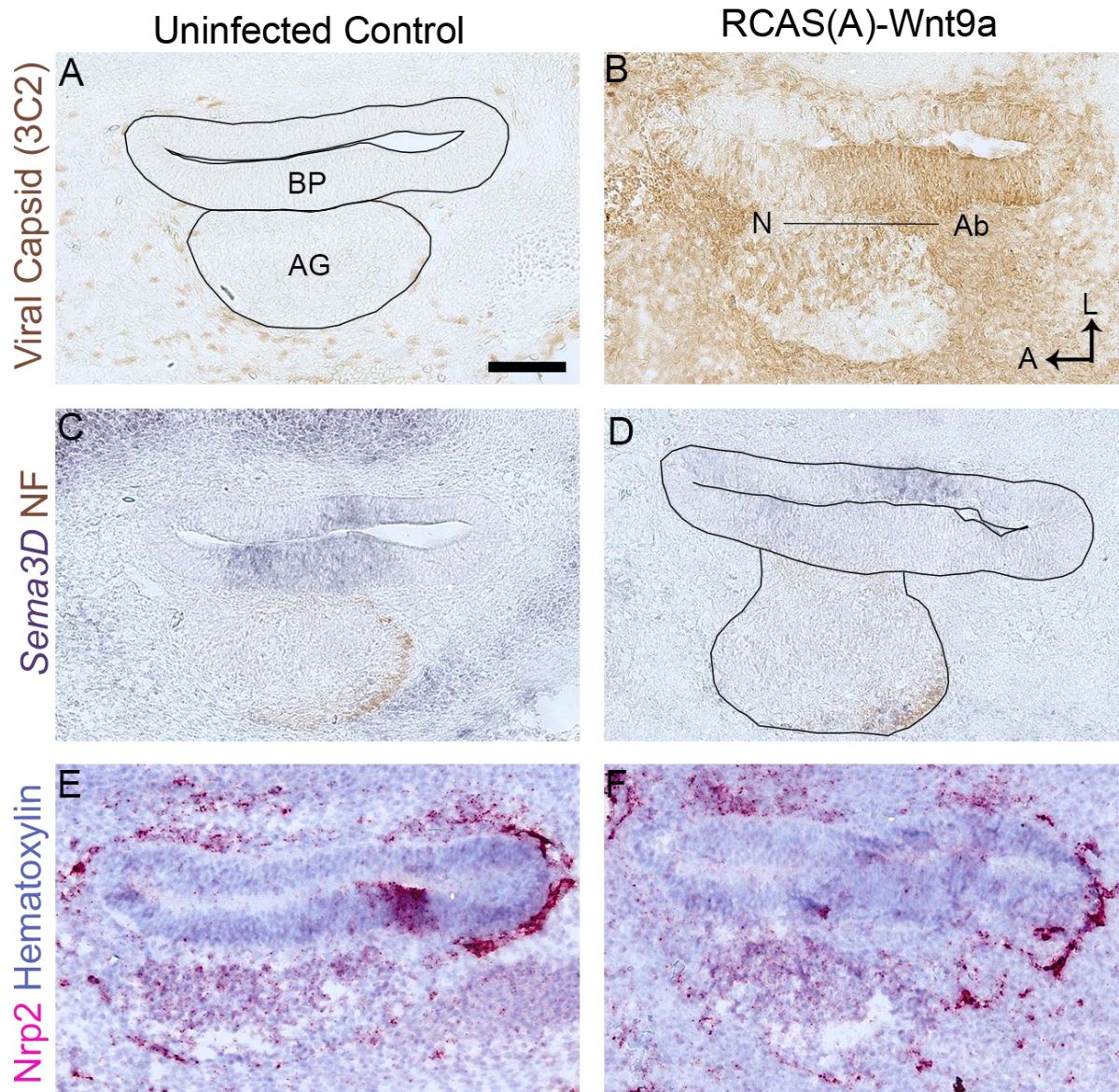


Figure 6.1 Semaphorin3D and Nrp2 decrease in the presence of exogenous Wnt9a

Serial horizontal cross sections are presented through both BPs of an E6 embryo, 3 days after injection of the right otocyst with RCAS(A)-Wnt9a. (A) the left BP was uninfected, with scattered virus, detected by immunolabeling for viral gag protein (3C2), present only in the periotic mesenchyme. (B) virus had spread to both the cochlear epithelium and periotic mesenchyme on the right side. (C-D) *Sema3D* transcripts are decreased in the sensory domain in the presence of exogenous *Wnt9a*. (E-F) *Nrp2* transcripts expressed on the abneural side of the BP are reduced in the presence of exogenous *Wnt9a*. n=3. Scale bar is 100 μ m. Abbreviations: Ab, abneural side of the BP; AG, auditory (cochlear) ganglion; BP, basilar papilla; N, neural side of the BP.

6.3 Time course of Semaphorin signaling gene expression in the inner ear

Within each inner ear compartment, regional expression is presented, with epithelial (sensory and nonsensory), neuronal, periotic mesenchymal and periotic vascular expression patterns described. A summary of expression for each timepoint and gene can be found at the bottom of figures 6.2 through 6.5. We examined time points for ages ranging from E4-E10; however, only expression patterns for E5, E6, E8, and E10 are described below. These specific time points were chosen based on changes in expression patterns that occurred at these time points for some genes. During the time range examined, critical events such as innervation, synaptogenesis, and differentiation of the prosensory domain are occurring. A summary of the number of *in situ* and immunofluorescent labels performed for each gene and time point can be found in table 6.1.

Table 6.1 Summary of *in situ* and immunohistochemistry replicates for uninfected embryos

Gene	HH 28, E5	HH 29, E6	HH 33, E8	HH 36, E10
<i>Sema3F</i>	4	4	3	3
<i>Sema3D</i>	5	5	4	4
<i>Nrp1</i>	4	4	6	3
<i>Nrp2</i>	5	4	4	3
<i>PlxnA1</i>	3	6	4	3

6.3.1 Expression results in the cristae, semicircular canals and endolymphatic sac

The expression patterns for *Sema3D*, *Sema3F*, *Nrp1*, *Nrp2*, and *PlxnA1* were similar in each of the cristae (anterior, posterior, and lateral). In figure 6.2, expression patterns are shown in the PCr. The anterior and lateral cristae are not shown.

Sema3F transcripts are weakly expressed in the mesenchyme immediately surrounding the inner ear from E5 to E8 (Fig. 6.2 A-C). In the epithelium, *Sema3F* is weakly expressed in the cristae (Fig. 6.2 A, bracket) and in the semicircular canals (Fig. 6.2 A, closed arrow) at E5. At E6 and E8, faint *Sema3F* flanks the cristae (Fig. 6.2 B-C, brackets). By E10, *Sema3F* is no longer expressed in the epithelium (Fig. 6.2 D).

Sema3D expression is clearly distinct from, and stronger than, *Sema3F*. *Sema3D* is expressed in the epithelium flanking the cristae (Fig. 6.2 E-G, brackets), in the semicircular canals (Fig. 6.2 E-G, closed arrows), in the mesenchyme, and in the endolymphatic duct (Fig. 6.2 E-F, closed

arrowheads; duct not shown in E8 image) from E5 to E8. By E10, this pattern has faded and *Sema3D* is expressed in a tight band (Fig. 6.2 H, open arrows) that lies just beyond the dye-stained vascular tissue surrounding the otic epithelium (Fig. 6.2 L, open arrows).

An anti-Nrp1 antibody labels within or near the vascular tissues surrounding the otic epithelium (Fig. 6.2 J-L, open arrows) from E6 to E10. At E8 it is also expressed in the epithelium and is strongest flanking the cristae (Fig. 6.2 K bracket).

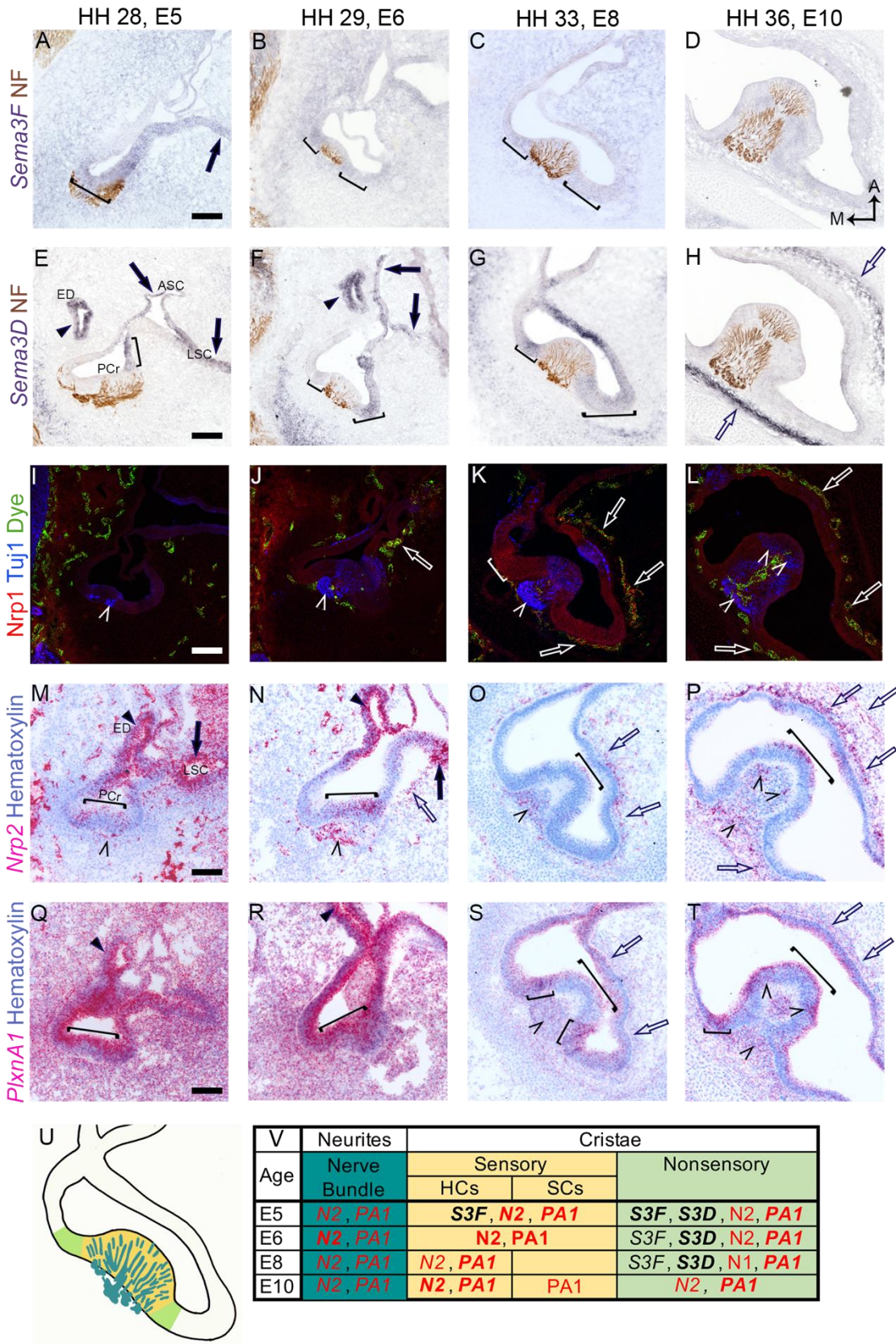
Nrp2 transcripts are expressed in the mesenchyme from E5 through E10. The staining overlaps spatially with vascular tissue surrounding the otic epithelium (Fig. 6.2 I-L, M-P, open arrows) and is intermingled among neurofilament-labeled axons of the vestibular ganglion (Fig 6.2 I-L, M-P, open arrowheads). At E10, two concentric bands of Nrp2 are found in the mesenchyme: a major band close to the otic epithelium that is superimposed with the vascular dye label and with Nrp1; and a minor band just beyond the vascular tissue that partially overlaps with *Sema3D* (Fig. 6.2 H, L, & P, open arrows). At E5-E6, Nrp2 is also found in the semicircular canals (Fig. 6.2 M-N, closed arrows) and the endolymphatic duct (Fig. 6.2 M-N, closed arrow heads). Nrp2 is expressed in the cristae (Fig. 6.2 M-P, brackets). At E5 and E6, it is unclear if Nrp2 is expressed by the sensory epithelium or by the neurites innervating it (Fig. 6.2 M-N, brackets). At E8 and E10, Nrp2 is expressed near the apical surface of the epithelium, where the HCs reside (Fig. 6.2 O-P, brackets).

PlxnA1 is strongly expressed in the mesenchyme and otic epithelium at E5 and E6 (Fig. 6.2 Q-R), including in the endolymphatic duct (Fig. 6.2 Q-R, closed arrow heads). After E6, *PlxnA1* decreases in both the mesenchyme and epithelium and becomes more specific. At E8 and E10, *PlxnA1* is strongly expressed in the epithelium flanking the innervated cristae (Fig. 6.2 S-T, brackets). At these ages, it is also expressed on the apical sensory epithelium, among the HCs (Fig. 6.2 S-T, brackets) and in the vascular tissue (Fig. 6.2 S-T, open arrows). *PlxnA1* is also found in the nerve bundles beneath the sensory organ (Fig. 6.2 S-T, open arrowheads).

Figure 6.2 U-V summarizes the results for the epithelia of the semicircular canals and the ampullae, as well as the associated nerve bundles innervating the cristae.

Figure 6.2 Semaphorin signaling gene expression in the posterior crista

(A-T) Horizontal cross sections through the posterior crista (PCr) are shown. Expression patterns for *Sema3F*, *Sema3D*, *Nrp1*, *Nrp2*, and *PlxnA1* in the other two cristae (anterior and lateral, not shown) are similar to the PCr. Brackets indicate expression in the sensory or nonsensory epithelia, as explained in the text. Closed arrows denote expression in the semicircular canals. Closed arrowheads highlight expression in the endolymphatic duct (ED). Open arrows indicate vascular tissue labeled by dye or an expression pattern in the vascular tissue or mesenchyme. Open arrowheads indicate neurites of the vestibular ganglion (VG) or an expression pattern in the neurites. (U-V) A summary of gene expression in each region is included at the bottom of the figure. The organ diagram (U) is of an E8 PCr and specific regions are color coded. These colors correspond to the same regions listed on the gene summary table (V). The nerve bundle is teal. The sensory domain, which contains both hair cells (HCs) and supporting cells (SCs) after E8, is labeled in yellow. The nonsensory domain containing transitional epithelial cells and dark cells is labeled in green. The remaining nonsensory epithelium is in white. In the tables of this and subsequent figures, red text is used to denote receptors, and bold text is used to denote high levels of expression. All scale bars are 100 μm . Abbreviations: A, anterior; ASC, anterior semicircular canal; E, embryonic day; HH, Hamburger Hamilton stage; LSC, lateral semicircular canal; M, medial.



6.3.2 Expression results in the saccule, utricle, and vestibular ganglion

Sema3F transcripts are expressed weakly in the nonsensory epithelium of the SM and UM, as well as in the proximal CD from E5-E8 (Fig. 6.3 A-C, closed arrows). At these ages, it is also expressed weakly in the periotic mesenchyme (Fig. 6.3 A-C). By E10, *Sema3F* is down-regulated in both the SM, UM, and in the surrounding mesenchyme.

Sema3D is strongly expressed in the vestibular ganglion from E5-E8 (Fig. 6.3 E-G, circles). It is expressed in the nonsensory cochlea from E5-E8 and in the nonsensory epithelium of the SM and UM at E8 (Fig. 6.3 E-G, closed arrows). By E10, *Sema3D* is no longer expressed in the vestibular ganglion (data not shown) or the inner ear (Fig. 6.3 H). *Sema3D* is expressed in the precartilaginous otic capsule at all ages tested at E5-E8, well beyond the *Sema3F*-positive loose mesenchyme (Fig. 6.3 E-G). By E10, *Sema3D* expression also appears as a narrow band on the inner edge of the cartilaginous otic capsule (Fig. 6.3 H, closed arrowhead).

Nrp1 is expressed in the otic epithelium near the junction of the cochlear and saccular ducts at E5-E6 (Fig. 6.3 I-J, closed arrows). At E5 it overlaps with capillary-rich tissue surrounding the otic epithelium and vestibular ganglion (Fig. 6.3 I, open arrows). At E6 and later ages, most *Nrp1* has faded in the mesenchyme but some blood vessels continue to express it (Fig. 6.3 J-L, open arrows).

Nrp2 is expressed in the vestibular ganglion at each of the time points we examined (Fig. 6.3 M-O, circles; data not shown for E10). Concurrently, *Nrp2* is strongly expressed in the sensory epithelium of the SM and weakly expressed in the sensory UM (Fig. 6.3 M-P, brackets). By E10, *Nrp2* is present in HCs of the SM and UM (fig. 6.3 P, bracket). We also observed *Nrp2* in the tissue surrounding the SM, UM, and vestibular ganglion (Fig. 6.3 M-P, closed arrowheads). This mesenchymal tissue is traversed by capillaries and neurites, precluding a definitive assignment of the cell type(s) that contribute to the *Nrp2* expression in this location.

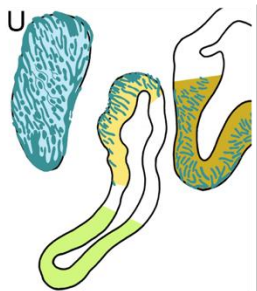
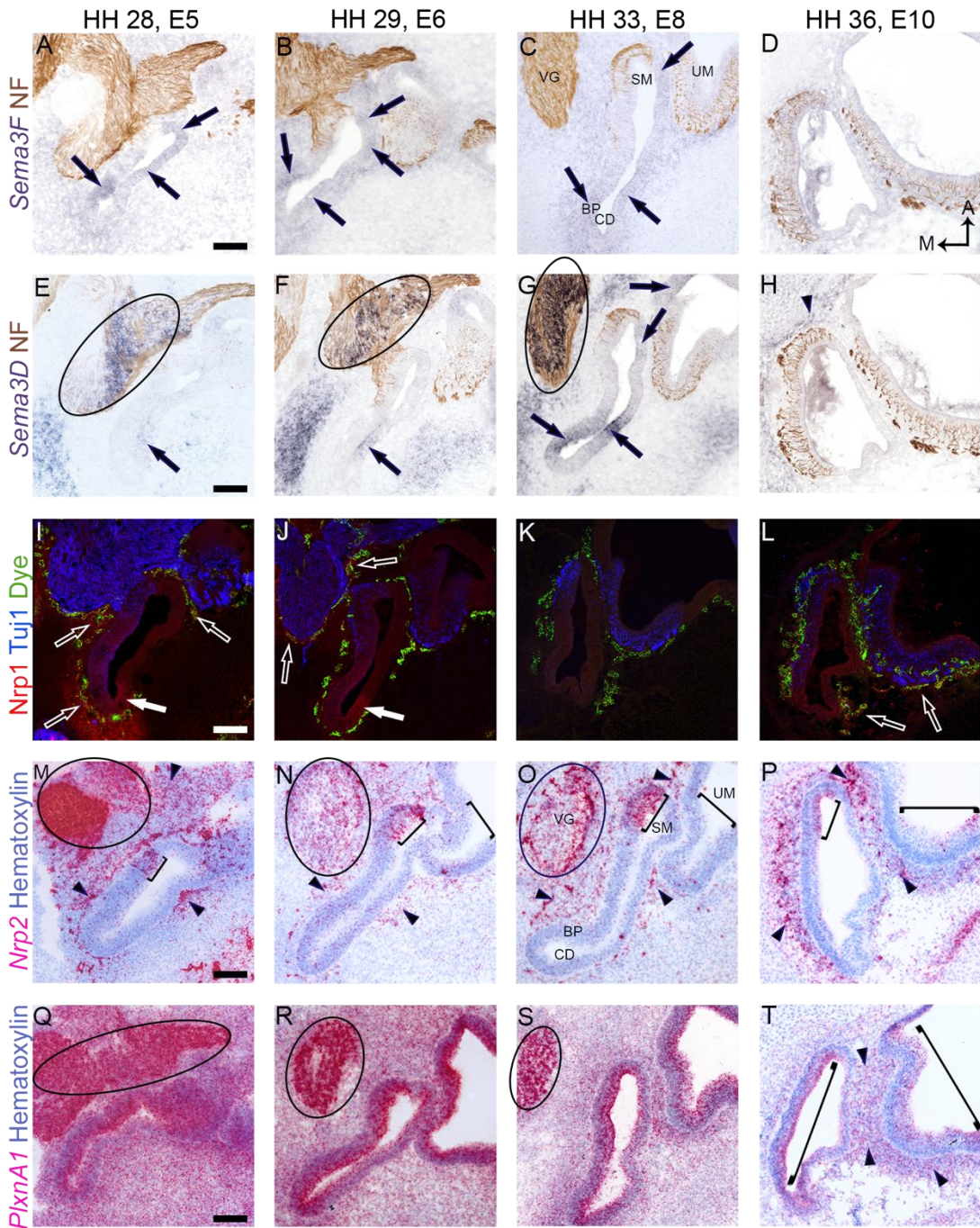
PlxnA1 is strongly expressed throughout the vestibular ganglion, epithelium, and mesenchyme at E5 (Fig. 6.3 Q). As embryo age increases, the intensity of expression decreases (Fig. 6.3 R-T). At all of the timepoints examined, *PlxnA1* is expressed in the vestibular ganglion (Fig. 6.3 Q-S, circles, vestibular ganglion for E10 not shown). At E8-10, this expression is localized to the larger (presumed neuronal) cell bodies. In the epithelium at E10, *PlxnA1* is most strongly expressed in the sensory epithelia of the SM and the UM (Fig. 6.3 T, brackets). In the mesenchyme at E10, *PlxnA1* is most intense immediately surrounding the SM and UM (Fig 6.3 T, closed arrowheads).

This tissue is rich in neurites and capillaries, suggesting that *PlxnA1* is expressed by the blood vessels and/or the vestibular ganglion neurites.

The major results for the vestibular ganglion and the middle compartments of the inner ear are summarized (Fig. 6.3 U-V).

Figure 6.3 Semaphorin signaling gene expression in the saccule, utricle, and vestibular ganglion

(A-T) Horizontal cross sections through the saccular macula (SM), utricular macula (UM), and vestibular ganglion (VG) are presented. In many cross sections the proximal cochlear duct (CD) can be seen ventral to the SM. Selected positive signals are highlighted in the sensory epithelium (brackets), the CD and/or the nonsensory epithelium (closed arrows) and the mesenchyme (closed arrowheads). Open arrows indicate vascular tissue labeled with dye or an expression pattern associated with the vascular tissue. Circles denote expression in the VG. A diagram of the E8 saccule, utricle, and VG (U) as well as a table summarizing gene expression at each age (V) is at the bottom of the figure, with corresponding color schemes. The VG and its neurites are blue. The sensory domain, containing hair cells (HCs) and supporting cells (SCs) at E8 and E10, is yellow for the SM and orange for the UM. Nonsensory epithelium of the CD is green. All other nonsensory epithelium is in white. All scale bars are 100 μm . Abbreviations: A, anterior; E, embryonic day; HH, Hamburger Hamilton stage; M, medial.



Age	Ganglion VG	Sacculus				Utriculus		
		Sensory		Nonsensory		Sensory		Non-sensory
		HCs	SCs	NS	CD	HCs	SCs	
E5	S3D, N2, PA1	N2, PA1		S3F, N1, N2, PA1	S3F, S3D, N1, N2	N2, PA1		PA1
E6	S3D, N2, PA1	N2, PA1		S3F, N2, PA1	S3F, S3D, N1, N2, PA1	N2, PA1		PA1
E8	S3D, N2, PA1	N2, PA1	N2, PA1	S3F, S3D, N2, PA1	S3F, S3D, N2, PA1	N2, PA1	N2, PA1	S3D, PA1
E10	N2, PA1	N2, PA1	N2, PA1	PA1		N2, PA1	PA1	PA1

6.3.3 Expression results in the lagena

Unlike the UM and SM, *Sema3F* is strongly expressed from E5-E8 in the sensory epithelium of the LM (Fig. 6.4 A-C, brackets). Additionally, it is weakly expressed in the nonsensory lagenar epithelium (Fig. 6.4 A-C, closed arrows). At E5-E8 it is also in the mesenchyme (Fig. 6.4 A-C). By E10, most of the *Sema3F* has faded (Fig. 6.4 D).

Sema3D is expressed in the nonsensory epithelium at E5 and this expression pattern becomes more intense at E6 and E8 (Fig. 6.4 E-G, closed arrows). By E10, *Sema3D* is no longer expressed in the epithelium (Fig. 6.4 H). At each of the time points we examined, *Sema3D* was expressed in the mesenchyme. Similar to other sensory organs of the inner ear, by E10, *Sema3D* is expressed in a tight band just outside of the capillary-rich region (Fig. 6.4 H, closed arrowheads).

Nrp1 is not expressed in the lagenar epithelium. It is seen in a small population of the capillaries surrounding the LM and around larger nearby blood vessels (Fig. 6.4 I-L, open arrows).

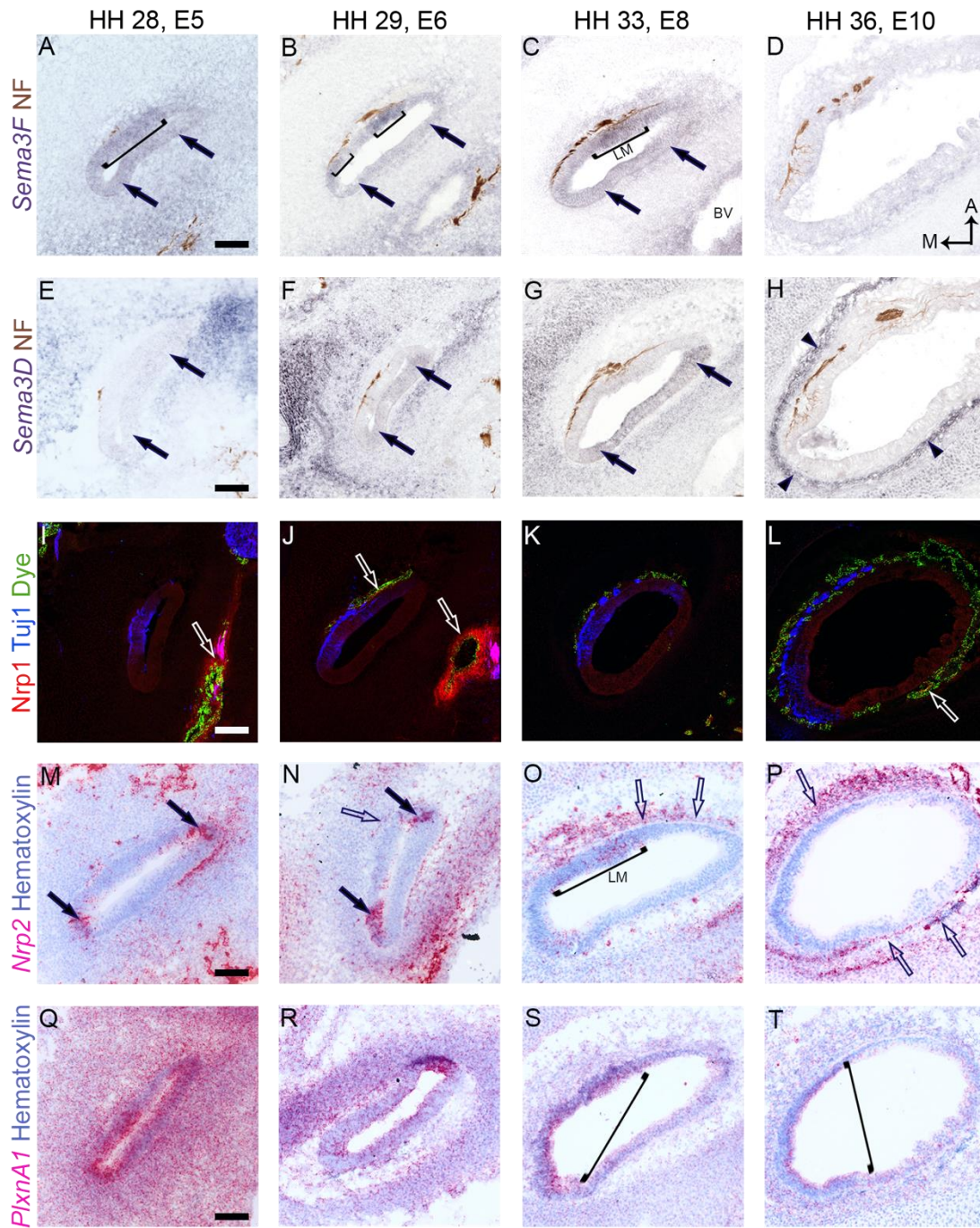
Nrp2 is expressed in the nonsensory epithelium flanking the LM at E5-E6 (Fig. 6.4 M-N, closed arrows). At E8, it is in the LM (Fig. 6.4 O, brackets). At each age we examined, *Nrp2* is also expressed in the mesenchyme and in the area enriched in capillaries (Fig. 6.4 M-P, open arrows).

PlxnA1 is strongly expressed throughout the epithelium and in the surrounding mesenchyme at E5 (Fig. 6.4 Q). The intensity of *PlxnA1* expression decreases with age. At E8-E10 *PlxnA1* is strongly expressed in the sensory epithelium of the LM (Fig. 6.4 S-T, brackets).

Figure 4 U-V highlights the major findings for the epithelial tissues of the lagena.

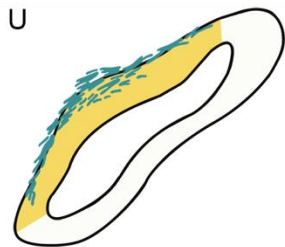
Figure 6.4 Semaphorin signaling gene expression in the lagena

(A-T) Representative cross sections through the lagena macula (LM) are shown. Selected positive signals are highlighted in the sensory epithelium (brackets), the nonsensory epithelium (closed arrows) and the mesenchyme (closed arrowheads). Open arrows indicate vascular tissue labeled with dye or an expression signal that is intermingled with the vascular tissue. A diagram of the E8 lagena illustrates sensory (yellow) and nonsensory (white) domains of the epithelium (U). The color coding in the diagram corresponds to the same regions in the expression summary table (V). All scale bars are 100 μm . Abbreviations: A, anterior; BV, blood vessel; E, embryonic day; HH, Hamburger Hamilton stage; M, medial.



Nrp2 Hematoxylin

Plxna1 Hematoxylin



Age	Lagena	
	Sensory	Nonsensory
E5	S3F, N2, PA1	S3F, S3D, N2, PA1
E6	S3F, N2, PA1	S3F, S3D, N2, PA1
E8	S3F, N2, PA1	S3F, S3D, N2, PA1
E10	PA1	PA1

6.3.4 Expression results in the cochlear duct and cochlear ganglion

For the purposes of this analysis, the nonsensory epithelium of the CD is divided into three domains in radial cross-sections; these domains presage the differentiation of specific cell types described previously (Oesterle *et al.*, 1992). A superior domain gives rise to homogeneous cells and clear cells. An inferior domain includes the future border cells, hyaline cells, vacuole cells and cuboidal cells. Between them on the lateral side of the CD is the primordium of the tegmentum vasculosum.

Sema3F is weakly expressed on the abneural side of the BP (Fig. 6.5 A-B, brackets) and in the nonsensory epithelium (Fig. 6.5 A-B, closed arrows) at E5-E6. By E8, *Sema3F* expression has faded in the epithelium (Fig. 6.5 C). At E10, it is expressed in the SCs and HCs in the BP (Fig. 6.5 D-D', brackets) and in the hyaline cells, cuboidal cells, and tegmentum vasculosum of the nonsensory epithelium (Fig. 6.5 D-D' closed arrows). *Sema3F* is also weakly expressed in the periotic mesenchyme at each age we examined (Fig. 6.5 A-D'). At E10, *Sema3F* is also observed at the periphery of the cartilaginous otic capsule (Fig. 6.5 D, closed arrowhead).

Sema3D is expressed throughout the prosensory domain of the BP (Fig. 6.5 E-H', brackets) from E5-E10. Note that the abneural side of the BP therefore expresses both *Sema3D* and *Sema3F* at E5-E6, whereas neurites approaching the neural side would encounter only one of these two potentially repulsive cues. At all ages examined, *Sema3D* is present in the primordium of the tegmentum vasculosum (Fig. 6.5 E-H, closed arrows), with a particularly strong band seen at E8. At E10, *Sema3D* is expressed in the SCs and HCs of the BP (Fig. 6.5 H-H', brackets). This expression appears to be highest on the abneural side. *Sema3D* is also expressed in the mesenchyme at each of the ages examined. *Sema3D* in the periotic mesenchyme is adjacent to the *Sema3F* expression domains described above.

Nrp1 is expressed in the capillary-rich region surrounding the cochlea at each of the timepoints examined (Fig. 6.5 I-L', open arrows). This overlaps with *Sema3F* expression and lies adjacent to *Sema3D* expressed in the mesenchyme surrounding the cochlea (described above). *Nrp1* is also expressed in the presumptive cuboidal cells of the nonsensory epithelium of the cochlea (Fig. 6.5 I-L', closed arrows). This *Nrp1* domain is adjacent to *Sema3D* expressed in the primordial tegmentum vasculosum and overlaps *Sema3F* expressed in the nonsensory epithelium.

Nrp2 is strongly expressed on the abneural side of the BP at E5 and E6 (Fig. 6.5 M-N, brackets). At E8 and E10, its expression is barely detectable in the BP. In the nonsensory epithelium, *Nrp2* is expressed by the cuboidal cell domain at E10 (Fig. 6.5 P, closed arrow). In the

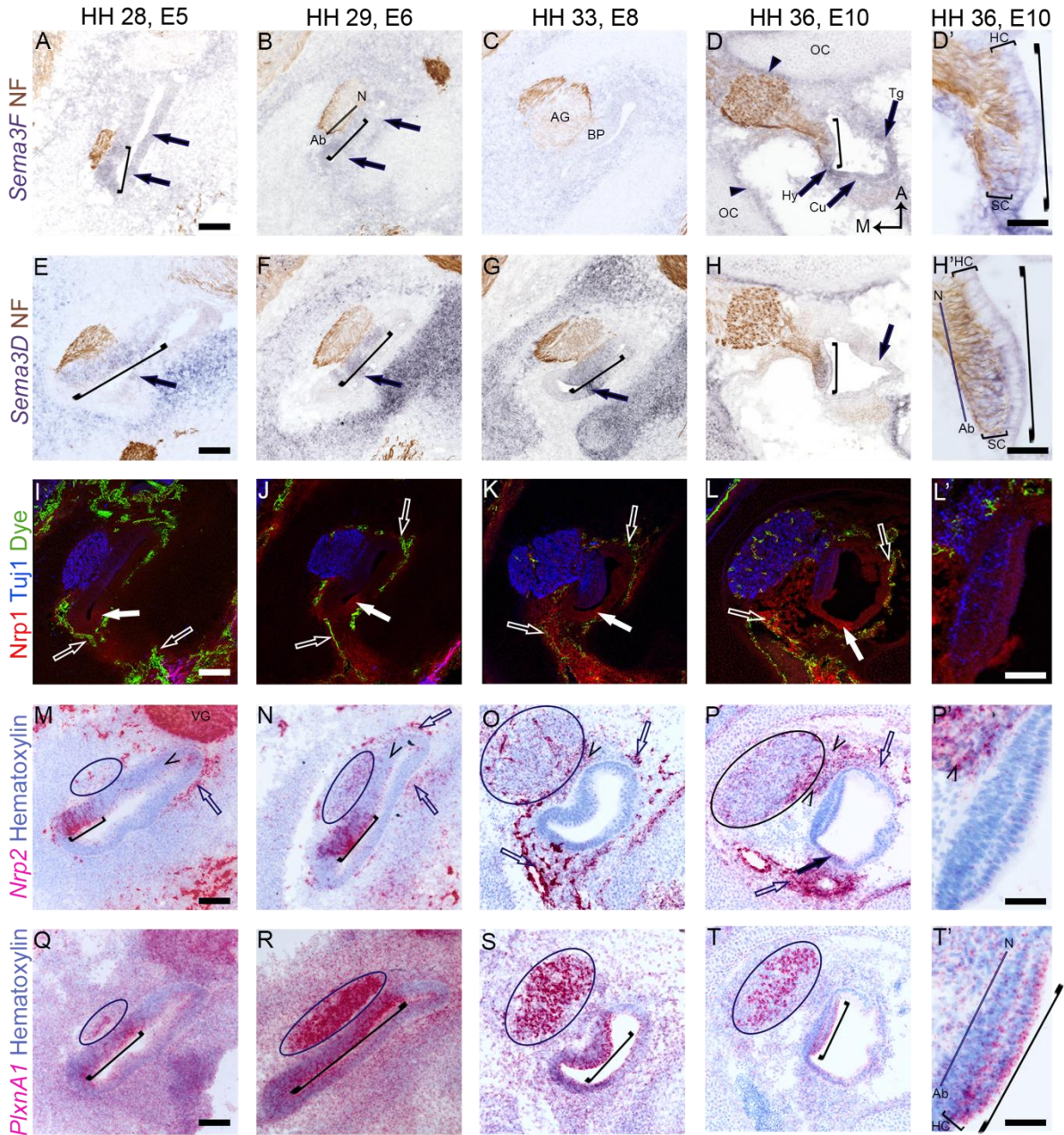
cochlear ganglion, *Nrp2* is expressed from E5 to E10 (Fig. 6.5 M-P, circles). In the mesenchyme, it is expressed at all timepoints, where it overlaps with the vascular tissue surrounding the CD (Fig. 6.5 M-P, open arrows; compare to green signal in Fig. 6.5 I-L). *Nrp2* expression is intermingled with neurites that lie beneath the sensory epithelium (Fig. 6.5 M-P', open arrowheads).

PlxnA1 is strongly expressed throughout the CD and periotic mesenchyme at E5 (Fig. 6.5 Q). As development progresses, the intensity of this expression decreases and the signal restricts to certain domains. At each age, *PlxnA1* is strongly expressed by the BP (Fig. 6.5 Q-T', brackets). At E8-E10, this sensory expression is strongest in the HC layer (Fig. 6.5 T', bracket). At E10, HCs on the abneural side express higher levels of *PlxnA1* than the neural side, especially at the base of the HCs. In the cochlear ganglion, *PlxnA1* is strongly expressed from E6 to E10 (Fig. 6.5 Q-T, circles). At E8 and E10, *PlxnA1* localizes to the cell bodies of the cochlear ganglion neurons.

Figure 6.5 U-V highlights expression data for the cochlear ganglion, the two radial halves (neural and abneural) of the BP, and three distinct nonsensory domains of the CD.

Figure 6.5 Semaphorin signaling gene expression in the cochlear duct, basilar papilla, and cochlear ganglion

(A-T) This orientation slices through the auditory (cochlear) ganglion (AG) and provides radial cross-sections through the cochlear duct, and its sensory organ, the basilar papilla (BP). (U-V) The cartoon image supports the table summarizing gene expression domains in the epithelium. Brackets indicate an expression pattern in the sensory BP (yellow in U-V). Smaller brackets in the right-most column distinguish hair cells (HC) and supporting cells (SC) in the BP. Closed arrows indicate an expression pattern in the nonsensory epithelium. The nonsensory epithelium includes the primordia of the tegmentum vasculosum (Tg, peach in U-V), cuboidal cells (Cu, green in U-V), and hyaline cells (Hy, green in U-V). Closed arrowheads highlight expression in the mesenchyme. Open arrows denote expression in the vascular tissue surrounding the inner ear epithelium. Open arrowheads indicate expression in the neurites. Circles denote expression in the AG. All scale bars are 100 μm . Abbreviations: Ab, abneural side; A, anterior; E, embryonic day; HH, Hamburger Hamilton stage; M, medial; N, neural side; OC, otic capsule.



Age	Ganglion AG	Sensory Cochlear Duct				Nonsensory Cochlear Duct		
		Neural		Abneural		Inferior	TG	Superior
		HCs	SCs	HCs	SCs			
E5	<i>N2, PA1</i>	<i>S3D, N2, PA1</i>		<i>S3F, S3D, N2, PA1</i>		<i>S3F, N1, N2, PA1</i>	<i>S3F, S3D, PA1</i>	<i>N2, PA1</i>
E6	<i>N2, PA1</i>	<i>S3D, N2, PA1</i>		<i>S3F, S3D, N2, PA1</i>		<i>S3F, N1, N2, PA1</i>	<i>S3F, S3D, PA1</i>	<i>N2, PA1</i>
E8	<i>N2, PA1</i>	<i>S3D, PA1</i>	<i>S3D, PA1</i>	<i>S3D, PA1</i>	<i>S3D, PA1</i>	<i>N1, PA1</i>	<i>S3D, PA1</i>	<i>PA1</i>
E10	<i>N2, PA1</i>	<i>S3F, PA1</i>	<i>S3F, S3D, PA1</i>	<i>S3F, S3D, PA1</i>	<i>S3F, S3D, PA1</i>	<i>S3F, N1, N2, PA1</i>	<i>S3F, S3D, PA1</i>	

6.4 Misexpression of Semaphorin3D in the inner ear results

To determine the function of *Sema3D* on the inner ear, *Sema3D* was over expressed using an RCAS(A) retrovirus. When the sensory epithelium of the UM was strongly infected, neurites still penetrated the sensory epithelium; however, there was a slight decrease in the number of neurites in epithelium and in the nerve bundle in the mesenchyme. Fewer neurites appeared to innervate the HC layer of the UM as well (Fig. 6.6). The subtlety of this effect on neurites could be due to the timing of the infection. In this experiment, embryos were injected with virus on E3, prior to when vestibular neurites begin projecting out to the vestibular epithelium. It is possible that by the time the virus infected the tissue and began transcribing and translating *Sema3D*, some neurites may have already entered the utricular epithelium. While multiple embryos from this batch were examined, this was the only embryo that was strongly infected in the vestibular sensory epithelium.

When the mesenchyme surrounding the CD was infected, mesenchyme adjacent to the posterior wall of the CD was less vascularized (Fig. 6.7, white arrows). Vasculature along the anterior wall of the CD seemed unaffected by ectopic *Sema3D*. Previous results have shown that most vasculature has already developed by E5 (Fig. 6.5 I); however, the time course of vasculogenesis of the inner ear is currently unknown. One possibility is that vasculogenesis along the anterior wall of the CD occurs earlier than E3 (time of virus injection) and was therefore unaffected by ectopic *Sema3D*. While multiple embryos from this batch were examined, this embryo had the strongest mesenchymal infection adjacent to the posterior wall of the CD. This is the only embryo this effect has been observed in.

When the sensory epithelium of the BP was infected, no changes in innervation were observed (n=4). Each replicate had varying degrees of infection along the longitudinal axis of the BP and infection was often patchy. The example in Fig. 6.7 shows faint overexpression.

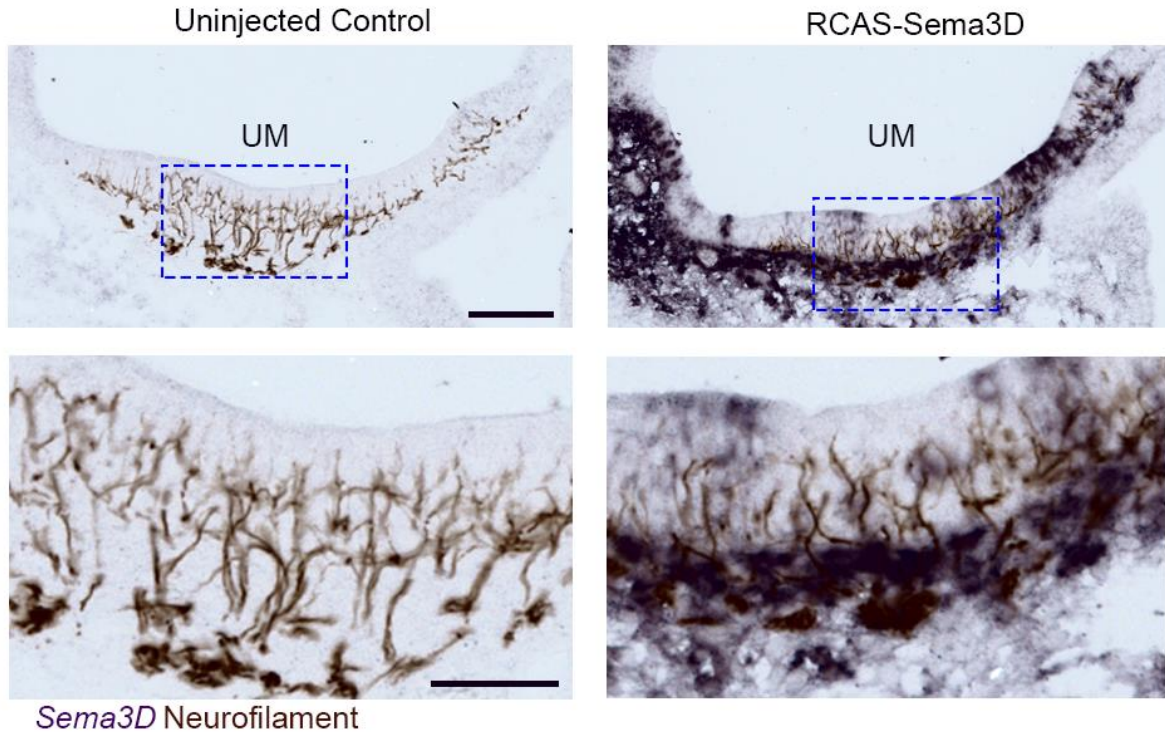


Figure 6.6 *Sema3D* misexpression in the sensory epithelium of the utricle
 The image on the left depicts results for the uninfected-control left ear of an E10 embryo. The image on the right depicts the results for the infected right ear of the same embryo at approximately the same location in the utricle. The bottom panels are zoomed in images of the areas in the blue boxes from the top panel. *Sema3D* transcripts were labeled by *in situ* hybridization and are shown in purple. DAB-histochemistry was used to label neurofilament associated protein shown in brown. N=1. Scale bar (top) = 100 μm . Scale bar (bottom) = 50 μm .

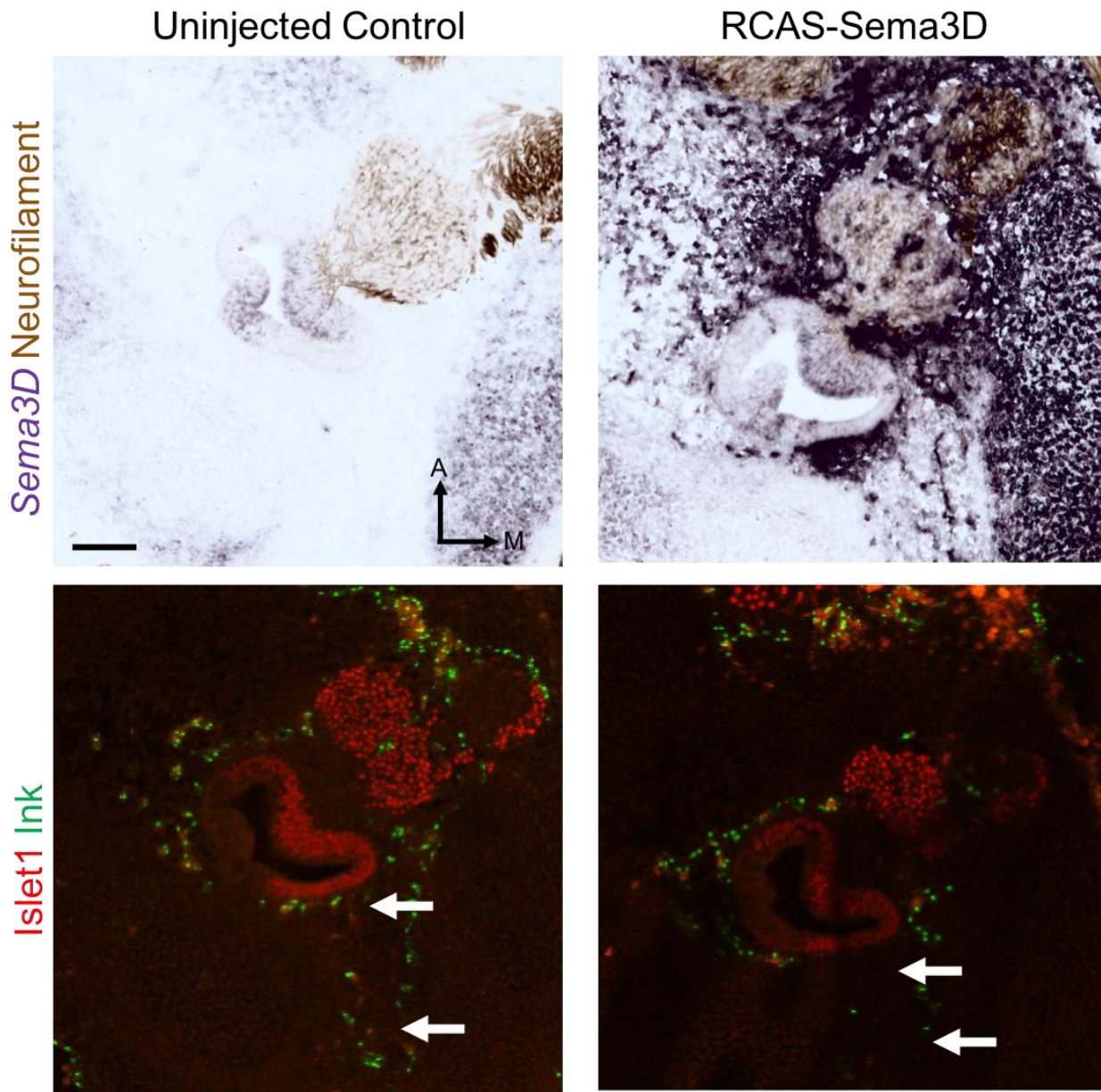


Figure 6.7 Misexpression of *Sema3D* in the mesenchyme and cochlear duct

The left panel is from the uninjected control left ear of an E10 embryo at approximately 50% through the longitudinal axis. The right panel is from the RCAS-Sema3D injected right ear from the same embryo at approximately the same location along the longitudinal axis. In the top panel, *Sema3D* transcripts are shown in purple and neurofilament associated protein is shown in brown. In the bottom panel, vascular tissue is labeled in green and Islet1 is labeled in red. Islet1 transcription factor labels the cochlear ganglion, BP, and nonsensory CD excluding the tegmentum vasculosum. N=1. Scale bar = 100 μ m. Abbreviations: A, anterior; M, medial.

6.5 Discussion

6.5.1 Semaphorin3D and Neuropilin2 are downstream of Wnt9a

We began our investigation of Semaphorin signaling genes by following up on the expression patterns of axon guidance factors, *Sema3D* and *Nrp2*, that were differentially expressed in uninfected control and Wnt9a-overexpressing BPs (Munnamalai *et al.*, 2017). Given that *Sema3F* has been previously reported to have asymmetric expression across the radial axis of the mammalian organ of Corti (present abneurally) and has a repulsive effect on type I afferents in the mouse (Coate *et al.*, 2015), we expected to find a homologous expression pattern in the bird cochlea. Indeed, while its expression is weak, *Sema3F* is confined to the abneural side of the BP on E5-E6 (Fig. 6.5 A-B). However, we also expected *Sema3D* to show a similar distribution to *Sema3F*, and that *Nrp2* would be in cochlear ganglion neurons. We further hypothesized that the down regulation of both genes in the presence of exogenous *Wnt9a* contributed to the increase in afferent innervation previously described (Munnamalai *et al.*, 2017)(Chapter 3). In accordance with our RNA sequencing data, *in situ* hybridization shows a severe reduction of both *Sema3D* and *Nrp2* in Wnt9a-infected BPs (Fig. 6.1 D, F). And yet, endogenous *Sema3D* is not restricted to the abneural-side but is expressed across the width of the prosensory domain (Fig. 6.1 C). Meanwhile, *Nrp2* is endogenously expressed in the ganglion (as expected) but is also in the epithelium on the abneural side of the CD (Fig. 6.1 E). Given these results, we suggest two possibilities: 1) the abneural side requires both *Sema3D* and *Sema3F* to effectively repel afferents; or 2) *Sema3D* and *Nrp2* are not involved in directing the radial patterning of afferents in the BP through a repulsive mechanism.

To get a better sense of the role these genes play in the developing inner ear, we examined the expression of several other Semaphorin signaling genes (*Sema3F*, *Nrp1*, and *PlxnA1*) in the inner ear across several time points (E5, E6, E8, E10). The sections below describe how these genes have appropriate spatiotemporal expression patterns to impact innervation, synaptogenesis, endothelial cell migration, boundary formation, and development of vestibular dark cells.

6.5.2 Semaphorin signaling genes in the ganglia suggest role in innervation

The receptors, *PlxnA1* and *Nrp2*, are both expressed in the cochlear ganglion (Fig. 6.5 M-T, V) and the vestibular ganglion (Fig. 6.3 M-O, Q-S, V) at E5 through E10 (vestibular ganglion for

E10 not shown). These receptors are also observed in the nerve bundles and in the sensory domains of the auditory and vestibular organs (Fig. 6.2 – 6.5, V). Given that RNAscope *in situ* hybridization is sensitive enough to detect mRNAs localized to axons (Baleriola *et al.*, 2015), it is difficult to distinguish if these mRNAs are expressed by the sensory epithelium or the neurites innervating that tissue. There are countless examples of Semaphorin signaling genes acting in axon guidance, as reviewed by Derijck *et al.* (2010) and Nakamura *et al.* (2000), and it is possible that the *PlxnA1* and *Nrp2* receptors expressed the ganglia and their projections may be involved in pathfinding of the peripheral processes of these sensory axons.

The ligands encoded by *Sema3D* and *Sema3F* are expressed in the nonsensory epithelial domains flanking the cristae (Fig. 6.2 B-C & E-G, V) and saccular macula (SM) (Fig. 6.3 A-C, E-G, V). At the same time, *Sema3D* is expressed in the prosensory domain of the BP (Fig. 6.5 E-H', brackets). It is tempting to speculate that *Nrp2*- and *PlxnA1*-positive neurites from the vestibular ganglion are averted from the nonsensory epithelia of the vestibular organs and from the sensory BP by Sema ligands. This theory is supported by our data showing that the UM is slightly less innervated when *Sema3D* is misexpressed (Fig. 6.6). One caveat to this theory, however, is that *Nrp2* and *PlxnA1* are also expressed in the cochlear ganglion (Fig. 6.5 V) and these neurons are able to innervate the prosensory domain of the BP despite the *Sema3D* expressed there. This raises the question: why would *Nrp2*- and *PlxnA1*-expressing neurites in the vestibular ganglion respond to *Sema3D* in the BP, while cochlear ganglion neurites expressing the same receptors do not? Various Sema receptors and co-receptors can form receptor complexes with one another. The composition of these holoreceptors impacts their affinity for specific ligands, intracellular signaling events, and the functional outcome of signaling (Zhou *et al.*, 2008). It is possible that there is another receptor we did not test in either the vestibular or auditory neurites that alters their response to *Sema3D* or *Sema3F*.

6.5.3 Semaphorin signaling genes in the hair cells suggest role in synaptogenesis

Semaphorins and their receptors have previously been shown to impact synapse formation as well as synaptic maintenance and elimination in the CNS (Tillo *et al.*, 2012). Some reports found that Semaphorins promote synapse and dendritic spine formation (Laht *et al.*, 2015; Morita *et al.*, 2006) as well as clustering of pre- and post-synaptic markers (Morita *et al.*, 2006). Conversely, other reports have found that Semaphorins inhibit dendritic spine formation and promote synapse

elimination (Bouzioukh *et al.*, 2006; Duan *et al.*, 2014; Laht *et al.*, 2015; Paradis *et al.*, 2007; Tran *et al.*, 2009). Semaphorin regulation (promotion or inhibition) of synaptogenesis and synaptic maintenance may depend on the specific ligand, receptors, and co-receptors involved as well as the function (excitatory or inhibitory) of the synapse.

Nrp2 and *PlxnA1* are expressed in the HCs of the cristae (Fig. 6.2 O-P, S-T, V) and SM (Fig. 6.3 O-P, T,V). In the BP, *Sema3F*, *Sema3D*, and *PlxnA1* are expressed in the HCs (Fig. 6.5 D', H', & T', brackets) at E10. *PlxnA1* transcripts are distributed along the apical surface of the HCs across the radial axis, while HCs on the abneural side of the BP have more *PlxnA1* at the base of the HCs compared to those on the neural side (Fig. 6.5 T'). From these data, it is difficult to distinguish if *PlxnA1* is expressed by the base of the HCs or by the efferent terminals, but in either case, it may influence synaptogenesis from either the pre- or the post-synaptic sides. *Sema3D* is more strongly expressed by the HCs of the abneural side (Fig. 6.5 H') while *Sema3F* is expressed in HCs more uniformly across the radial axis (fig. 6.5 D').

Afferents and efferents synapse onto vestibular HCs at approximately E6 (Ginzberg & Gilula, 1980) and E10 (Meza & Hinojosa, 1987), respectively. *Nrp2* in the HCs of the cristae and SM may be involved in synaptogenesis, although neither of the Sema ligands examined seem to be present at these time points. Afferents and efferents synapse onto BP HCs at approximately E8-9 (Whitehead & Morest, 1985b) and E14 (Rebillard & Pujol, 1983), respectively. Based on the timing of the expression we observe, *Sema3D*, *Sema3F*, and *PlxnA1* may be involved in synapse formation in the BP. Neuronal cell adhesion molecule (NrcAM) has been shown to associate with *Nrp2* (Julien *et al.*, 2005) and recent work in the mammalian inner ear has shown that it is involved in limiting ribbon synapses in the HCs, likely through inhibiting synapse formation or promoting pruning (Harley *et al.*, 2018). RNA sequencing data failed to detect NrcAM transcripts in the chicken BP at E6 (Munnamalai *et al.*, 2017), although this time point precedes synapse formation in this organ.

6.5.4 The presence of Semaphorin signaling genes in the mesenchyme suggest a role in endothelial migration

While Sema signaling is most commonly associated with its role in axon guidance, it can also have effects on endothelial cell migration (Hamm *et al.*, 2016; Serini *et al.*, 2003), vasculogenesis (Bates *et al.*, 2003; Serini *et al.*, 2003), vascular patterning (Fiore *et al.*, 2005), and tumor angiogenesis (Kessler *et al.*, 2004; Serini *et al.*, 2003). Semaphorins can impact blood vessels by

repelling Nrp- or Plxn-expressing blood vessels (Bates *et al.*, 2003), blocking the effects of vascular endothelial growth factor (VEGF) (Bagnard *et al.*, 2001; Miao *et al.*, 1999), or regulating endothelial cell responsiveness to integrins (Serini *et al.*, 2003). In the inner ear, *Nrp1* conditional knock out mice had enlarged vessels in the stria vascularis (homologous to avian tegmentum vasculosum) (Salehi *et al.*, 2017). In the context of this literature, it is interesting to find Semaphorin signaling genes in the periotic mesenchyme of the inner ear. *Nrp1* and *Nrp2* are localizing to the dye-filled blood vessels (Fig. 6.2 – 6.5, I-L, M-P). In the vestibular organs, a tight band of *Sema3D* is expressed in the mesenchyme immediately adjacent to the vascular tissue surrounding the epithelium of the cristae (Fig. 6.2 H, open arrows), SM (Fig. 6.3 H, closed arrowhead), and LM (Fig. 6.4 H, closed arrowhead). One possibility is that this pattern of *Sema3D* channels or maintains these blood vessels in close proximity to the inner ear.

In the mesenchyme surrounding the cochlear duct, another interesting pattern is observed. There is a *Nrp1*-positive patch of cells extending from a blood vessel (not shown in images) to the abneural side of the CD (Fig. 6.5, I-L, open arrows). These *Nrp1*-positive cells are rich in vasculature and also express *Nrp2* after E8 (Fig. 6.5, O-P, open arrows). This band of *Nrp1* positive cells is immediately flanked by *Sema3D* in the mesenchyme. We speculate that these *Nrp1*- and *Nrp2*-expressing cells are migrating endothelial cells and are channeled to their proper location surrounding the inner ear by the repulsive cue, *Sema3D*. This theory is supported when *Sema3D* is misexpressed in the mesenchyme adjacent to the posterior wall of the CD. These data show less vasculature in the presence of robust ectopic *Sema3D*.

6.5.5 Semaphorin signaling genes in the nonsensory epithelium of the cochlear duct may influence boundary formation

Previous work in zebrafish has examined Semaphorins in hindbrain boundary formation and maintenance. In zebrafish, *sema4D* is expressed at the rhombomere boundaries of the developing hindbrain. When *sema4D* was knocked down using morpholinos, the expression of odd-numbered rhombomere markers, *wnt1* and *epha4a*, as well as hindbrain marker, *foxb1.2*, increased; however, the localization of these markers did not change. Malformations of the hindbrain were also observed in *sema4d* morphants (Yang *et al.*, 2013). *Sema3fb* and *sema3gb* are also expressed at the hindbrain rhombomere boundaries. When Terriente and colleagues knocked down *sema3fb* and *sema3gb* or *nrp2a* using morpholinos, they found reduced clustering of *fgf20a*-expressing neurons in the rhombomeres (Terriente *et al.*, 2012). The authors propose a model in which *fgf20a*-

expressing neurons also express the *nrp2a* receptor and are restricted from migrating away from the center of the rhombomere by repulsive *sema3fb* and *sema3gb* at the rhombomere boundaries.

Expression patterns identified in this paper suggest that *Sema* signaling may also be involved in restricting cell migration or mixing at boundaries in the CD. At each of the ages we examined, *Sema3D* is expressed by the future tegmentum vasculosum (Fig. 6.5 E-H, V) while *Nrp1* is strongly expressed by the cubodial cell domain adjacent to the abneural edge of the BP (Fig. 6.5 I-L, V). *Nrp2* and *Sema3F* are also weakly expressed in the future cubodial cells at E5-E8 (Fig. 6.5 A-C, M-O, V). At E10, the expression of these genes increases, but *Sema3F* spreads to the tegmentum vasculosum as well. *PlxnA2* is weakly expressed throughout the entire nonsensory epithelium (Fig. 6.5 Q-T, V). We speculate that, in the CD, *Sema3D* expressed in the future tegmentum vasculosum repels *Nrp1*-expressing cubodial cells. This would create or maintain a boundary between these two regions, allowing them to differentiate appropriately.

6.5.6 Semaphorin signaling genes in the vestibular dark cells suggest role in producing endolymph and Meniere's disease

Vestibular dark cells flanking the vestibular sensory organs function in maintaining proper endolymph composition by transporting potassium into the endolymph (Kimura, 1969; Wangemann, 1995). Individuals diagnosed with Meniere's disease may experience vertigo and endolymphatic hydrops (Hallpike & Cairns, 1938). When Masutani and colleagues examined the histology of ampulla sections from patients with hydrops diagnosed with Meniere's disease, they found a significant decrease in the number of dark cells compared to controls. Many of the dark cells in the Meniere's disease samples also displayed a swollen cytoplasm and displacement of the nucleus. These observed changes in the dark cells in patients diagnosed with Meniere's disease suggest that they are involved in Meniere's disease pathology (Masutani *et al.*, 1992).

In our expression data, we found *Sema3D* to be expressed in the non-sensory epithelium flanking the sensory cristae (Fig. 6.3.1 E-G) in the location where dark cells reside. Given that a rare missense mutation in *Sema3D* was recently identified in patients from the same family diagnosed with Meniere's disease (Martín-Sierra *et al.*, 2016), we speculate that *Sema3D* is necessary for the proper development or maintenance of vestibular dark cells near the cristae and that the mutation of *Sema3D* may contribute to some of the symptoms observed in Meniere's disease (J. A. Lopez-Escamez, personal communication).

While preliminary data *Sema3D* misexpression experiments are presented in this dissertation, further in depth analyses will need to be done to tests these hypotheses and elucidate the role of *Sema3* and its receptors in the inner ear.

CHAPTER 7. ANATOMY AND TIMECOURSE OF EFFERENT INNERVATION IN THE BASILAR PAPILLA

7.1 Efferent projections from the auditory brainstem to the basilar papilla

In the auditory organ of birds and mammals, short HCs and outer HCs are primarily innervated by efferents with large cup like terminals on the HC. While tall HCs and inner HCs are primarily innervated by afferents, they also receive efferent terminals directly onto the HC or on the afferents (Fig. 1.1 C) (Koppl, 2011). This efferent innervation provides feedback from the auditory brainstem to the HCs and afferents (Guinan, 2017) and may serve several functions in hearing. In experiments where efferents are lesioned in the brainstem or where efferent projections are cut, increased thresholds after exposure to acoustic trauma (Darrow *et al.*, 2007; Kujawa & Liberman, 1997) and increased difficulties in discriminating speech from background noise (Dewson III, 1967; Giraud *et al.*, 1997) were observed. These data suggest that efferent feedback helps protect the auditory organ from damage due to acoustic trauma and enhances important sounds, such as speech, from background noise in the environment (Frank & Goodrich, 2018; Guinan Jr, 2006).

While auditory afferent cell bodies are located in the cochlear ganglion, auditory efferent cell bodies are located in the brainstem in the superior olivary complex (Rasmussen, 1946, 1953). In mammals, these olivocochlear efferents can be grouped into lateral and medial systems (Warr, 1975; Warr & Guinan Jr, 1979). Lateral olivocochlear efferents have cell bodies in the lateral superior olive that primarily project to ipsilateral type I afferents; medial olivocochlear efferents have cell bodies in the ventral nucleus of the trapezoid body that project to the ipsilateral and contralateral outer hair cells (Frank & Goodrich, 2018; Guinan *et al.*, 1984; Liberman & Brown, 1986; Simmons, 2002; Warr *et al.*, 1997; Warr & Guinan Jr, 1979). Efferent projections are present in the spiral ganglion as early as E12.5 (Bruce *et al.*, 1997) and by E14.5 efferent fibers have begun to penetrate the sensory epithelium and branch below HCs (Fritzsche, 1996). By E16.5 efferents have projected to the inner HCs and by E18.5 efferents have projected to the outer HCs (Simmons, 2002; Simmons *et al.*, 2011).

While extensive work has been done in mammals, less is known about the timing and destination of these projections in the bird. Previous work in the bird shows that auditory efferent cell bodies are located in the ventral hindbrain, near the facial branchial motor nuclei and these

efferents have ipsilateral and contralateral projections to the cochlea (Whitehead & Morest, 1985a). It is unknown if there are two distinct populations of efferents that go to the tall HC or short HC. While previous work in the chick suggests that efferents begin projecting out of the brainstem as early as S17 (E3) and entering the BP at S30 (E7) (Fritsch & Nichols, 1993), it is currently unknown if the time course of these projections differs for ipsilateral and contralateral projections. In this chapter, these questions are examined in the chicken BP.

7.2 Filter implant analysis

7.2.1 Filter implant approaches

The goal of inserting filters into the brainstem was to target the efferent cell bodies located in the ventral pons (Fig. 2.8) but not the afferent projections located in the cochlear nucleus. To determine the best approach to inserting the filters, data on each implant were recorded during the procedure and then later examined to evaluate the position of the insert in the brainstem and correlate that with the success (or failure) of labeling the target in the inner ear. The variables we tested for this procedure are summarized in table 7.1. For each embryo, the subject (embryo) number and the age (HH stage) were recorded. The placement along the anterior to posterior axis (%A-P) was recorded (Fig. 2.8) along with the filter size and shape. For wedge shaped filters (Fig. 2.8) the smallest length is recorded with the shape. The distance of the filter placement from the midline was also recorded.

After the filter was implanted, embryos with filter implants in the brainstem were incubated in 2% or 4% PFA at 37 °C or 55 °C. Ipsilateral projections had a shorter distance to travel than contralateral projections and were incubated for a shorter period of time. The incubation time (days) was dependent of the age, temperature, and side relative to the implant. Projections labeled in the BP are represented in the last two columns as E (efferents) and A (afferents). The success of the implant (only hitting efferents) was considered when deciding how to proceed with future implants. Highly successful implants with clear and distinct labeling of efferents are highlighted in bright and pale yellow. Embryos highlighted in bright yellow are represented in the figures in chapter 7.3. Embryo 42-1 ipsilateral BP was considered highly successful even though it only hit efferents in the cochlear ganglion. Given the young age (HH 35), it is possible that efferents have not yet projected beyond the nerve to penetrate the BP.

In general, wedge filters that spanned the anterior-to-posterior axis were most successful. Incubation at 55 °C was occasionally successful but often resulted in no labeling or, if incubated too long, excessive diffusion in the brain stem that resulted in afferent labeling. Implants that reached 0.5 mm or 0.75 mm from the dorsal midline were most successful. Clear efferent labeling was observed in embryos incubated with 2% or 4% PFA, suggesting that this variable made little impact on the diffusion.

Table 7.1 Summary of filter implants

Embryo Information		Filter Implant Information								Results	
Embryo #	Age (HH Stage)	PFA	%A-P	Filter size	Filter Shape	Distance from midline	Temp (C)	Ipsi.: time (d)	Contra: time (d)	Ipsilateral projections	Contralateral Projections
46-5	30	4%	0%-100%	3mmX0.5mm	Rectangle	0.75mm	37	10	45	Only in LM	E (few/weak)
42-1	35	4%	0%-100%	1.5mmX0.5mm	wedge, 1mm	0.5mm	37	10	25	E only in CG	A
42-2	35	4%	0%-100%	2mmX0.25mm	wedge, 1.5mm	0.5mm	37	11	25	A	A
41-15	36	4%	0%-100%	2.5mmX0.5mm	Rectangle	0.5mm	37	14	42	No	No
46-4	36.5	4%	0%-85%	2.5mmX0.5mm	Rectangle	0.5mm	37	14	42	No	No
55-5	37	2%	0%-100%	2.5mmX0.5mm	Wedge, 1.5mm	0.5mm	37	14	21	E & few A	E (few)
55-11	37	4%	0%-100%	3mm X 0.5mm	Wedge, 2.5mm	0.5 mm	37	14	22	E (few)	E&A
55-12	37	4%	0%-100%	3mm X 0.5mm	Wedge, 2.5mm	0.5mm	37	14	14	E & A	A
55-9	37	4%	0%-100%	3mm X 0.5mm	Wedge, 2mm	0.5mm	37	15	25	E & A	No
55-10	37	4%	0%-100%	3mm X 0.5mm	Wedge, 2mm	0.5mm	37	20	25	E & A	No
41-13	38	4%	0%-100%	3mmX0.5mm	Wedge, 2.5mm	0.5mm	37	19	31	E & few A	E (weak)
41-9	38	4%	0%-100%	3mmX0.5mm	Wedge, 2.5mm	0.5mm	37	19	31	E & A	E & A
55-15	38	2%	0%-100%	3.5mmX0.5mm	Wedge, 3mm	0.5mm	37	8	23	No	E (few/weak)
55-16	38	2%	0%-100%	3.5mmX0.5mm	Wedge, 3mm	0.75 mm	37	8	21	LM only	E (few/weak)
55-14	38	2%	0%-100%	3mm X 0.5mm	Wedge, 2.5mm	0.5mm	37	20	34	E & A	E (few/weak)
55-13	38	2%	0%-100%	3mm X 0.5mm	Wedge, 2.5mm	0.75mm	37	20	34	E & A	E & A
41-10	38	4%	0%-100%	3.5mm X0.5mm	Wedge, 2.5mm	0.5mm	37	20	31	E & A	No
41-11	38	4%	0%-100%	3.5mm X 0.5mm	Wedge, 2.5mm	0.5mm	37	20	31	E & A	No
41-18	38	4%	0%-100%	3mm X 0.5mm	Wedge, 2mm	0.25mm	37	20	31	E & A	E & A
41-14	38	4%	0%-100%	3mm X 0.5 mm	Wedge, 2mm	0.25mm	37	20	31	E & A	E & A
46-8	38.5	4%	0%-100%	3mmX0.5mm	Wedge, 2mm	0.5mm	37	21	35	E & A	E (weak)
55-8	38.5	2%	0%-100%	2.5mmX0.5mm	Rectangle	0.25mm	55	22	22	E & A	A & E
55-7	38.5	2%	0%-100%	2.5mmX0.5mm	Wedge, 2mm	0.75mm	37	22	22	E & A	A
55-6	38.5	2%	0%-100%	2mmX0.5mm	Wedge, 1mm	0.75mm	55	7	7	E & A	No

Table 7.1 continued

46-6	39	4%	0%-100%	3mmX0.5mm	Rectangle	0.5mm	37	10	45	No	No
48-4	40	4%	0%-100%	4mmX0.75mm	Wedge, 2.5mm	1mm	37	21	42	E & A	E & A
54-8	40	2%	CG	1mmX0.5mm	Rectangle	n/a	37	n/a	35	No	No
54-9	40	2%	CG	2.5mmX0.5mm	Rectangle	n/a	37	n/a	35	E & A?	E (few)?
41-22	41	4%	0%-100%	4.5mmX0.75mm	Wedge, 3mm	0.5mm	37	21	49	No	E only in CG
48-5	41	4%	0%-100%	4mmX0.75mm	Wedge, 2.5mm	0.5mm	37	21	42	E & few A	E & A
54-10	41	2%	0%-100%	3.5mmX0.5mm	Wedge, 3mm	0.5mm	55	14	21	E & few A	A
48-6	41.5	2%	0%-100%	3.5mmX0.5mm	Wedge, 2mm	0.5mm	37	21	33	E (few/weak)	E only in CG
46-13	42	4%	25%-75%	3mmX0.5mm	Rectangle	not recorded	55	7	14	No	No
41-23	42	4%	0%-100%	5mmX0.75mm	Wedge, 3mm	0.5mm	37	21	49	No	No
48-10	42	4%	0%-100%	4mmX0.75mm	Wedge, 2.5mm	0.5mm	37	21	42	E	E & A
48-7	42	4%	0%-100%	3.5mmX0.5mm	Wedge, 2mm	0.75mm	37	21	34	E & few A	No
46-11	43	4%	0%-50%	3mmX0.5mm	Rectangle	not recorded	55	7	14	No	No
46-10	43	4%	50%-100%	3mmX0.5mm	Rectangle	not recorded	55	7	14	No	No
41-20	43	4%	0%-100%	5mmX0.75mm	Wedge, 3mm	0.75mm	55	10	18	No	No
41-19	43	4%	0%-100%	4mmX0.75mm	Rectangle	0.75mm	55	10	18	No	No
41-21	43	4%	0%-100%	4.5mmX0.75mm	Wedge, 3mm	0.5mm	55	7	18	No	No
41-24	43	4%	0%-50%	3mmX0.5mm	Rectangle	not recorded	55	7	14	No	No
54-15	43	4%	0%-100%	4.5mmX0.75mm	Wedge, 3mm	0.75mm	37	44	49	E	No
54-14	43	2%	CG	2mmX0.5mm	Rectangle	n/a	37	n/a	48	No	No
54-17	43	2%	CG & VG	0.5mmX0.5mm	Rectangle	n/a	37	n/a	49	No	No
48-12	43.5	4%	0%-100%	3.5mmX0.5mm	Wedge, 2mm	0.5 mm	37	22	45	No	No
40-4	44	4%	0%-100%	4.5mmX0.75mm	Wedge, 3mm	0.75mm	37	21	49	No	E (only in CG)
54-16	44	4%	0%-100%	4mmX0.75mm	Wedge, 3mm	0.75mm	37	30	54	E (few/weak)	No
48-16	45	4%	0%-100%	3.5mmX0.5mm	Wedge, 2mm	0.5mm	37	27	45	E (few/weak)	E (few)

7.2.2 Filter placement analysis

After both the BPs and cochlear ganglia were removed from the embryo, the brainstems containing the implant were sectioned and the angle and depth of the filter were analyzed (Fig. 2.8). This data is summarized in table 7.2. The subject (embryo) number and age (HH stage) as well as the projections labeled in the ipsi- and contralateral BPs are included in the first two and last two columns. The filter angle was measured from the midline (Fig. 2.8). In a few cases, the filter angle is negative, indicating that the filter was incorrectly angled towards the midline. The distance of the filter was measured from the ventral edge of the brainstem, therefore, larger depth measurements indicate a shallower insert from the dorsal side. These measurements were taken from three sections (approximately 25%, 50%, and 75%) through the brainstem. In some cases, when heavy damage occurred to the brainstem or its sections, all three measurements could not be taken. The results shown in table 7.2 are the average of those one to three measurements. In some cases, the implant was angled along the anterior-to-posterior axis, resulting in a larger standard deviation. Of the BPs with cleanly labeled efferents, the angle of the implant ranged from 9.59° to 30.83° and the depth of the implant ranged from $182.60\ \mu\text{m}$ to $750.90\ \mu\text{m}$.

Table 7.2 Summary of filter angle and depth analysis

Embryo Information		Fliter Implant Analysis			Results	
Embryo #	Age (HH Stage)	Filter Angle Avg (Std)	Filter Depth. (µm) Avg (Std)	Notes:	Ipsilateral projections	Contralateral Projections
46-5	30	76.90 (10.03)	134.59 (38.91)		Only in LM	E (few/weak)
42-1	35	21.15 (1.46)	182.60 (30.09)	LARGE Diffusion across midline= 590.28(57.55)	E only in CG	A
42-2	35	22.13 (1.90)	198.20 (38.96)	Diffusion across midline=303.48(63.21)	A	A
41-15	36	17.53 (1.85)	49.40 (19.02)		No	No
46-4	36.5	18.10 (2.65)	549.71 (51.22)		No	No
55-5	37	22.13 (1.89)	465.67 (56.35)	Diffusion across midline= 36.75 (73.5)	E & few A	E (few)
55-11	37	9.43 (3.09)	4.53 (9.05)	Diffusion across midline: 530.395 (62.48) // filter parallel to midline	E (few)	E & A
55-12	37	69.36548	539.98 (318.46)	Filter in midline // heavy damage to sections	E & A	A
55-9	37	19.36 (1.34)	132.50 (33.50)	Diffusion across midline: 110.5 (72.12) // very faint diffusion	E & A	No
55-10	37	5.70 (1.90)	323.90 (65.20)		E & A	No
41-13	38	30.83 (1.80)	705.97 (92.40)	average diffusion past midline: 251.135 (28.74)	E & few A	E (weak)
41-9	38	24.45 (2.24)	339.01 (65.86)	faint diffusion; two had no diffusion past midline	E & A	E & A
55-15	38	29.62 (3.33)	390.12 (73.707)	Diffusion across midline: 387.3 (24.769)	No	E (few/weak)
55-16	38	342.07 (2.50)	282.62 (24.30)	Diffusion across midline: 191.85	LM only	E (few/weak)
55-14	38	-16.56 (5.29)	338.12 (70.17)	Diffusion across midline: 328.52 (154.9) // filter in midline at angle	E & A	E (few/weak)
55-13	38	-14.13 (1.31)	82.012 (97.16)	Diffusion across midline: 388.7 (95.123)	E & A	E & A
41-10	38	33.13 (3.12)	217.80 (88.11)	Diffusion across midline: 62.66 (66.2) //very faint diffusion	E & A	No
41-11	38			too much damage to assess	E & A	No
41-18	38			too much damage to assess	E & A	E & A
41-14	38	15.60 (1.49)			E & A	E & A
46-8	38.5	40.68 (4.09)	139.39 (136.82)	Filter shifted in posterior sections	E & A	E (weak)
55-8	38.5	18.0 (0.84)	586.96 (100.79)	Diffusion across midline= 404.88 (56.4)	E & A	A & E

Table 7.2. continued

55-7	38.5	20.00 (0.94)	993.90 (87.43)	Diffusion across midline= 672.7 (121.9) // filter through midline on post. End	E & A	A
55-6	38.5	32.74 (1.96)	366.70 (178.40)	Diffusion across midline= 40.0 (47.478)	E & A	No
46-6	39	21.59 (3.61)	0 (0)		No	No
48-4	40	25.25 (12.83)	245.86 (42.64)		E & A	E & A
54-8	40				No	No
54-9	40				E & A?	E (few)?
41-22	41	26.04 (4.13)	354.51 (409.22)	large standard deviation on depth of filter	No	E (only in CG)
48-5	41	9.58 (3.13)	578.79 (73.81)		E & few A	E & A
54-10	41	29.14 (2.17)	478.70 (251.73)	Diffusion across midline= 443.8 (85.02)	E & few A	A
48-6	41.5				E (few/weak)	E (only in CG)
46-13	42	48.31 (4.48)	181.67 (91.00)		No	No
41-23	42	24.20 (1.82)	186.75 (56.00)		No	No
48-10	42	22.85 (2.32)	474.83 (96.53)	Filter popped out. Faint diffusion across midline	E	E & A
48-7	42	19.45 (2.19)	750.90 (59.18)	Diffusion across midline= 207.5(66.4)	E & few A	No
46-11	43	-44.90 (0.61)	688.83 (0)	Damaged sections.	No	No
46-10	43	-10.04 (5.09)	151.31 (94.69)		No	No
41-20	43	16.89 (3.43)	489.95 (211.12)	Large standard deviation on depth of filter	No	No
41-19	43	26.71 (2.00)	53.13 (39.13)		No	No
41-21	43	15.42 (2.00)	241.37 (241.51)		No	No
41-24	43	38.03 (1.88)	335.62 (124.30)	large standard deviation on depth of filter	No	No
54-15	43	27.80 (1.34)	437.31 (56.90)	Diffusion across midline= 114.315 (91.69)	E	No
54-14	43				No	No
54-17	43				No	No
48-12	43.5	20.66 (2.28)	614.23 (109.66)	Diffusion across midline= 269.34 (82.27)	No	No
40-4	44	25.59 (0.58)	345.72 (160.15)		No	E (only in CG)
54-16	44	30.55 (2.50)	751.67 (89.30)	Diffusion across midline= 250.5 (36.09)	E (few/weak)	No
48-16	45	28.79 (0.83)	565.05 (109.74)	Diffusion across midline= 150.18 (24.33)	E (few/weak)	E (few)

7.3 Time course of ipsilateral and contralateral auditory efferents in the BP

7.3.1 Ipsilateral auditory efferents at HH stage 37

Figure 7.1 depicts an ipsilateral HH 37 (E11) cochlear ganglia and BP with strong NeuroVue label in the auditory neurons. The cochlear ganglia shows strong labeling in the fibers of the efferent bundle (yellow arrow). Some afferent cell bodies were also labeled in the ganglion suggesting that some of the label in the BP could be afferents. In fact, we suspect that much of the label on the neural side of the BP is from afferents. In the BP, most labeling is at the habenula perforata (white arrows) which runs the length of the BP and is where the neurites enter the BP. At this age, very few efferents have extended all the way to the abneural edge of the ipsilateral BP.

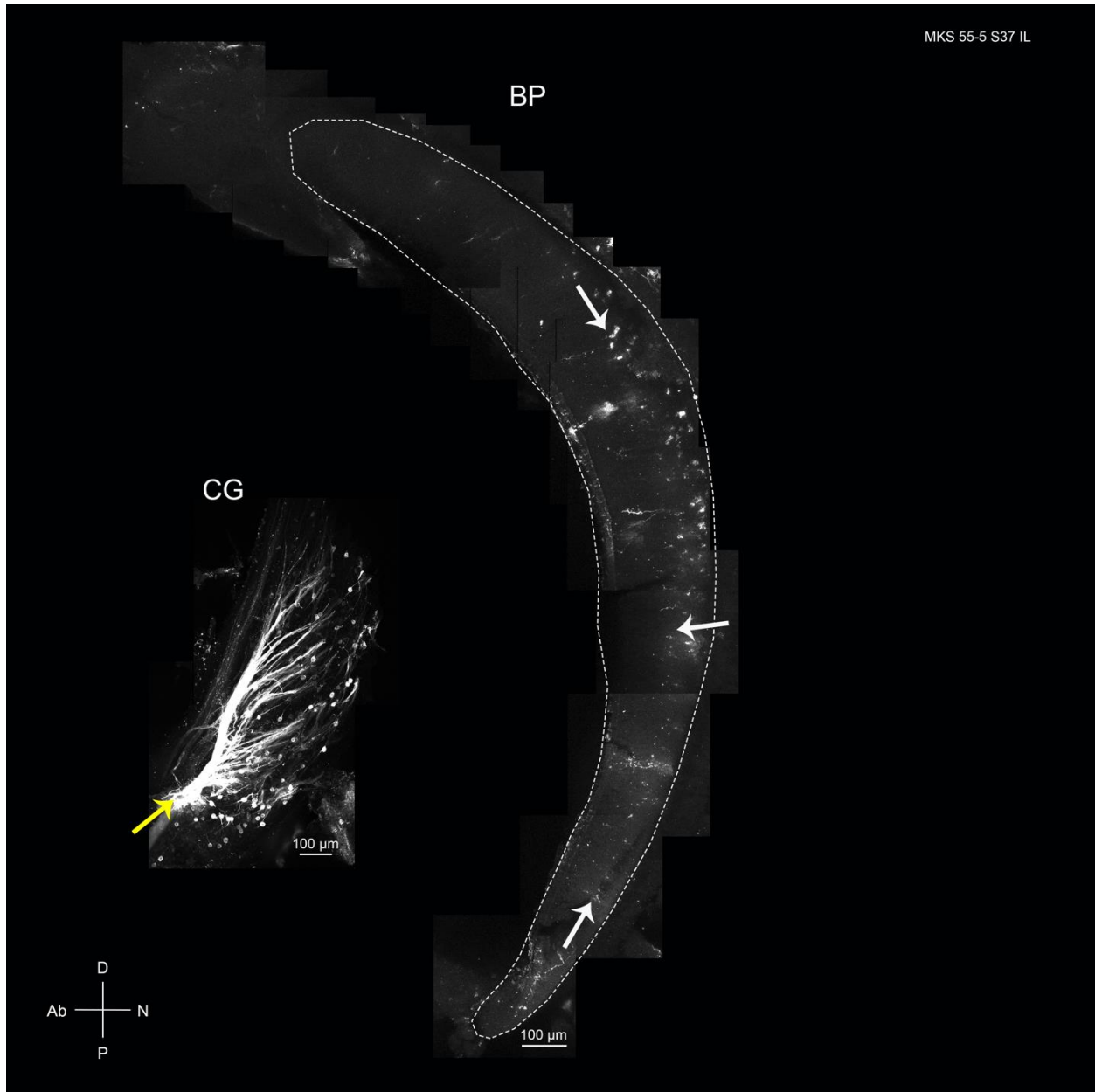


Figure 7.1 Ipsilateral stage 37 (E11) cochlear ganglion and BP

The cochlear ganglion (CG) and BP from embryo number 55-5. The cochlear ganglion and BP show NeuroVue labeling in efferents and a few afferents. The efferent bundle in the cochlear ganglion is indicated by the yellow arrow. The habenula perforate runs the length of the BP and white arrows label it at the proximal, middle, and distal BP. Abbreviations: Ab, abneural; D, distal; N, neural; P, proximal. Scale bars are 100 μ m. N=1.

7.3.2 Contralateral auditory efferents at HH stage 37

In figure 7.2, the contralateral HH 37 (E11) cochlear ganglion shows strong labeling in the efferent bundle (yellow arrow) and little to no label in the afferent cell bodies. This suggests that the label in the BP is in the efferents. At this age, the contralateral BP appears have very few efferents. All of the labeled fibers are at the proximal end and middle of the BP. Most efferents have not made it to the abneural edge of the BP. We speculate that puncta along the fibers are growth cones or branch points forming.



Figure 7.2 Contralateral stage 37 (E11) cochlear ganglion and BP

A contralateral HH 37 cochlear ganglion (CG) and BP from embryo number 55-5 are shown. This and all other contralateral images were flipped to present them in the same orientation as the ipsilateral images. NeuroVue dye is present in the efferents bundle (yellow arrow) but not afferents. A 60X image (box) provides a detailed view of the dashed box located in the middle of the BP. Abbreviations: Ab, abneural; D, distal; N, neural; P, proximal. Scale bars are 100 μm and 50 μm . N=1.

7.3.3 Ipsilateral auditory efferents at HH stage 38

The ipsilateral HH 38 (E12) cochlear ganglion in figure 7.3 shows strong labeling in the efferent bundle (yellow arrow) with only a few afferent cell bodies labeled. This suggests most of the label seen in the BP is in the efferent projections. Compared to the HH37 ipsilateral BP, there are more projections along the longitudinal axis of the BP. The proximal end of the BP contains more fibers than the distal end. Some efferents have made it to the abneural edge of the BP but are not projecting distally yet. Bright puncta are present along the efferent fibers. These could be growth cones or branching points. Looking through the z-stack, these puncta are present throughout the depth of the tissue, suggesting they are not terminals synapsing onto hair cells, but varicosities along the axons.

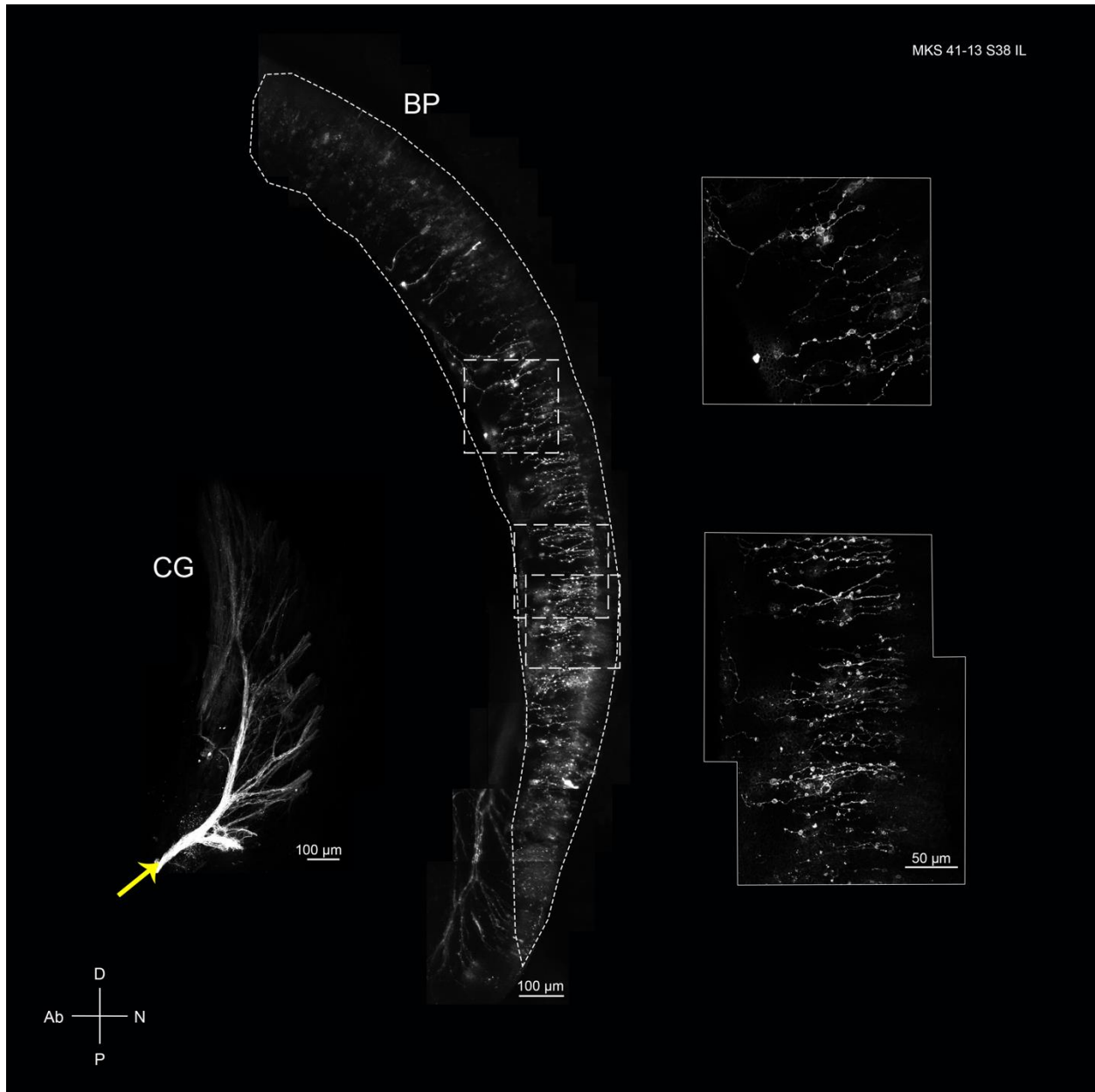


Figure 7.3 Ipsilateral stage 38 (E12) cochlear ganglion and BP

The ipsilateral cochlear ganglion (CG) and are from a HH 38 embryo (embryo number 41-13). The efferent bundle (yellow arrow) is strongly labeled with NeuroVue dye and only a few afferents are labeled. 60X images (boxes) are provided for the areas of the BP in the dashed boxes. Abbreviations: Ab, abneural; D, distal; N, neural; P, proximal. Scale bars are 100 μm and 50 μm . N=1.

7.3.4 Contralateral auditory efferents at HH stage 38

The HH 38 (E12) contralateral cochlear ganglion shows weak labeling in the efferent bundle (yellow arrow) with little to no label in afferent cell bodies, suggesting that the label in the BP is in efferents but not all efferents are labeled. There are far more efferents at this age compared to the contralateral S37 BP. The distal end of the BP still lacks efferent projections. Some efferents have made it to the abneural edge of the BP but are not yet projecting distally. Bright puncta are present along the efferent fibers. These could be growth cones or branch points. Looking through the z-stack, these puncta are present throughout the depth of the tissue, suggesting they are not exclusively efferent terminals synapsing onto hair cells which should be confined to more apical slices of the stack (Fig. 7.4)

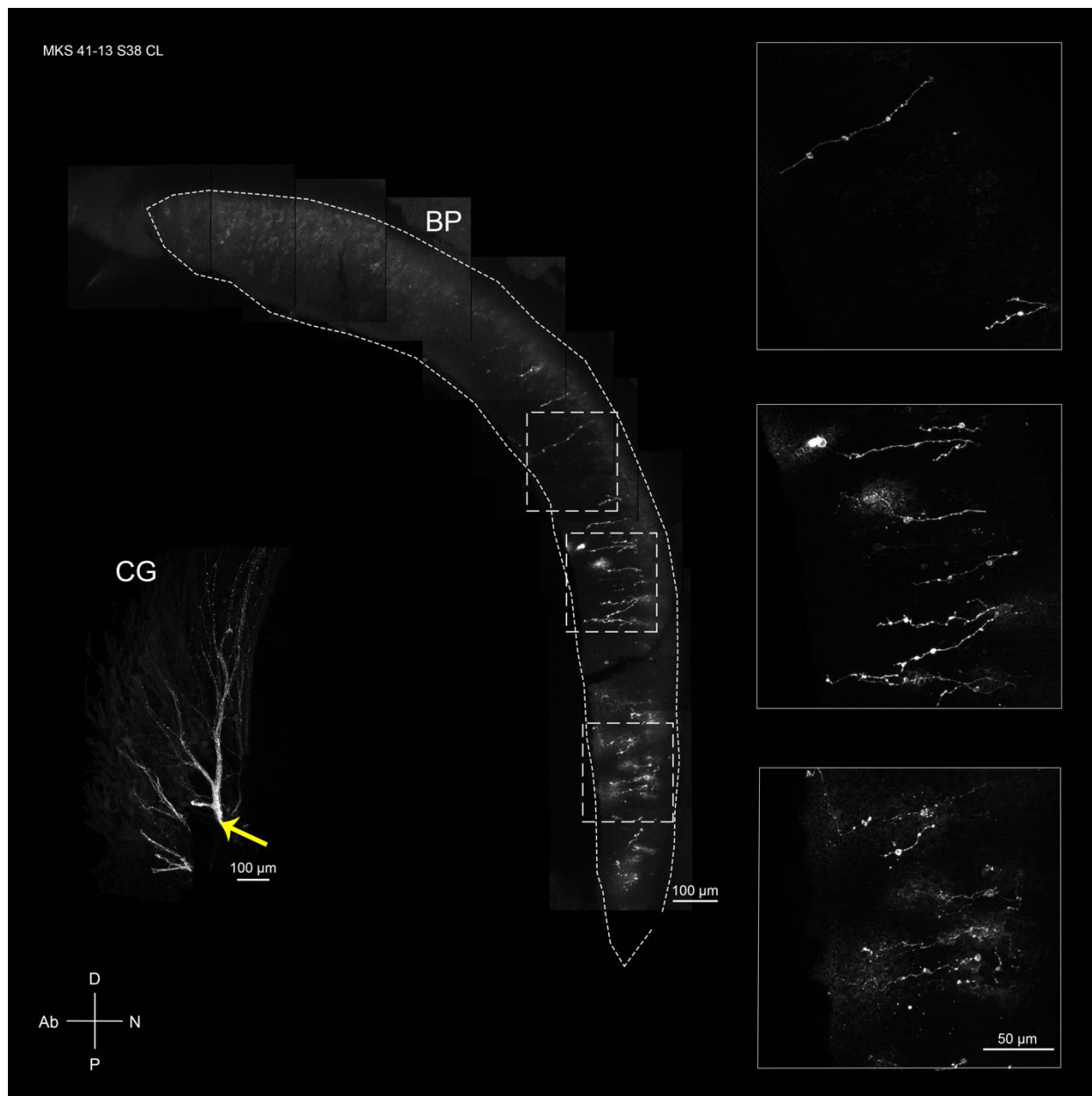


Figure 7.4 Contralateral stage 38 (E12) cochlear ganglion and BP

The contralateral cochlear ganglion (CG) and BP from embryo number 41-13 are shown above. The NeuroVue label only appears to be in the efferents (efferent bundle, yellow arrow); however, that label is somewhat weak. It is possible that not all of the efferents are labeled. A close up of the dashed boxes in the BP are shown in the boxes to the right. Abbreviations: Ab, abneural; D, distal; N, neural; P, proximal. Scale bars are 100 μ m and 50 μ m. N=1.

7.3.5 Ipsilateral auditory efferents at HH stage 41

In figure 7.5, the efferent bundle (yellow arrow) of the cochlear ganglion is labeled with NeuroVue dye along with only a few afferent cell bodies. This suggests that the label in the BP is mostly efferent labeling. At HH 41 (E15), most, if not all, of the efferents have made it to the abneural edge of BP are branching along the abneural edge (white arrows). For this age, no contralateral cochlear ganglia and BPs attempted showed strong labeling in the efferent bundle with few to no afferents. No contralateral data is presented for this age.

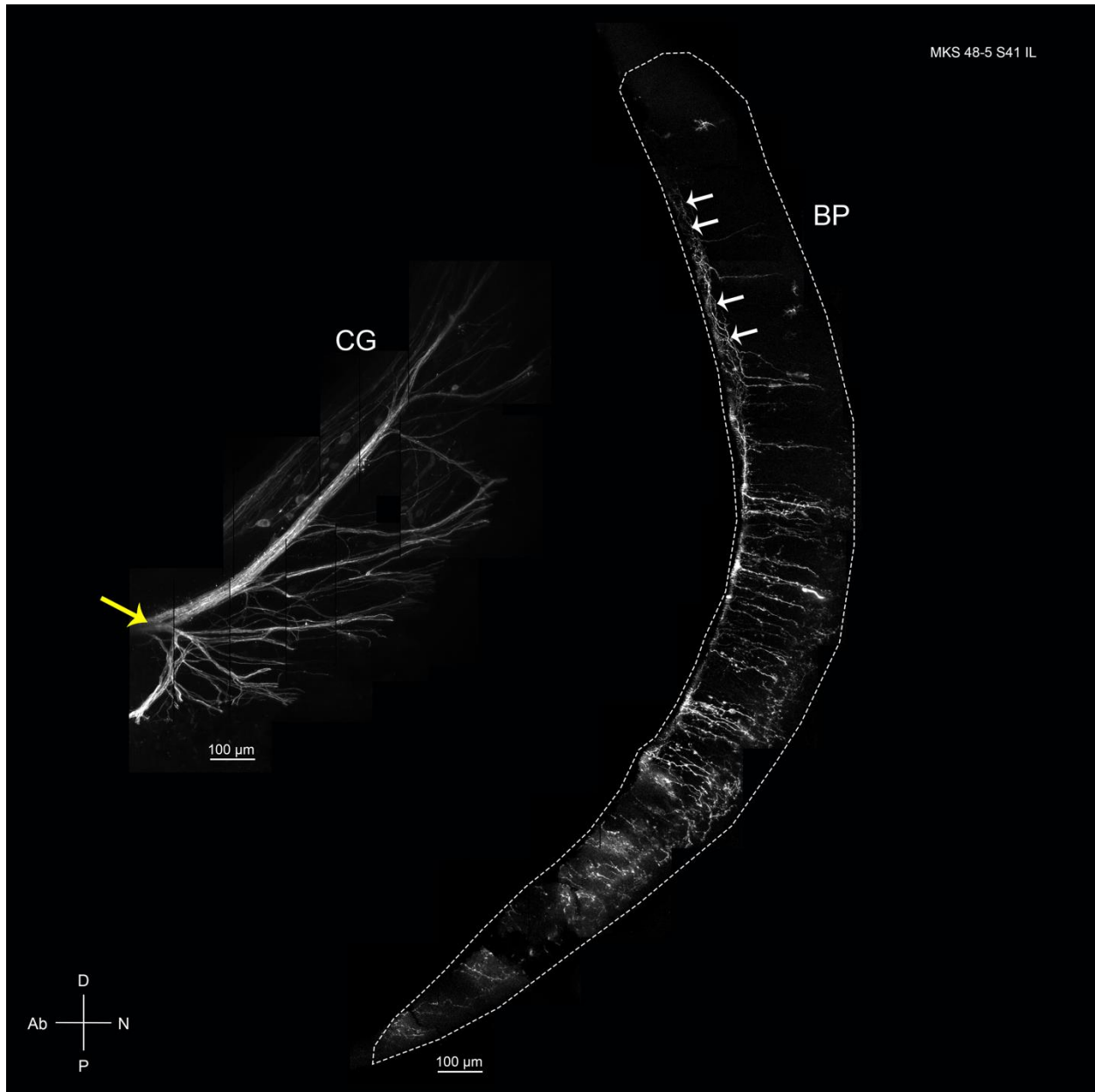


Figure 7.5 Ipsilateral stage 41 (E15) cochlear ganglion and BP

The ipsilateral cochlear ganglion (CG) and BP from embryo number 48-5 are shown above. The embryo was HH 41 at the time of harvest. The yellow arrow indicates the efferent bundle. White arrows point to efferent fibers projecting distally. Abbreviations: Ab, abneural; D, distal; N, neural; P, proximal. Scale bars are 100 μ m. N=2.

7.3.6 Ipsilateral auditory efferents at HH stage 42

In figure 7.6, the efferent bundle (yellow arrow) of the ipsilateral cochlear ganglion is well labeled. Only a few afferent cell bodies are labeled. The label in the BP is mostly in the efferents. Most, if not all, of the efferents have made it to the abneural edge of BP are branching along the abneural edge (white arrows). Dense fibers are observed at the proximal end and get less dense distally. Compared to the HH 41 BP, efferent fibers are more dense throughout the length of the BP. The attempted contralateral cochlear ganglia and BPs did not receive optimum labeling to allow for accurate conclusions, thus only data for the ipsilateral side is presented here.

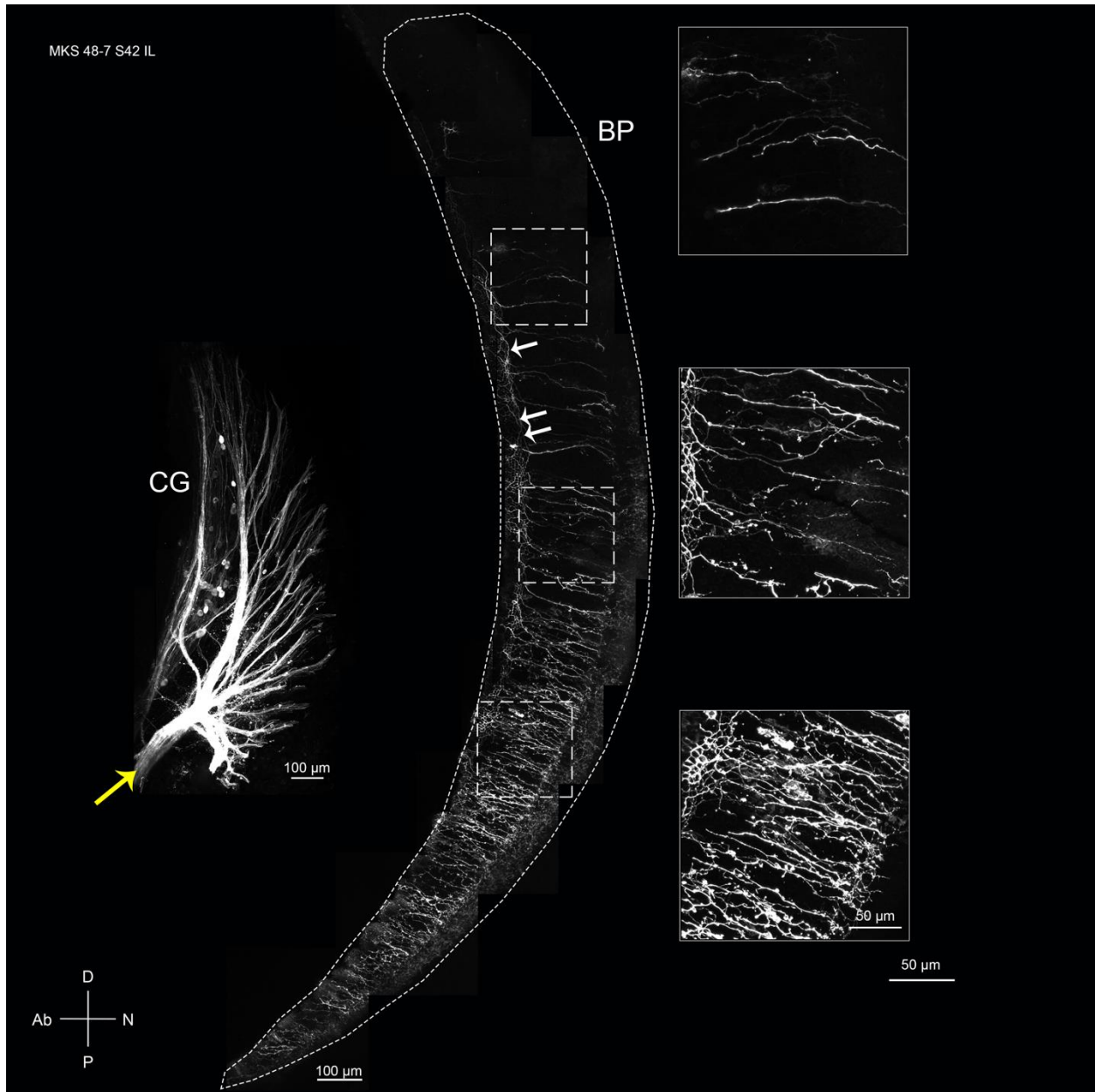


Figure 7.6 Ipsilateral stage 42 (E16) cochlear ganglion and BP

The efferent bundles (yellow arrow) of the ipsilateral cochlear ganglion (CG) are strongly labeled and only a few afferent cell bodies (bright puncta within the cochlear ganglion at this power) are labeled with NeuroVue dye. Efferents are branching distally (white arrows).

Abbreviations: Ab, abneural; D, distal; N, neural; P, proximal. Scale bars are 100 μ m and 50 μ m. N=2.

7.3.7 Ipsilateral auditory efferents at HH stage 43

In figure 7.7, while only a few afferents are labeled in the cochlear ganglion, the efferent labeling is weak in the bundle (yellow arrow) and it does not appear that all efferents are labeled. This likely explains the abrupt cutoff in labeled fibers that occurs at the middle of the BP. Although the distribution of labeled fibers is not ideal in this example, given the lack of label in the afferents, we are still able to observe proximal efferent fibers.



Figure 7.7 Ipsilateral S43 cochlear ganglion and BP

The ipsilateral cochlear ganglion (CG) and BP are shown for a HH 43 embryo (54-15). Although the efferent bundle (yellow arrow) is labeled with only a few afferent cell bodies, it appears that only a portion of efferents were labeled in the cochlear ganglion. This likely resulted in incomplete label in the BP. A 60X image of the boxed region of the BP is included.

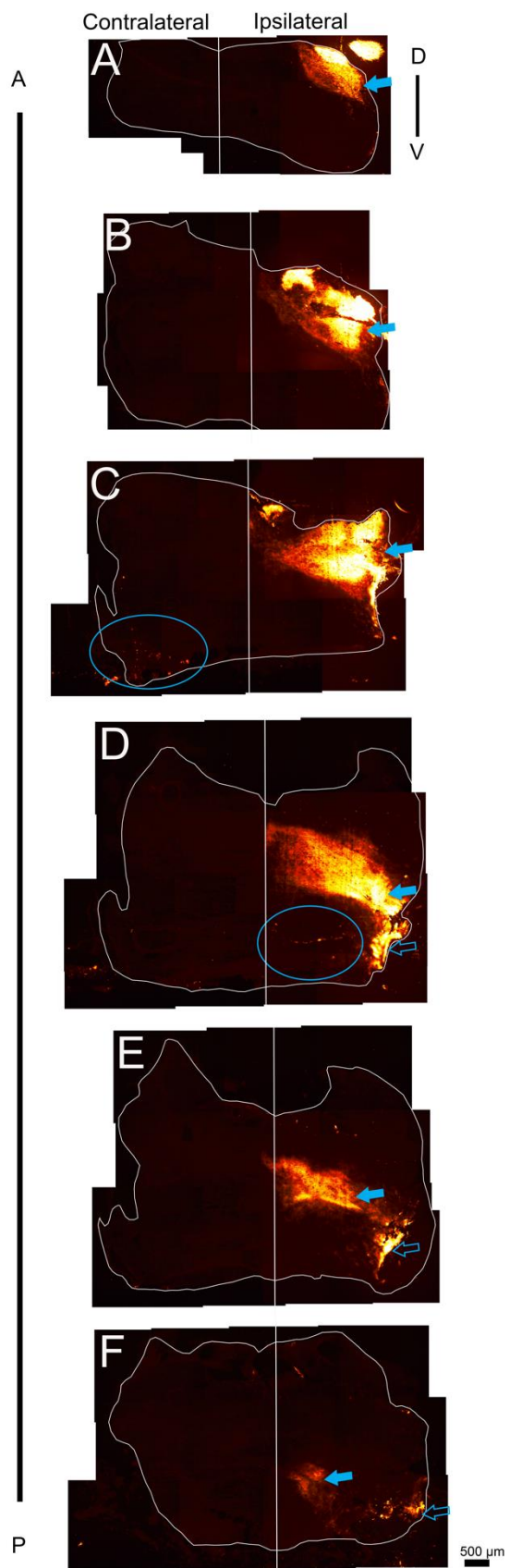
Abbreviations: Ab, abneural; D, distal; N, neural; P, proximal. Scale bars are 100 μm and 50 μm . N=1.

7.4 Tracing auditory projections from the cochlear ganglion to the brainstem

In an attempt to determine a precise location of the efferent cell bodies in the brain stem, we placed NeuroVue filters against the auditory ganglion (embryos 54-17, 54-14, 54-8, 54-9 in table 7.1 and 7.2). Although we made several attempts to replicate this data, embryo 54-9 was the only successful attempt. Based on the location of the NeuroVue label in the brainstem, we speculate that NeuroVue is labeling auditory/vestibular afferents, auditory efferents, and facial neurons. A detailed description of this can be found in the caption.

Figure 7.8 Projections from the cochlear ganglion to the brainstem

From top to bottom, these coronal sections go from most anterior/rostral (A) to most posterior/caudal (P). Each brainstem section is outlined in white and another white line down the center of the image approximates the location of the midline. The right and left sides of the sections are asymmetric. The ipsilateral side is located to the right of the midline and the contralateral side is to the left of the midline. For sections (A-C), we speculate that NeuroVue is labeling the nucleus angularis (homologous to the mammalian cochlear nucleus) (solid blue arrow). It is also possible that vestibular afferents are labeled here as well. We speculate that the circled label in section (C) may be contralateral efferents. In sections (D-E) labeled tissue indicated by the solid blue arrow could be nucleus angularis afferents, efferents, or facial neurons. We suspect the label indicated by the blue open arrow may be ipsilateral efferents and the circled fibers in section (D) are efferents projecting contralaterally. In section (F) the closed and open arrows may indicate two populations of efferents or the label indicated by the closed arrow could be efferents crossing to the contralateral side. Abbreviations: D, dorsal; V, ventral. N=1.



7.5 Discussion

7.5.1 Optimal filter implant conditions

Information was recorded on the size, shape, and location of each filter as well as the conditions of incubation. The goal was to determine the following: 1) the best combination of conditions for successfully labeling only the auditory efferents; and 2) if there are two populations of efferent cell bodies in the brainstem and where they are located. For the filter implant conditions, we examined several variables that may impact the success of labeling only efferents. The success of only labeling efferents was determined by examining the ganglia for label in afferent cell bodies.

We preferred wedge-shaped filters over rectangular-shaped filters. These filters could hit a greater range along the dorsal-to-ventral axis without cutting all the way through the ventral hindbrain (Fig. 2.8). In addition, the angle from the midline and depth from the ventral edge of the filter may also be important variables in determining the success of targeting only efferents. In our most successful examples, the angle from the midline ranged from 9.58° to 30.83° and the depth from the ventral edge ranged from $182.60\ \mu\text{m}$ to $750.90\ \mu\text{m}$. These variables on the shape and location of the filter likely determined how close the filter was placed to the efferent cell bodies.

Once a filter is placed, the dye diffuses through the efferent fibers to the BP. Dye also diffuses to the surrounding tissue. If the dye diffuses dorsally to label axons entering the nucleus angularis or nucleus magnocellularis (homologous to mammalian cochlear nucleus), afferent neurons might be back-labeled. This issue was particularly problematic in younger embryos, where there was less distance between the filter and the afferents. Higher incubation temperatures and times result in increased dye diffusion so the time and temperature of incubation needed to be balanced to make sure that efferents were labeled but afferents were not. Given that we frequently observed labeling of afferents, we attempted to reduce the incubation time by raising the temperature to $55\ ^\circ\text{C}$. Higher fixative concentrations can also increase diffusion times so we also tried incubating in 2% paraformaldehyde. We did not find that these changes increased our chances of not hitting afferents.

7.5.2 Efferent labeling in the BP and cochlear ganglion

The youngest age at which we were able to successfully label efferents was HH 37 (E11). At this age we observed only a few efferent projections into the proximal half of the BP. As the age

of the embryo increases, efferent projections in the BP increase and more efferent projections are found distally. Although, even in the adult, the distal BP received far fewer efferent fibers than the proximal BP (Fischer, 1992; Tanaka & Smith, 1978). At HH 38, varicosities are present along the length of the efferent fibers. Some of these puncta may be branching points where efferent fibers are beginning to send out back branches to the short HCs. At S41, ipsilateral efferent projections have reached the abneural edge of the BP and appear to be innervating the hyaline cells as previously observed in the mature BP by Zidanic (2002). At each stage when we have data for ipsilateral and contralateral BPs, we observed that ipsilateral BPs have more efferent fibers than the contralateral BPs for the given age.

While our data suggests that at HH37 efferents are still in the process of penetrating the sensory epithelium, we recognize that using NeuroVue dye can result in incomplete labeling of all the efferents. It is possible that not all of the efferents were labeled in the S37 embryo; however, the fact that we see strong labeling of the efferent bundle in the cochlear ganglion of this embryo supports that a large number of efferents were indeed labeled.

7.5.3 Examining populations of efferent cell bodies in the brainstem

In an attempt to determine if there are two populations of efferent cell bodies that project ipsilaterally or contralaterally, we implanted filters unilaterally into the cochlear ganglion, hoping to backfill efferent cell bodies on both sides of the brainstem. While we did get robust label in the brainstem of one of our replicates, this label was not specific to auditory efferents. Label in the nucleus angularis (Fig. 7.8) is likely from the terminal projections of the central processes of auditory afferents (Whitehead & Morest, 1981). It is also possible that diffusion near the ganglion occurred, labeling facial neurons as well. We did observe label in a similar location to the ipsilateral efferent cell bodies previously observed by (Whitehead & Morest, 1981) (Fig. 7.8 E-F). We additionally observed label on the contralateral side of the brainstem near the ventral edge of the tissue (Fig. 7.8 C). These occur more anterior than the presumptive ipsilateral efferents we observed; however, this could be due to the asymmetry of the sections on the ipsi- and contralateral sides.

Although we did observe label in one replicate after implanting a filter into the cochlear ganglion, this method may not be the best for examining efferent cell bodies in the brainstem. Due to the dye diffusion and filter placement, it is difficult to target only the efferents. In addition, we

were unable to replicate these results. In all other attempted replicates, we observed little to no label in the brainstem. Although gauze was tightly packed over the filter to keep it in place, it is possible that over the course of the lengthy incubation period the packed gauze loosened separating the filter from the ganglion thus weakening the label.

CHAPTER 8. SUMMARY, CONCLUSIONS, AND FUTURE DIRECTIONS

To date, several regulators of radial afferent innervation patterns have been identified (Coate *et al.*, 2015; Defourny *et al.*, 2013; Ghimire *et al.*, 2018). Ectopic expression of a morphogen, *Wnt9a*, has been shown to increase afferent innervation across the radial axis of the BP. This effect on innervation is likely not a direct effect as vestibular and auditory neurites have been shown to be unresponsive to *Wnt9a in vitro* (Fantetti, 2011).

In this study, we attempt to knock down *Wnt9a* using siRNAs to complement *Wnt9a* overexpression work and to use RNA sequencing of the E6 transcriptome as a starting point to identify genes down stream of *Wnt9a* that could influence innervation. We found that siRNAs carried by Tol2 plasmids or RCAS retroviruses are not a reliable method to knock down *Wnt9a* as we observed little to no knock down using these tools (CHAPTER 3). Recent work in the chicken embryo had used CRISPR/Cas9 genome editing to achieve loss-of-function. The Marcelle lab has developed Tol2 plasmids for carrying guide RNAs and Cas9 (Veron *et al.*, 2015) and has generously shared these plasmids with us. These may be more reliable tools to use in future loss-of-function experiments.

RNA deep sequencing comparing *Wnt9a* overexpressing and control BPs identified axon guidance factors down stream of *Wnt9a*. Of these, this dissertation examined *Slit2* (CHAPTER 4), *Cntn6* (CHAPTER 5), and *Sema3D/Nrp2* (CHAPTER 6). We predicted that axon guidance genes that were upregulated in the presence of exogenous *Wnt9a* (*Slit2* and *Cntn6*) would be endogenously present on the neural side of the BP and support the development of the neural-side identity or repress the abneural-side identity. Additionally, we expected that axon guidance genes downregulated in the presence of exogenous *Wnt9a* (*Sema3D* and *Nrp2*) would be endogenously expressed on the abneural side of the BP and promote the abneural-side identity or repress the neural-side identity. We attempted to validate candidate genes identified by RNA sequencing using RT-qPCR but found that this resulted in high variability. This is likely due to the varying levels of *Wnt9a* overexpression that occur when *Wnt9a* is overexpressed using RCAS (CHAPTER 3). We therefore used *in situ* hybridization to validate RNA sequencing results. While this dissertation followed up on the four genes listed above, other genes identified by RNA sequencing could be followed up on in future experiments. Examples of some of these genes can be found in the table 8.1. This table includes the number of transcripts in the control BP, the fold change, and the

canonical pathways identified by the Ingenuity Pathway Analysis run by Vidyha Munnamalai and Adam Lorch (Fekete Lab). One gene of particular note is *Fgf19*, which has been previously shown to promote the survival and outgrowth of cultured cochleovestibular ganglion neurites by our lab (Fantetti & Fekete, 2011).

Table 8.1 Candidates downstream of *Wnt9a*

Gene Name	# transcripts	Fold change	Canonical pathways
<i>Cdh8</i>	1127.5	0.74	Cell adhesion, cytoskeletal regulation, ECM organization
<i>Fgf3</i>	476.7	2.66	Cytoskeletal regulation
<i>Fgf19</i>	899.9	1.63	Cytoskeletal regulation
<i>Fzd10</i>	1792.2	0.56	Axon guidance signaling
<i>Rac3</i>	1271.2	1.39	Axon guidance signaling, regulation of actin-based motility by Rho, cytoskeletal signaling, Ephrin-B signaling
<i>Isl1</i>	3119.4	0.74	Transcriptional regulatory network in embryonic stem cells

In this study we examined the radial expression of *Slit2* and its Robo receptors (CHAPTER 4). Contrary to our hypothesis, in *Wnt9a* overexpressing BPs, we conclude that the increase in *Slit2* identified by RNA sequencing is likely due to a slight expansion of the *Slit2*-expression domain that was caused by an increase in proliferation. In control BPs, *Slit2* is expressed in the nonsensory CD flanking the prosensory domain while *Robo1* and *Robo2* are expressed in the prosensory domain in a gradient highest on the abneural side. When we transiently overexpressed *Slit2*, we did not observe any changes in innervation, proliferation, or β -catenin activation. When a dominant-negative Robo1 was transiently overexpressed, we did observe a reduction in ganglion size in some but not all samples. From this result, we speculate that Slit-Robo signaling could be involved in neuroblast delamination and/or migration from the otic epithelium. To further test this, the dominant-negative Robo1 should be overexpressed using delivery methods designed for long-term overexpression, such as Tol2 plasmids or RCAS retrovirus.

RNA sequencing data indicated that *Cntn6* transcripts increase in the presence of exogenous *Wnt9a*. We attempted to validate these results using *in situ* hybridization (CHAPTER 5). We conclude that *in situ* hybridization is not sensitive enough to validate these results due to the low number of transcripts present in both control and *Wnt9a*-overexpressing BPs.

This study also validated *Sema3D* using *in situ* hybridization as well as examine the expression another class III Semaphorin and Semaphorin receptors (CHAPTER 6). The expression patterns of class III Semaphorins and their receptors that we examined do not support our original hypothesis that they are involved in establishing or maintaining radial innervation patterns within the auditory sensory organ; however, they do suggest that they could be involved in vestibular innervation, synaptogenesis, endothelial cell migration, and other functions. To test this, we overexpressed *Sema3D* using RCAS retrovirus. Our preliminary data suggests that *Sema3D* may be involved in channeling endothelial cell migration to the inner ear and in channeling neurites to the vestibular epithelium. In this data set, overexpression may be beginning after vestibular neurites have begun to penetrate the vestibular epithelium. In future experiments, virus injections should be done at an earlier time point or a Tol2 plasmid could be used to deliver *Sema3D*. Nicolas Daudet has kindly provided us with the Tol2 plasmids used in Freeman and Daudet (2012) and Mann *et al.* (2017).

In addition to investigating potential molecular regulators of radial innervation downstream of *Wnt9a*, we also examined the time course and arrangement of efferents in the BP and brainstem using NeuroVue lipophilic tracer dye (CHAPTER 7). We focused our attention on this understudied population because some of the guidance factors we had identified in the E6 BP might impact the peripheral projections of the efferents, but the timecourse of when we should expect this pathfinding to be occurring needed to be determined. Our data supports that efferents have begun to penetrate the sensory epithelium by E11 and have begun sending branches to short HCs by E12. By E15, efferents appear to have reached the abneural edge of the BP and are innervating the hyaline cells. These data suggest that a separate transcriptomic analysis at a later time point might be useful to identify candidate molecules that direct efferents in the sensory periphery. At each age we examined where we have ipsilateral and contralateral BPs to compare, we find that the ipsilateral BP has more efferent fibers. Given the success rate of this method, future work should aim to replicate the ages for which we have collected data.

REFERENCES

- Adam, J., Myat, A., Le Roux, I., Eddison, M., Henrique, D., Ish-Horowicz, D., & Lewis, J. (1998). Cell fate choices and the expression of Notch, Delta and Serrate homologues in the chick inner ear: parallels with *Drosophila* sense-organ development. *Development*, *125*, 4645-4654.
- Agerman, K., Hjerling-Leffler, J., Blanchard, M. P., Scarfone, E., Canlon, B., Nosrat, C., & Ernfors, P. (2003). BDNF gene replacement reveals multiple mechanisms for establishing neurotrophin specificity during sensory nervous system development. *Development*, *130*(8), 1479-1491.
- Andrews, W., Barber, M., Hernadez-Miranda, L. R., Xian, J., Rakic, S., Sundaresan, V., Rabbitts, T. H., Pannell, R., Rabbitts, P., Thompson, H., Erskine, L., Murakami, F., & Parnavelas, J. G. (2008). The role of Slit-Robo signaling in the generation, migration and morphological differentiation of cortical interneurons. *Developmental Biology*, *313*(2), 648-658. doi:10.1016/j.ydbio.2007.10.052
- Bagnard, D., Vaillant, C., Khuth, S. T., Dufay, N., Lohrum, M., Puschel, A. W., Belin, M. F., Bolz, J., & Thomasset, N. (2001). Semaphorin 3A-vascular endothelial growth factor-165 balance mediates migration and apoptosis of neural progenitor cells by the recruitment of shared receptor. *Journal of Neuroscience*, *21*(10), 3332-3341.
- Baleriola, J., Jean, Y., Troy, C., & Hengst, U. (2015). Detection of Axonally Localized mRNAs in Brain Sections Using High-Resolution In Situ Hybridization. *Jove-Journal Of Visualized Experiments*, *2015*(100). doi:10.3791/52799
- Bao, Z. Z., & Jin, Z. (2006). Sema3D and Sema7A have distinct expression patterns in chick embryonic development. *Developmental Dynamics*, *235*(8), 2282-2289. doi:10.1002/dvdy.20882
- Bates, D., Taylor, G. I., Minichiello, J., Farlie, P., Cichowitz, A., Watson, N., Klagsbrun, M., Mamluk, R., & Newgreen, D. F. (2003). Neurovascular congruence results from a shared patterning mechanism that utilizes Semaphorin3A and Neuropilin-1. *Developmental Biology*, *255*(1), 77-98.
- Battisti, A. C., Fantetti, K. N., Moyers, B. A., & Fekete, D. M. (2014). A subset of chicken statoacoustic ganglion neurites are repelled by Slit1 and Slit2. *Hear Res*, *310*, 1-12. doi:10.1016/j.heares.2014.01.003
- Battisti, A. C., & Fekete, D. M. (2008). Slits and robos in the developing chicken inner ear. *Developmental Dynamics*, *237*(2), 476-484.
- Berglund, A. M., & Ryugo, D. K. (1987). Hair cell innervation by spiral ganglion neurons in the mouse. *Journal of Comparative Neurology*, *255*(4), 560-570. doi:10.1002/cne.902550408
- Birmingham-McDonogh, O., Oesterle, E. C., Stone, J. S., Hume, C. R., Huynh, H. M., & Hayashi, T. (2006). Expression of Prox1 during mouse cochlear development. *Journal of Comparative Neurology*, *496*(2), 172-186. doi:10.1002/cne.20944
- Bouzioukh, F., Daoudal, G., Falk, J., Debanne, D., Rougon, G., & Castellani, V. (2006). Semaphorin3A regulates synaptic function of differentiated hippocampal neurons. *European Journal of Neuroscience*, *23*(9), 2247-2254. doi:10.1111/j.1460-9568.2006.04783.x

- Bromberg-White, J. L., Webb, C. P., Patacsil, V. S., Miranti, C. K., Williams, B. O., & Holmen, S. L. (2004). Delivery of short hairpin RNA sequences by using a replication-competent avian retroviral vector. *Journal of Virology*, 78(9), 4914-4916.
- Brose, K., Bland, K. S., Wang, K. H., Arnott, D., Henzel, W., Goodman, C. S., Tessier-Lavigne, M., & Kidd, T. (1999). Slit proteins bind Robo receptors and have an evolutionarily conserved role in repulsive axon guidance. *Cell*, 96(6), 795-806.
- Bruce, L. L., Kingsley, J., Nichols, D. H., & Fritsch, B. (1997). The development of vestibulocochlear efferents and cochlear afferents in mice. *International Journal of Developmental Neuroscience*, 15(4-5), 671-692.
- Carney, P. R., & Couve, E. (1989). Cell polarity changes and migration during early development of the avian peripheral auditory system. *The Anatomical Record*, 225, 156-164.
- Chandler, J. P. (1984). Light and electron microscopic studies of the basilar papilla in the duck, *Anas platyrhynchos*. I. The Hatchling. *The Journal of Comparative Neurology*, 222, 506-522.
- Chen, M., Payne, W. S., Hunt, H., Zhang, H., Holmen, S. L., & Dodgson, J. B. (2008). Inhibition of Marek's disease virus replication by retroviral vector-based RNA interference. *Virology*, 377(2), 265-272. doi:10.1016/j.virol.2008.03.019
- Chrysostomou, E., Gale, J. E., & Daudet, N. (2012). Delta-like 1 and lateral inhibition during hair cell formation in the chicken inner ear: evidence against cis-inhibition. *Development*, 139(20), 3764-3774. doi:10.1242/dev.074476
- Clevers, H., & Nusse, R. (2012). Wnt/beta-catenin signaling and disease. *Cell*, 149(6), 1192-1205. doi:10.1016/j.cell.2012.05.012
- Coate, T. M., & Kelley, M. W. (2013). Making connections in the inner ear: recent insights into the development of spiral ganglion neurons and their connectivity with sensory hair cells. *Seminars in Cell & Developmental Biology*, 24(5), 460-469. doi:10.1016/j.semcdb.2013.04.003
- Coate, T. M., Spita, N. A., Zhang, K. D., Isgrig, K. T., & Kelley, M. W. (2015). Neuropilin-2/Semaphorin-3F-mediated repulsion promotes inner hair cell innervation by spiral ganglion neurons. *Elife*, 4. doi:10.7554/eLife.07830
- Cohen, G. M., & Cotanche, D. A. (1992). Development of the sensory receptors and their innervation in the chick cochlea. In R. Romand (Ed.), *Development of Auditory and Vestibular Systems 2* (1 ed., pp. 101-138). Amsterdam: Elsevier.
- Cohen, G. M., & Fermin, C. D. (1978). The development of hair cells in the embryonic chick's basilar papilla. *Acta Otolaryngol*, 86, 342-358.
- Coppola, V., Kucera, J., Palko, M. E., Martinez-De Velasco, J., Lyons, W. E., Fritsch, B., & Tessarollo, L. (2001). Dissection of NT3 functions in vivo by gene replacement strategy. *Development*, 128(21), 4315-4327.
- Cotanche, D., & Sulik, K. (1982). Scanning electron microscopy of the developing chick tegmentum vasculosum. *Scan Electron Microsc*(Pt 3), 1283-1294.
- Cotanche, D. A., Henson, M. M., & Henson, O. W., Jr. (1992). Contractile proteins in the hyaline cells of the chicken cochlea. *Journal of Comparative Neurology*, 324(3), 353-364.
- Cotanche, D. A., & Sulik, K. K. (1983). Early differentiation of hair cells in the embryonic chick basilar papilla. *Archives of Otorhinolaryngology*, 237, 191-195.
- D'Amico-Martel, A., & Noden, D. M. (1983). Contributions of placodal and neural crest cells to avian cranial peripheral ganglia. *American Journal of Anatomy*, 166, 445-468.

- Dale, T. C. (1998). Signal transduction by the Wnt family of ligands. *Biochemical Journal*, 329(Pt 2), 209-223.
- Darrow, K. N., Maison, S. F., & Liberman, M. C. (2007). Selective removal of lateral olivocochlear efferents increases vulnerability to acute acoustic injury. *Journal of Neurophysiology*, 97(2), 1775-1785.
- Das, R. M., Van Hateren, N. J., Howell, G. R., Farrell, E. R., Bangs, F. K., Porteous, V. C., Manning, E. M., McGrew, M. J., Ohyama, K., Sacco, M. A., Halley, P. A., Sang, H. M., Storey, K. G., Placzek, M., Tickle, C., Nair, V. K., & Wilson, S. A. (2006). A robust system for RNA interference in the chicken using a modified microRNA operon. *Developmental Biology*, 294(2), 554-563.
- Defourny, J., Poirrier, A. L., Lallemand, F., Mateo Sanchez, S., Neef, J., Vanderhaeghen, P., Soriano, E., Peuckert, C., Kullander, K., Fritsch, B., Nguyen, L., Moonen, G., Moser, T., & Malgrange, B. (2013). Ephrin-A5/EphA4 signalling controls specific afferent targeting to cochlear hair cells. *Nat Commun*, 4, 1438. doi:10.1038/ncomms2445
- Derijck, A. A., Van Erp, S., & Pasterkamp, R. J. (2010). Semaphorin signaling: molecular switches at the midline. *Trends in Cell Biology*, 20(9), 568-576. doi:10.1016/j.tcb.2010.06.007
- Devarajan, K., Forrest, M. L., Detamore, M. S., & Staecker, H. (2013). Adenovector-mediated gene delivery to human umbilical cord mesenchymal stromal cells induces inner ear cell phenotype. *Cell Rerogram*, 15(1), 43-54. doi:10.1089/cell.2011.0097
- Dewson III, J. H. (1967). Olivocochlear Bundle: Relationships to Signal Discrimination in Noise. *The Journal of the Acoustical Society of America*, 42(5), 1189-1189.
- Dickson, B. J., & Gilestro, G. F. (2006). Regulation of commissural axon pathfinding by slit and its Robo receptors. *Annual Review of Cell and Developmental Biology*, 22, 651-675.
- Drenckhahn, D., Merte, C., von Düring, M., Smolders, J., & Klinke, R. (1991). Actin, myosin and alpha-actinin containing filament bundles in hyaline cells of the caiman cochlea. *Hear Res*, 54(1), 29-38.
- Duan, Y., Wang, S. H., Song, J., Mironova, Y., Ming, G. L., Kolodkin, A. L., & Giger, R. J. (2014). Semaphorin 5A inhibits synaptogenesis in early postnatal- and adult-born hippocampal dentate granule cells. *Elife*, 3. doi:10.7554/eLife.04390
- Duncan, J., Kersigo, J., Gray, B., & Fritsch, B. (2011). Combining lipophilic dye, in situ hybridization, immunohistochemistry, and histology. *Journal of visualized experiments: JoVE*(49).
- Ernfors, P., Van De Water, T., Loring, J., & Jaenisch, R. (1995). Complementary roles of BDNF and NT-3 in vestibular and auditory development. *Neuron*, 14, 1153-1164.
- Fantetti, K. N. (2011). *Responsiveness of chick statoacoustic ganglion neurons to morphogens*: Purdue University.
- Fantetti, K. N., & Fekete, D. M. (2011). Members of the BMP, Shh and FGF morphogen families promote chicken statoacoustic ganglion neurite outgrowth and neuron survival in vitro. *Dev Neurobiol*. doi:10.1002/dneu.20988
- Fantetti, K. N., Zou, Y., & Fekete, D. M. (2011). Wnts and Wnt inhibitors do not influence axon outgrowth from chicken statoacoustic ganglion neurons. *Hear Res*, 278(1-2), 86-95. doi:S0378-5955(11)00106-7 [pii]10.1016/j.heares.2011.04.005
- Farinas, I., Jones, K. R., Tessarollo, L., Vigers, A. J., Huang, E., Kirstein, M., de Caprona, D. C., Coppola, V., Backus, C., Reichardt, L. F., & Fritsch, B. (2001). Spatial shaping of cochlear innervation by temporally regulated neurotrophin expression. *Journal of Neuroscience*, 21(16), 6170-6180.

- Fiore, R., Rahim, B., Christoffels, V. M., Moorman, A. F., & Puschel, A. W. (2005). Inactivation of the Sema5a gene results in embryonic lethality and defective remodeling of the cranial vascular system. *Molecular and Cellular Biology*, 25(6), 2310-2319. doi:10.1128/mcb.25.6.2310-2319.2005
- Fischer, F. P. (1992). Quantitative analysis of the innervation of the chicken basilar papilla. *Hear Res*, 61(1-2), 167-178.
- Frank, M. M., & Goodrich, L. V. (2018). Talking back: Development of the olivocochlear efferent system. e324.
- Freeman, S., Chrysostomou, E., Kawakami, K., Takahashi, Y., & Daudet, N. (2012). Tol2-mediated gene transfer and in ovo electroporation of the otic placode: a powerful and versatile approach for investigating embryonic development and regeneration of the chicken inner ear. *Methods Mol Biol*, 916, 127-139. doi:10.1007/978-1-61779-980-8_10
- Freeman, S. D., & Daudet, N. (2012). Artificial induction of Sox21 regulates sensory cell formation in the embryonic chicken inner ear. *PLoS One*, 7(10), e46387.
- Fritsch, B. (1996). Development of the labyrinthine efferent system. *Annals of the New York Academy of Science*, 781, 21-33.
- Fritsch, B., Dillard, M., Lavado, A., Harvey, N. L., & Jahan, I. (2010). Canal cristae growth and fiber extension to the outer hair cells of the mouse ear require Prox1 activity. *PLoS One*, 5(2), e9377. doi:10.1371/journal.pone.0009377
- Fritsch, B., Muirhead, K. A., Feng, F., Gray, B. D., & Ohlsson-Wilhelm, B. M. (2005). Diffusion and imaging properties of three new lipophilic tracers, NeuroVue Maroon, NeuroVue Red and NeuroVue Green and their use for double and triple labeling of neuronal profile. *Brain Research Bulletin*, 66(3), 249-258. doi:10.1016/j.brainresbull.2005.05.016
- Fritsch, B., & Nichols, D. H. (1993). DiI reveals a prenatal arrival of efferents at the differentiating otocyst of mice. *Hear Res*, 65(1-2), 51-60.
- Gennarini, G., Durbec, P., Boned, A., Rougon, G., & Goridis, C. (1991). Transfected F3/F11 neuronal cell surface protein mediates intercellular adhesion and promotes neurite outgrowth. *Neuron*, 6(4), 595-606.
- Ghimire, S. R., Ratzan, E. M., & Deans, M. R. J. D. (2018). A non-autonomous function of the core PCP protein VANGL2 directs peripheral axon turning in the developing cochlea. *145(12)*, dev159012.
- Ginzberg, R. D., & Gilula, N. B. (1980). Synaptogenesis in the vestibular sensory epithelium of the chick embryo. *Journal of Neurocytology*, 9(3), 405-424.
- Giraud, A. L., Garnier, S., Micheyl, C., Lina, G., Chays, A., & Chéry-Croze, S. (1997). Auditory efferents involved in speech-in-noise intelligibility. *Neuroreport*, 8(7), 1779-1783.
- Glasgow, E., & Tomarev, S. I. (1998). Restricted expression of the homeobox gene prox 1 in developing zebrafish. *Mech Dev*, 76(1-2), 175-178. bin/cas/tree/store/mod/cas_sub/browse/browse.cgi?year=1998&volume=1976&issue=1991-1992&aid=1964.
- Goodyear, R. J., & Richardson, G. P. (2018). Structure, Function, and Development of the Tectorial Membrane: An Extracellular Matrix Essential for Hearing. *Curr Top Dev Biol*, 130, 217-244. doi:10.1016/bs.ctdb.2018.02.006
- Gu, C., Rodriguez, E. R., Reimert, D. V., Shu, T., Fritsch, B., Richards, L. J., Kolodkin, A. L., & Ginty, D. D. (2003). Neuropilin-1 conveys semaphorin and VEGF signaling during neural and cardiovascular development. *Developmental Cell*, 5(1), 45-57.

- Guinan, J. J. (2017). Olivocochlear efferents: their action, effects, measurement and uses, and the impact of the new conception of cochlear mechanical responses. *Hearing Research*.
- Guinan, J. J., Jr., Warr, W. B., & Norris, B. E. (1984). Topographic organization of the olivocochlear projections from the lateral and medial zones of the superior olivary complex. *Journal of Comparative Neurology*, 226(1), 21-27. doi:10.1002/cne.902260103
- Guinan Jr, J. J. (2006). Olivocochlear efferents: anatomy, physiology, function, and the measurement of efferent effects in humans. *Ear and hearing*, 27(6), 589-607.
- Hallpike, C. S., & Cairns, H. (1938). Observations on the Pathology of Ménière's Syndrome. *The Journal of Laryngology & Otology*, 53(10), 625-655. doi:10.1017/S0022215100003947
- Hamburger, V., & Hamilton, H. L. (1951). A series of normal stages in the development of the chick embryo. *Journal of Morphology*, 88, 49-91.
- Hamm, M. J., Kirchmaier, B. C., & Herzog, W. (2016). Sema3d controls collective endothelial cell migration by distinct mechanisms via Nrp1 and PlxnD1. *The Journal of Cell Biology*, 215(3), 415-430. doi:10.1083/jcb.201603100
- Hammond, R., Vivancos, V., Naeem, A., Chilton, J., Mambetisaeva, E., Andrews, W., Sundaresan, V., & Guthrie, S. (2005). Slit-mediated repulsion is a key regulator of motor axon pathfinding in the hindbrain. *Development*, 132(20), 4483-4495.
- Harley, R. J., Murdy, J. P., Wang, Z., Kelly, M. C., Ropp, T. J. F., Park, S. H., Maness, P. F., Manis, P. B., & Coate, T. M. J. D. D. (2018). Neuronal cell adhesion molecule (NrCAM) is expressed by sensory cells in the cochlea and is necessary for proper cochlear innervation and sensory domain patterning during development.
- Hartmann, C., & Tabin, C. J. (2001). Wnt-14 plays a pivotal role in inducing synovial joint formation in the developing appendicular skeleton. *Cell*, 104(3), 341-351.
- Hemond, S. G., & Morest, D. K. (1991). Ganglion formation from the otic placode and the otic crest in the chick embryo: mitosis, migration, and the basal lamina. *Anat Embryol (Berl)*, 184(1), 1-13.
- Holmes, G., & Niswander, L. (2001). Expression of slit-2 and slit-3 during chick development. *Developmental Dynamics*, 222(2), 301-307.
- Huelsken, J., & Birchmeier, W. (2001). New aspects of Wnt signaling pathways in higher vertebrates. *Current Opinion in Genetics & Development*, 11(5), 547-553.
- Ishiyama, E., Cutt, R. A., & Keels, E. W. (1970). Ultrastructure of the tegmentum vasculosum and transitional zone. *Ann Otol Rhinol Laryngol*, 79(5), 998-1009. doi:10.1177/000348947007900520
- Jacques, B. E., Montgomery, W. H. t., Uribe, P. M., Yatteau, A., Asuncion, J. D., Resendiz, G., Matsui, J. I., & Dabdoub, A. (2014). The role of Wnt/beta-catenin signaling in proliferation and regeneration of the developing basilar papilla and lateral line. *Dev Neurobiol*, 74(4), 438-456. doi:10.1002/dneu.22134
- Jacques, B. E., Puligilla, C., Weichert, R. M., Ferrer-Vaquero, A., Hadjantonakis, A. K., Kelley, M. W., & Dabdoub, A. (2012). A dual function for canonical Wnt/beta-catenin signaling in the developing mammalian cochlea. *Development*, 139(23), 4395-4404. doi:10.1242/dev.080358
- Jin, Z., Chau, M. D., & Bao, Z. Z. (2006). Sema3D, Sema3F, and Sema5A are expressed in overlapping and distinct patterns in chick embryonic heart. *Developmental Dynamics*, 235(1), 163-169. doi:10.1002/dvdy.20614

- Julien, F., Bechara, A., Fiore, R., Nawabi, H., Zhou, H., Hoyo-Becerra, C., Bozon, M., Rougon, G., Grumet, M., Püschel, A. W., Sanes, J. R., & Castellani, V. (2005). Dual Functional Activity of Semaphorin 3B Is Required for Positioning the Anterior Commissure. *Neuron*, 48(1), 63-75. doi:<https://doi.org/10.1016/j.neuron.2005.08.033>
- Katayama, A., & Corwin, J. T. (1989). Cell production in the chicken cochlea. *Journal of Comparative Neurology*, 281(1), 129-135.
- Katayama, K., Imai, F., Suto, F., & Yoshida, Y. (2013). Deletion of Sema3a or plexinA1/plexinA3 causes defects in sensory afferent projections of statoacoustic ganglion neurons. *PLoS One*, 8(8), e72512. doi:10.1371/journal.pone.0072512
- Kawakami, K. (2007). Tol2: a versatile gene transfer vector in vertebrates. *Genome Biol*, 8 Suppl 1, S7. doi:10.1186/gb-2007-8-s1-s7
- Kessler, O., Shraga-Heled, N., Lange, T., Gutmann-Raviv, N., Sabo, E., Baruch, L., Machluf, M., & Neufeld, G. (2004). Semaphorin-3F is an inhibitor of tumor angiogenesis. *Cancer Research*, 64(3), 1008-1015.
- Kim, D., Pertea, G., Trapnell, C., Pimentel, H., Kelley, R., & Salzberg, S. L. (2013). TopHat2: accurate alignment of transcriptomes in the presence of insertions, deletions and gene fusions. *Genome Biol*, 14(4), R36. doi:10.1186/gb-2013-14-4-r36
- Kim, K. A., Wagle, M., Tran, K., Zhan, X., Dixon, M. A., Liu, S., Gros, D., Korver, W., Yonkovich, S., Tomasevic, N., Binnerts, M., & Abo, A. (2008). R-Spondin family members regulate the Wnt pathway by a common mechanism. *Mol Biol Cell*, 19(6), 2588-2596. doi:10.1091/mbc.E08-02-0187
- Kimura, R. S. (1969). Distribution, Structure, and Function of Dark Cells in the Vestibular Labyrinth. *Annals of Otology, Rhinology & Laryngology*, 78(3), 542-561. doi:10.1177/000348946907800311
- Knowlton, V. Y. (1967). Correlation of the development of membranous and bony labyrinths, acoustic ganglia, nerves, and brain centers in the chick embryo. *Journal of Morphology*, 121, 179-208.
- Kohn, A., & Moon, R. (2005). Wnt and calcium signaling: β -Catenin-independent pathways. *Cell Calcium*, 38(3-4), 439-446. doi:10.1016/j.ceca.2005.06.022
- Koppl, C. (2011). Birds--same thing, but different? Convergent evolution in the avian and mammalian auditory systems provides informative comparative models. *Hear Res*, 273(1-2), 65-71. doi:10.1016/j.heares.2010.03.095
- Koundakjian, E. J., Appler, J. L., & Goodrich, L. V. (2007). Auditory neurons make stereotyped wiring decisions before maturation of their targets. *Journal of Neuroscience*, 27(51), 14078-14088. doi:10.1523/JNEUROSCI.3765-07.2007
- Kuijpers, W. H., N. M. D.; Bonting, S. L. (1970). Distribution and properites of ATPase activities in the cochlea of the chicken. *Comparative Biochemistry and Physiology*, 36(4), 669-670.
- Kujawa, S. G., & Liberman, M. C. (1997). Conditioning-related protection from acoustic injury: effects of chronic deafferentation and sham surgery. *Journal of Neurophysiology*, 78(6), 3095-3106.
- Laht, P., Tammaru, E., Otsus, M., Rohtla, J., Tiismus, L., & Veske, A. (2015). Plexin-B3 suppresses excitatory and promotes inhibitory synapse formation in rat hippocampal neurons. *Experimental Cell Research*, 335(2), 269-278. doi:10.1016/j.yexcr.2015.05.007
- Lewis, E. R., Leverenz, E. L., & Bialek, W. S. (1985). *The vertebrate inner ear*: CRC PressI Llc.

- Li, H., Takeda, Y., Niki, H., Ogawa, J., Kobayashi, S., Kai, N., Akasaka, K., Asano, M., Sudo, K., Iwakura, Y., & Watanabe, K. (2003). Aberrant responses to acoustic stimuli in mice deficient for neural recognition molecule NB-2. *European Journal of Neuroscience*, *17*(5), 929-936.
- Liberman, M. C., & Brown, M. C. (1986). Physiology and anatomy of single olivocochlear neurons in the cat. *Hear Res*, *24*(1), 17-36.
- Loftus, S. K., Larson, D. M., Watkins-Chow, D., Church, D. M., & Pavan, W. J. (2001). Generation of RCAS vectors useful for functional genomic analyses. *DNA Research*, *8*(5), 221-226.
- Love, M. I., Huber, W., & Anders, S. (2014). Moderated estimation of fold change and dispersion for RNA-seq data with DESeq2. *Genome Biol*, *15*(12), 550. doi:10.1186/s13059-014-0550-8
- Maiorana, C. R., & Staecker, H. (2005). Advances in inner ear gene therapy: exploring cochlear protection and regeneration. *Current Opinion in Otolaryngology & Head and Neck Surgery*, *13*(5), 308-312.
- Mann, Z. F., Galvez, H., Pedreno, D., Chen, Z., Chrysostomou, E., Zak, M., Kang, M., Canden, E., & Daudet, N. (2017). Shaping of inner ear sensory organs through antagonistic interactions between Notch signalling and Lmx1a. *Elife*, *6*. doi:10.7554/eLife.33323
- Martín-Sierra, C., Gallego-Martinez, A., Requena, T., Frejo, L., Batuecas-Caletrío, A., & Lopez-Escamez, J. A. (2016). Variable expressivity and genetic heterogeneity involving DPT and SEMA3D genes in autosomal dominant familial Meniere's disease. *European Journal of Human Genetics*, *25*, 200. doi:10.1038/ejhg.2016.154
- Masutani, H., Takahashi, H., & Sando, I. (1992). Dark Cell Pathology in Meniere's Disease. *Acta Otolaryngol*, *112*(3), 479-485. doi:10.3109/00016489209137429
- Meier, S. (1978). Development of the embryonic chick otic placode. I. Light microscope analysis. *The Anatomical Record*, *191*, 447-458.
- Mercati, O., Huguet, G., Danckaert, A., Andre-Leroux, G., Maruani, A., Bellinzoni, M., Rolland, T., Gouder, L., Mathieu, A., Buratti, J., Amsellem, F., Benabou, M., Van-Gils, J., Beggiato, A., Konyukh, M., Bourgeois, J. P., Gazzellone, M. J., Yuen, R. K., Walker, S., Delepine, M., Boland, A., Regnault, B., Francois, M., Van Den Abbeele, T., Mosca-Boidron, A. L., Faivre, L., Shimoda, Y., Watanabe, K., Bonneau, D., Rastam, M., Leboyer, M., Scherer, S. W., Gillberg, C., Delorme, R., Cloez-Tayarani, I., & Bourgeron, T. (2017). CNTN6 mutations are risk factors for abnormal auditory sensory perception in autism spectrum disorders. *Molecular Psychiatry*, *22*(4), 625-633. doi:10.1038/mp.2016.61
- Meza, G., & Hinojosa, R. (1987). Ontogenetic approach to cellular localization of neurotransmitters in the chick vestibule. *Hear Res*, *28*(1), 73-85.
- Miao, H. Q., Soker, S., Feiner, L., Alonso, J. L., Raper, J. A., & Klagsbrun, M. (1999). Neuropilin-1 mediates collapsin-1/semaphorin III inhibition of endothelial cell motility: functional competition of collapsin-1 and vascular endothelial growth factor-165. *Journal of Cell Biology*, *146*(1), 233-242.
- Miko, I. J., Henkemeyer, M., & Cramer, K. S. (2008). Auditory brainstem responses are impaired in EphA4 and ephrin-B2 deficient mice. *Hear Res*, *235*(1-2), 39-46. doi:10.1016/j.heares.2007.09.003
- Miyazaki, N., Furuyama, T., Takeda, N., Inoue, T., Kubo, T., & Inagaki, S. (1999). Expression of mouse semaphorin H mRNA in the inner ear of mouse fetuses. *Neuroscience Letters*, *261*(1-2), 127-129.

- Mlodzik, M. (2002). Planar cell polarization: do the same mechanisms regulate *Drosophila* tissue polarity and vertebrate gastrulation? *Trends in Genetics*, *18*(11), 564-571.
- Morgan, B. A., & Fekete, D. M. (1996). Manipulating gene expression with replication-competent retroviruses. *Methods Cell Biol*, *51*, 185-218.
- Morita, A., Yamashita, N., Sasaki, Y., Uchida, Y., Nakajima, O., Nakamura, F., Yagi, T., Taniguchi, M., Usui, H., Katoh-Semba, R., Takei, K., & Goshima, Y. (2006). Regulation of Dendritic Branching and Spine Maturation by Semaphorin3A-Fyn Signaling. *The Journal of Neuroscience*, *26*(11), 2971.
- Mulvaney, J. F., Yatteau, A., Sun, W. W., Jacques, B., Takubo, K., Suda, T., Yamada, W., & Dabdoub, A. (2013). Secreted factor R-Spondin 2 is involved in refinement of patterning of the mammalian cochlea. *Developmental Dynamics*, *242*(2), 179-188. doi:10.1002/dvdy.23908
- Munnamalai, V., & Fekete, D. M. (2013). Wnt signaling during cochlear development. *Seminars in Cell & Developmental Biology*, *24*(5), 480-489. doi:10.1016/j.semcdb.2013.03.008
- Munnamalai, V., & Fekete, D. M. (2016). Notch-Wnt-Bmp crosstalk regulates radial patterning in the mouse cochlea in a spatiotemporal manner. *Development*, *143*(21), 4003-4015. doi:10.1242/dev.139469
- Munnamalai, V., Sienknecht, U. J., Duncan, R. K., Scott, M. K., Thawani, A., Fantetti, K. N., Atallah, N. M., Biesemeier, D. J., Song, K. H., Luethy, K., Traub, E., & Fekete, D. M. (2017). Wnt9a Can Influence Cell Fates and Neural Connectivity across the Radial Axis of the Developing Cochlea. *Journal of Neuroscience*, *37*(37), 8975-8988. doi:10.1523/jneurosci.1554-17.2017
- Murakami, Y., Suto, F., Shimizu, M., Shinoda, T., Kameyama, T., & Fujisawa, H. (2001). Differential expression of plexin-A subfamily members in the mouse nervous system. *Developmental Dynamics*, *220*(3), 246-258.
- Nakamura, F., Kalb, R. G., & Strittmatter, S. M. (2000). Molecular basis of semaphorin-mediated axon guidance. *Journal of Neurobiology*, *44*(2), 219-229.
- Nickel, R., Becker, D., & Forge, A. (2006). Molecular and functional characterization of gap junctions in the avian inner ear. *Journal of Neuroscience*, *26*(23), 6190-6199. doi:10.1523/jneurosci.1116-06.2006
- Oesterle, E. C., Cunningham, D. E., & Rubel, E. W. (1992). Ultrastructure of hyaline, border, and vacuole cells in chick inner ear. *Journal of Comparative Neurology*, *318*(1), 64-82.
- Ogawa, J., Lee, S., Itoh, K., Nagata, S., Machida, T., Takeda, Y., & Watanabe, K. (2001). Neural recognition molecule NB-2 of the contactin/F3 subgroup in rat: Specificity in neurite outgrowth-promoting activity and restricted expression in the brain regions. *Journal of Neuroscience Research*, *65*(2), 100-110. doi:10.1002/jnr.1133
- Paradis, S., Harrar, D. B., Lin, Y., Koon, A. C., Hauser, J. L., Griffith, E. C., Zhu, L., Brass, L. F., Chen, C., & Greenberg, M. E. (2007). An RNAi-based approach identifies molecules required for glutamatergic and GABAergic synapse development. *Neuron*, *53*(2), 217-232. doi:10.1016/j.neuron.2006.12.012
- Rasmussen, G. L. (1946). The olivary peduncle and other fiber projections of the superior olivary complex. *Journal of Comparative Neurology*, *84*(2), 141-219.
- Rasmussen, G. L. (1953). Further observations of the efferent cochlear bundle. *Journal of Comparative Neurology*, *99*(1), 61-74.
- Rebillard, M., & Pujol, R. (1983). Innervation of the chicken basilar papilla during its development. *Acta Otolaryngol*, *96*(5-6), 379-388.

- Rhee, J., Buchan, T., Zukerberg, L., Lilien, J., & Balsamo, J. (2007). Cables links Robo-bound Abl kinase to N-cadherin-bound beta-catenin to mediate Slit-induced modulation of adhesion and transcription. *Nature Cell Biology*, 9(8), 883-892. doi:10.1038/ncb1614
- Rhee, J., Mahfooz, N. S., Arregui, C., Lilien, J., Balsamo, J., & VanBerkum, M. F. (2002). Activation of the repulsive receptor Roundabout inhibits N-cadherin-mediated cell adhesion. *Nature Cell Biology*, 4(10), 798-805. doi:10.1038/ncb858
- Roberts, A., Pimentel, H., Trapnell, C., & Pachter, L. (2011). Identification of novel transcripts in annotated genomes using RNA-Seq. *Bioinformatics*, 27(17), 2325-2329. doi:10.1093/bioinformatics/btr355
- Robinson, M. D., McCarthy, D. J., & Smyth, G. K. (2010). edgeR: a Bioconductor package for differential expression analysis of digital gene expression data. *Bioinformatics*, 26(1), 139-140. doi:10.1093/bioinformatics/btp616
- Salehi, P., Ge, M. X., Gundimeda, U., Michelle Baum, L., Lael Cantu, H., Lavinsky, J., Tao, L., Myint, A., Cruz, C., Wang, J., Nikolakopoulou, A. M., Abdala, C., Kelley, M. W., Ohyama, T., Coate, T. M., & Friedman, R. A. (2017). Role of Neuropilin-1/Semaphorin-3A signaling in the functional and morphological integrity of the cochlea. *PLoS Genetics*, 13(10), e1007048. doi:10.1371/journal.pgen.1007048
- Sanchez-Calderon, H., Martin-Partido, G., & Hidalgo-Sanchez, M. (2004). Otx2, Gbx2, and Fgf8 expression patterns in the chick developing inner ear and their possible roles in otic specification and early innervation. *Gene Expr Patterns*, 4(6), 659-669.
- Schneider, M. E., Cotanche, D. A., Fambrough, D. M., Saunders, J. C., & Matschinsky, F. M. (1987). Immunocytochemical and quantitative studies of Na⁺,K⁺-ATPase distribution in the developing chick cochlea. *Hear Res*, 31(1), 39-53.
- Serini, G., Valdembri, D., Zanivan, S., Morterra, G., Burkhardt, C., Caccavari, F., Zammataro, L., Primo, L., Tamagnone, L., Logan, M., Tessier-Lavigne, M., Taniguchi, M., Puschel, A. W., & Bussolino, F. (2003). Class 3 semaphorins control vascular morphogenesis by inhibiting integrin function. *Nature*, 424(6947), 391-397. doi:10.1038/nature01784
- Shimoda, Y., & Watanabe, K. (2009). Contactins: emerging key roles in the development and function of the nervous system. *Cell Adh Migr*, 3(1), 64-70.
- Sienknecht, U. J., & Fekete, D. M. (2008). Comprehensive Wnt-related gene expression during cochlear duct development in chicken. *Journal of Comparative Neurology*, 510(4), 378-395. doi:10.1002/cne.21791
- Sienknecht, U. J., & Fekete, D. M. (2009). Mapping of Wnt, frizzled, and Wnt inhibitor gene expression domains in the avian otic primordium. *Journal of Comparative Neurology*, 517(6), 751-764. doi:10.1002/cne.22169
- Simmons, D. (2002). Development of the inner ear efferent system across vertebrate species. *Journal of Neurobiology*, 53(2), 228-250. doi:10.1002/neu.10130
- Simmons, D. D., Duncan, J., Crapon de Caprona, D., & Fritsch, B. (2011). Development of the inner ear efferent systems. In D. K. Ryugo, R. R. Fay, & A. N. Popper (Eds.), *Auditory and Vestibular Efferents*. New York: Springer.
- Slusarski, D. C., Corces, V. G., & Moon, R. T. (1997). Interaction of Wnt and a Frizzled homologue triggers G-protein-linked phosphatidylinositol signalling. *Nature*, 390(6658), 410-413.
- Später, D., Hill, T. P., O'Sullivan, R. J., Gruber, M., Conner, D. A., & Hartmann, C. J. D. (2006). Wnt9a signaling is required for joint integrity and regulation of Ihh during chondrogenesis. *Development*, 133(15), 3039-3049.

- Stevens, C. B., Davies, A. L., Battista, S., Lewis, J. H., & Fekete, D. M. (2003). Forced activation of Wnt signaling alters morphogenesis and sensory organ identity in the chicken inner ear. *Developmental Biology*, *261*(1), 149-164.
- Stoller, M. L., Chang, H. C., & Fekete, D. M. (2013). Bicistronic Gene Transfer Tools for Delivery of miRNAs and Protein Coding Sequences. *Int J Mol Sci*, *14*(9), 18239-18255. doi:10.3390/ijms140918239
- Stoller, M. L., & Fekete, D. M. (2016). Tol2-Mediated Delivery of miRNAs to the Chicken Otocyst Using Plasmid Electroporation. *Methods Mol Biol*, *1427*, 27-42. doi:10.1007/978-1-4939-3615-1_2
- Stone, J. S., Shang, J. L., & Tomarev, S. (2003). Expression of Prox1 defines regions of the avian otocyst that give rise to sensory or neural cells. *Journal of Comparative Neurology*, *460*(4), 487-502.
- Takasaka, T., & Smith, C. A. (1971). The structure and innervation of the pigeon's basilar papilla. *J Ultrastruct Res*, *35*(1), 20-65.
- Takase, Y., Tadokoro, R., & Takahashi, Y. (2013). Low cost labeling with highlighter ink efficiently visualizes developing blood vessels in avian and mouse embryos. *Development Growth & Differentiation*, *55*(9), 792-801. doi:10.1111/dgd.12106
- Tanaka, K., & Smith, C. A. (1978). Structure of the chicken's inner ear: SEM and TEM study. *Am J Anat*, *153*(2), 251-271.
- Terriente, J., Gerety, S. S., Watanabe-Asaka, T., Gonzalez-Quevedo, R., & Wilkinson, D. G. (2012). Signalling from hindbrain boundaries regulates neuronal clustering that patterns neurogenesis. *Development*, *139*(16), 2978-2987. doi:10.1242/dev.080135
- Tessarollo, L., Coppola, V., & Fritsch, B. (2004). NT-3 replacement with brain-derived neurotrophic factor redirects vestibular nerve fibers to the cochlea. *Journal of Neuroscience*, *24*(10), 2575-2584.
- Tillo, M., Ruhrberg, C., & Mackenzie, F. (2012). Emerging roles for semaphorins and VEGFs in synaptogenesis and synaptic plasticity. *Cell Adh Migr*, *6*(6), 541-546. doi:10.4161/cam.22408
- Toyoshima, M., Sakurai, K., Shimazaki, K., Takeda, Y., Nakamoto, M., Serizawa, S., Shimoda, Y., & Watanabe, K. (2009a). Preferential localization of neural cell recognition molecule NB-2 in developing glutamatergic neurons in the rat auditory brainstem. *Journal of Comparative Neurology*, *513*(4), 349-362. doi:10.1002/cne.21972
- Toyoshima, M., Sakurai, K., Shimazaki, K., Takeda, Y., Shimoda, Y., & Watanabe, K. (2009b). Deficiency of neural recognition molecule NB-2 affects the development of glutamatergic auditory pathways from the ventral cochlear nucleus to the superior olivary complex in mouse. *Developmental Biology*, *336*(2), 192-200. doi:10.1016/j.ydbio.2009.09.043
- Tran, T. S., Rubio, M. E., Clem, R. L., Johnson, D., Case, L., Tessier-Lavigne, M., Hagan, R. L., Ginty, D. D., & Kolodkin, A. L. (2009). Secreted semaphorins control spine distribution and morphogenesis in the postnatal CNS. *Nature*, *462*, 1065. doi:10.1038/nature08628
- Trapnell, C., Hendrickson, D. G., Sauvageau, M., Goff, L., Rinn, J. L., & Pachter, L. (2013). Differential analysis of gene regulation at transcript resolution with RNA-seq. *Nature Biotechnology*, *31*(1), 46-53. doi:10.1038/nbt.2450
- Trapnell, C., Roberts, A., Goff, L., Pertea, G., Kim, D., Kelley, D. R., Pimentel, H., Salzberg, S. L., Rinn, J. L., & Pachter, L. (2012). Differential gene and transcript expression analysis of RNA-seq experiments with TopHat and Cufflinks. *Nat Protoc*, *7*(3), 562-578. doi:10.1038/nprot.2012.016

- Trapnell, C., Williams, B. A., Pertea, G., Mortazavi, A., Kwan, G., van Baren, M. J., Salzberg, S. L., Wold, B. J., & Pachter, L. (2010). Transcript assembly and quantification by RNA-Seq reveals unannotated transcripts and isoform switching during cell differentiation. *Nature Biotechnology*, *28*(5), 511-515. doi:10.1038/nbt.1621
- Van Amerongen, R., & Nusse, R. (2009). Towards an integrated view of Wnt signaling in development. *Development*, *136*(19), 3205-3214. doi:10.1242/dev.033910
- Varkonyi-Gasic, E., Wu, R., Wood, M., Walton, E. F., & Hellens, R. P. (2007). Protocol: a highly sensitive RT-PCR method for detection and quantification of microRNAs. *Plant Methods*, *3*, 12. doi:10.1186/1746-4811-3-12
- Veron, N., Qu, Z., Kipen, P. A., Hirst, C. E., & Marcelle, C. (2015). CRISPR mediated somatic cell genome engineering in the chicken. *Developmental Biology*, *407*(1), 68-74. doi:10.1016/j.ydbio.2015.08.007
- Von Bartheld, C. S., Patterson, S. L., Heuer, J. G., Wheeler, E. F., Bothwell, M., & Rubel, E. W. (1991). Expression of nerve growth factor (NGF) receptors in the developing inner ear of chick and rat. *Development*, *113*, 455-470.
- Wang, S. Z., Ibrahim, L. A., Kim, Y. J., Gibson, D. A., Leung, H. C., Yuan, W., Zhang, K. K., Tao, H. W., Ma, L., & Zhang, L. I. (2013). Slit/Robo signaling mediates spatial positioning of spiral ganglion neurons during development of cochlear innervation. *Journal of Neuroscience*, *33*(30), 12242-12254. doi:10.1523/jneurosci.5736-12.2013
- Wangemann, P. (1995). Comparison of ion transport mechanisms between vestibular dark cells and strial marginal cells. *Hearing Research*, *90*(1), 149-157. doi:https://doi.org/10.1016/0378-5955(95)00157-2
- Warr, W. B. (1975). Olivocochlear and vestibular efferent neurons of the feline brain stem: their location, morphology and number determined by retrograde axonal transport and acetylcholinesterase histochemistry. *Journal of Comparative Neurology*, *161*(2), 159-181.
- Warr, W. B., Boche, J. B., & Neely, S. T. (1997). Efferent innervation of the inner hair cell region: origins and terminations of two lateral olivocochlear systems. *Hearing Research*, *108*(1-2), 89-111.
- Warr, W. B., & Guinan Jr, J. J. (1979). Efferent innervation of the organ of Corti: two separate systems. *Brain Research*, *173*(1), 152-155.
- Weisz, C. J., Glowatzki, E., & Fuchs, P. A. (2014). Excitability of type II cochlear afferents. *Journal of Neuroscience*, *34*(6), 2365-2373. doi:10.1523/jneurosci.3428-13.2014
- Whitehead, M. C., & Morest, D. K. (1981). Dual populations of efferent and afferent cochlear axons in the chicken. *Neuroscience*, *6*(11), 2351-2365.
- Whitehead, M. C., & Morest, D. K. (1985a). The development of innervation patterns in the avian cochlea. *Neuroscience*, *14*, 255-276.
- Whitehead, M. C., & Morest, D. K. (1985b). The growth of cochlear fibers and the formation of their synaptic endings in the avian inner ear: A study with the electron microscope. *Neuroscience*, *14*, 277-300.
- Wu, D. K., & Oh, S. H. (1996). Sensory organ generation in the chick inner ear. *Journal of Neuroscience*, *16*(20), 6454-6462.
- Yamagata, M., & Sanes, J. R. (2012). Expanding the Ig superfamily code for laminar specificity in retina: expression and role of contactins. *Journal of Neuroscience*, *32*(41), 14402-14414. doi:10.1523/jneurosci.3193-12.2012

- Yang, J., Zeng, Z., Wei, J., Jiang, L., Ma, Q., Wu, M., Huang, X., Ye, S., Li, Y., Ma, D., & Gao, Q. (2013). Sema4d is required for the development of the hindbrain boundary and skeletal muscle in zebrafish. *Biochemical and Biophysical Research Communications*, *433*(2), 213-219. doi:<https://doi.org/10.1016/j.bbrc.2013.02.085>
- Yazdani, U., & Terman, J. R. (2006). The semaphorins. *Genome Biol*, *7*(3), 211. doi:10.1186/gb-2006-7-3-211
- Zhang, K. D., Stoller, M. L., & Fekete, D. M. (2015). Expression and Misexpression of the miR-183 Family in the Developing Hearing Organ of the Chicken. *PLoS One*, *10*(7), e0132796. doi:10.1371/journal.pone.0132796
- Zhou, Y., Gunput, R. A., & Pasterkamp, R. J. (2008). Semaphorin signaling: progress made and promises ahead. *Trends in Biochemical Sciences*, *33*(4), 161-170. doi:10.1016/j.tibs.2008.01.006
- Zidanic, M. (2002). Cholinergic innervation of the chick basilar papilla. *Journal of Comparative Neurology*, *445*(2), 159-175.

VITA

I graduated from Indiana University – Purdue University Indianapolis (IUPUI) with a Bachelor's in Biology and minors in Chemistry and Dance in 2011. As an undergraduate, I interned in the neurodiagnostic lab at Clarian Health Partners. Under the mentorship of Ryan Lau, our research investigated the effectiveness of various methods and materials used for long-term electroencephalogram monitoring for diagnostic purposes. I also worked as a research technician in the lab of John Hofstetter at the Roudebush Veterans Affairs Medical Center where I studied quantitative trait loci for circadian period and locomotor activity in mice. After graduating, I continued my work in John Hofstetter's lab as the laboratory manager. I additionally took on a part-time role as a clinical interviewer under the mentorship of Aimee Mayeda where we worked on identifying coding region variants correlated with the diagnosis of schizophrenia and bipolar illnesses. In 2013 I began my graduate studies at Purdue University in the PULSe program and in 2014 I joined Donna Fekete's lab. In 2016, I was awarded a two-year NRSA predoctoral fellowship from the NIDCD. I have accepted a position at the Jackson Laboratory as a postdoctoral associate in Vidhya Munnamalai's lab where I will continue to study inner ear development.

PUBLICATIONS

Scott, M. K., Yue, J., Bieseimer, D. J., Lee, J., Fekete, D. M. (2018). Expression of Semaphorins and their receptors in the developing chicken inner ear. (accepted for publication in *The Journal of Comparative Neurology*).

Coate, T. M., **Scott, M. K.**, Gurjar, M. C. (2018). Current concepts in cochlear ribbon synapse formation: a view from the postsynaptic side. (accepted for publication in *Synapse*).

Munnamalai, V., Sienknecht, U. J., Duncan, R. K., **Scott, M. K.**, Thawani, A., Fantetti, K. N., Atallah, N. M., Bieseimer, D. J., Song, K. H., Luethy, K., Traub, E., Fekete, D. M. (2017). Wnt9a can influence cell fates and neural connectivity across the radial axis of the developing cochlea. *The Journal of Neuroscience*, 1554-1517.